Investigating the Potential Use of Photovoltaic Thermal System for the Dairy Industries in Ethiopia

M.Sc. Thesis

By

Nahom Adugna Worku

Thermal and Aerospace Engineering Program

School of Mechanical, Chemical and Materials Engineering

Adama Science and Technology University

Adama, Ethiopia

July 2019

Investigating the Potential Use of Photovoltaic Thermal System for the Dairy Industries in Ethiopia

A Thesis Submitted to Thermal and Aerospace Engineering Program of School of Mechanical, Chemical and Materials Engineering, Adama Science and Technology University in partial fulfilment of the requirements for the award of the degree of **Master of Science in Thermal Engineering.**

By

Nahom Adugna Worku

Advisor: Dr. Addis Bekele

Adama, Ethiopia

July 2019

APPROVAL OF BOARD OF EXAMINERS

We, the undersigned, members of the board of examiners of the final open defence by Nahom Adugna have read and evaluated his thesis entitled "Investigating the Potential Use of Photovoltaic Thermal System for the Dairy Industries in Ethiopia" and examined the candidate. This is, therefore, to certify that the thesis has been accepted in partial fulfilment of the requirement of the Degree of Masters of Science in Thermal Engineering.

____________________________	____________	____________
Chairperson	Signature	Date
____________________________	____________	____________
Internal Examiner	Signature	Date
____________________________	____________	____________
External Examiner	Signature	Date

Declaration

I hereby declare that this M.Sc. Thesis entitled "Investigating the Potential Use of Photovoltaic Thermal System for the Dairy Industries in Ethiopia" in partial fulfilment of the requirements for the award of the degree of Master of Science in Thermal Engineering is an authentic record of my own work carried out from April 2017 to July 2019 under supervision of Dr. Addisu Bekele, Assistant Professor of Thermal Engineering Program, Adama Science and Technology University.

The matter embedded in this thesis has not been submitted for the award of a degree or diploma in any other university. All relevant resource information used in this paper has been duly acknowledged.

Name: Nahom Adugna Signature: …………………. Date ……………….

This is to certify that the above statement made by the candidate is correct to the best of our knowledge and belief. This has been submitted for examination with our approval.

Dr Addisu Bekele Signature …………………. Date ……………

Acknowledgement

Before all, I would like to express my deepest and sincere gratitude to my advisor Dr. Addisu Bekele for his deserving guidance and encouragement without hesitation until this level. He is committed and dedicated to help me at anytime and anywhere as I need his support.

Second, I am also giving my deepest thanks to Mr. Samuel G/Mariam for his kindness to help me as much as he can for any request for support of the program with admirable facial expression.

Third, I would like to give my praise to all my teachers those showed me this direction from the beginning up to this level, without their determined effort I may not.

Finally, my deepest love and respect wished to reach at the place they live to my classmates, colleagues, family and friends those played a great role in giving constructive idea for my work and irreplaceable support.

Abstract

Using solar energy is an engineering art that need improved device to extract solar energy at maximum level with the main target of reducing solar energy dissipated in the form of heat, which easily managed with hybrid solar device. The hybrid solar device used to enhance the electrical efficiency and to decrease the temperature of PV module by trapping the excess heat from module which used for medium heating applications in dairy industry. The daily average solar energy collected in all month of the year for both Adama and Addis Ababa weather show the greater energy harnessed by hybrid system. The PV module temperature comparison shows the module highly affected and the efficiency of the device lower in Adama due to high ambient temperature, which implies that the location is more advisable for thermal collector application and the PV module need cooling than Addis Ababa. The Module temperature increment by 20℃ above reference temperature cause the module efficiency drop by more than 0.66% which shorten the device life. For the same fluid inlet temperature more temperature obtained Adama PV-T collector, more combined efficiency, more fluid outlet temperature and finally more useful energy gained with a smaller number of collector and space. The economic evaluations results show the cost of hybrid system (0.57birr/kWh) less expensive than diesel and PV system cost, with this cost the payback period required for PV and PV-T system 54 and 33months respectively. Generally, the hybrid collector for dairy processing is more advantages in all aspects of energy generations if installed in Adama (hot area) rather than Addis Ababa (colder) under this cooling technique.

Keyword: Photovoltaic, photocurrent, PV glazing and Dairy

Table of Content

List of Tables

List of Figures

List of Symbols and Abbreviations

A	area [m^2]
q	electrical energy [w]
V	Operating voltage [V]
v	Wind Velocity [m/s]
W	Tube centre to centre distance [m]
I_T	Irradiance [W/m^2]
h	Heat transfer coefficient [W/m^2K]
I	Current [A] or irradiation [W/m^2]
IAM	Incident Angle Modifier [-]
k	Thermal conductivity [W/m K]
L	Length of the tube [m]
ṁ	Mass flow rate [kg/s]
Q_u	Useful heat gain
Ac	Area of PVT collector[m^2]
D_i	Storage tank internal diameter[m]
D_o	Storage tank internal diameter[m]
F'	Collector efficiency factor
F_R	Heat removal factor
F	Collector fin efficiency factor
R	Heat Transfer Resistance [m^2k/W]
D	Diameter [m]
PV	Photovoltaic
PV-T	Photovoltaic-Thermal
PV-TC	photovoltaic thermal collector
PCM	phase change material
ATpv	Adama PV module temperature (°C)
AATpv	Addis Ababa PV module temperature (°C)

Subscripts

p	Absorber plate
b	beam/back
d	Diffuse
el	Electrical
g	glass
u	Useful

Greek

α	Absorptance
β	tilt angle [◦]
θ	incidence angle [◦]
ε	Emissivity
δ	thickness [m]
η	Efficiency [%]
σ	Stefan-Boltzmann constant [W/m^2K^4]
τ	Transmittance

CHAPTER ONE

INTRODUCTION

1.1 Introduction

As the land fuels diminished through time, evidence shows that the use of those fuels is harmful to our economy, our health and our environment[1]. High prices for energy and power disruptions not only cause inconvenience, but also raise prices for nearly everything we buy, diminishing real disposable income and hurting economic growth. The problems are clear; the next step is finding and implementing the green energy (like wind, solar, hydro, geothermal, etc.).

A photovoltaic (PV) cell transforms the solar energy incident on it into electricity, but the Photovoltaic module depends on the operating temperature of the module which reduce the electrical efficiency and the device efficiency increased if thermal energy is properly collected by using a cooling medium. Such a system is known as a photovoltaic thermal (PV-T) system.

A look at the world map of mean solar radiations potential distribution reveal, Africa as a continent receives the highest amounts of solar radiation annually[2]. This makes the African continent of which Ethiopia is a part, extremely suitable for solar energy utilizations at any level.

The cost of energy will increase from time to time and attracts the attention of the producer regarding to the overall cost of milk production in the dairy industry which is the greater issue in the net profit obtained from milk production under this circumstance. Having this in mind the direct sunlight that falls on Ethiopian earth with an average of sunny day throughout the year has vast potential to drive industries such as milk and food processing industries to mitigate the negative effects of high-energy prices and climate change by turning sunshine into heat and electricity using solar photovoltaic thermal collector[1]. In dairy industry, the processing of raw milk mainly involves heat treatment operation usually known as pasteurization and sterilization at suitable temperature.[3], [4] this research studies the possible substitutions of the conversional energy source by using the solar radiation falling on PV cells at optimum levels.

1.2 Problem statement

All most all dairy processing industries in Ethiopia utilize power from national grid and in case of unavailability of electric supply, diesel generators are providing energy for processing of the milk. Dairy production includes the rural farms (pastoralists, agro-pastoralists, and mixed crop livestock producers that contribute to 98% of the total milk production in Ethiopia) and urban dairy farms only contribute 2% of the total milk production of the country[5]. Many Ethiopian farmers live in rural areas (where there is no electricity). Hence, where the large potential of raw milk is found there is no milk industry to collect and process this resource[6].

In the solar electricity generation, more than 80% of the solar radiation falling on PV cells either reflected back or converted to heat energy. This leads to an increase in the PV cells working temperature as much as 40°C-50°C above the ambient temperature[7], which causes 0.3% to 0.6 % of efficiency loss per rise in PV cell temperature and permanent damage in the structure of PV module if the thermal stress remains for a long period of time[7].

To overcome those problems, this research is going to study the possible use of solar energy for milk processing industries. Especially, the photovoltaic-thermal concept offers an opportunity to increase overall efficiency of the PV by circulating a colder fluid through PV module. The heat from PV modules is removed to enhance the electrical performance of the PV module and this recovered heat can be converted into useful thermal energy. As a result, PV-T collectors can generate more solar energy per unit surface area than it can if side-by-side photovoltaic modules and solar thermal collectors are used.

1.3 Objectives of the study

1.3.1 General Objective

The general objective of this research is to study the possible use of integrated Photovoltaic-thermal system and to power dairy process with a better efficiency device per capital per area required to install than separately used photovoltaic collector or solar thermal energy collector for milk processing industries in Ethiopia.

1.3.2 Specific objectives

a) To investigate the potential of solar energy available at dairy processing areas
b) To identify the electricity and process heat demand of selected potential dairy industries in Ethiopia
c) To design appropriate solar photovoltaic-thermal systems that can satisfy the demand of the selected dairy industries.
d) To study the effect of temperature on PV module efficiency.
e) To investigate the power generation capability of this hybrid system.
f) To develop a numerical model of PV-T systems that simulates the study.
g) To simulate and analysis of the desired Solar PV-T systems for selected dairy industries.
h) To conduct economic analysis of the desired PV-T systems.

1.4 Purpose of the study

The importance of this study is to increase and create the awareness of using solar energy at industrial level in Ethiopia. Which can save the amount of money paid for electricity, to satisfy process heat demand and electricity for different industries. Also, it reduces the energy scarcity at national level by applying this solar energy technology for the hot water consuming industries (milk) using solar photovoltaic-thermal (PV-T) collector system combined in a single unit.

1.5 Scope of the Study

The scope of this research is to investigate a solar energy potential at some specified locations and compare that at the same design input, but at different geographical, metrological and environmental conditions under some controlled input. And also, to design and interpret the PV-T systems which combines solar electrical and solar thermal components to study the technical and economic feasibility.

1.6 Limitation

Due to high material cost to perform experimental study, this research only limited to the technical investigation and numerical analysis of flat plate Photovoltaic-thermal collector with oscillatory pipe to cool the collector and supply hot water at medium range temperature for milk industries.

CHAPTER TWO

LITERATURE REVIEW

Many researchers have conducted both theoretical and experimental studies on PV-T hybrid systems. For the need optimum energy output of the PV-T systems investigation continued over the last 20 years and also hire farther research on this topic.

Chow et al (2012) perform the study for glazing of PV-T collectors almost doubled the useful thermal output, but the electrical efficiency dropped from 10% to 9%. The glazing may also make the PV module more sensitive to hotspots, the bypass diodes may get overheated, reflection losses may reduce electrical performance, and the increased temperature levels may lower the electrical yield. However, the electrical gains due to the cooling of the PV by the water are of the same order as the optical loss of the PV-T collector due to the reflection at the glass cover.

Ibrahim et al (2009) Glazed hybrid PV-T collectors without Tedlar, give the best performance of all the configurations compared which investigated by. A covered PV-T system with a heat pump using an ambient heat source gives a good performance. Condensation formation on the front glazing changed the transmissivity of the glazing, and

Ozgoren et al. (2013) experimentally prove the coverless PV-T collector produced 8% more electrical energy than a standard PV module, and 41% of the thermal energy of the FPC. The total energy of the coverless PV-T collector was 11% higher than that of the PV module, and 12.87% higher than that of the Flat Plate Collector.

Chatzopoulou, et al.(2017) proposed the working fluid in liquid type collector usually water, oil or liquid with a low freezing point. Freezing of the water in the collector and the corrosion are the major challenges, but a liquid PV-T collector can generate up to 40% more energy than PV and solar-thermal panels installed side by side over the same area.

Joe et al (2015) investigate the glazed PV-T collector with a Direct Solar Floor system, the maximum temperature reached at the PV modules is above 100℃, due to the oversize of the collectors during summer. Hence, amorphous cells or uncovered PV-T collector are a more suitable configuration. consequently, led to a reduction in thermal and electrical efficiency. The glazing may cause edge shading, which reduces the electrical output substantially. In addition, the stagnation temperature can reach a maximum of 120℃ to 140℃.

Khelifa et al. (2016) investigate the electrical efficiency of the photovoltaic (PV) module depends on the operating temperature of the PV module. If the operating temperature of the PV module reduced, then the electrical efficiency of the PV module increased. In addition to increased electrical efficiency of the PV module, additional thermal energy increase, if thermal energy properly collected by either water or air**.** And also, Duperat et al investigation shows that the PV-T collectors operating up to 80°C.

Zondag et al. (2003) investigate the integrated of PV module and solar thermal collector into one design fundamentally changes the characteristics of both the electrical yield of PV-cells and the thermal energy yield of the collector changed based on inflow temperature, heat transfer resistance between the absorber and the fluid. Those scholars study the comparative analyses of different type of photovoltaic thermal collector.

Guarracino, et al. (2017) confirm that the combined PV and solar thermal collector generate the same electricity and a useful thermal output from the same aperture area. This technique increases the longevity of the PV cells and the benefit arises from the fact the solar cells in PV-T collectors suffer lower temperature stresses. The Experimental results and the maximum thermal efficiency of the PV-T system found to be **51%** and the maximum electrical efficiency of PV and PV-T systems are **11.5%** and **13.6%,** respectively.

Ozgoren et al. (2013) prove that high operating temperatures cause the shorten life cycle of the PV module due to damaging the module material which substantially eliminated by cooling the PV cell. For this reason, prolonged payback time of the PV system decrease and increase the life of the materials used in PV modules.

Tripanagnostopoulos (2016) perform dual heat extraction operation, either with water or with air circulation to investigate the temperature effect on PV electrical efficiency presented experimental on hybrid PV-T collector.

Ibrahim et al. (2009) investigate the PV-T collector arrays installed on multi -family buildings could save about 38% in area. This is very vital due to the availability of the roof top space per house which is not used for another purpose. The disadvantage of this system is that the shading angle of PV-T collector smaller than conventional solar thermal collector because of the shading effect does.

Ghoneim and Mohammedein (2016) perform experiments to investigate the effect of mass flow rates on the electrical and thermal efficiencies of combined PV-T system. Water used as a heat transfer medium in spiral flow absorber collector and air for the Single pass rectangular tunnel absorber collector. Results showed that the single flow absorber collector generates combined PV-T efficiency of 64%, electrical efficiency of 11% and power maximum achieved at 25.35W. Its concluded that the best mass flow rate achieved for spiral flow absorber collector is 0.011kg/s at surface temperature of 55 and 0.0754kg/s at surface temperature of 39°C for single pass rectangular collector absorber. It recommends using other type of photovoltaic cell such as amorphous silicon cell that possess the black mat surfaces property that will improve its thermal absorption.

Joe et al (2015) prove that the efficiency of a PV-T system increased as mass flow rate increase from 0.01 to 0.4kg/s with an optimal flow rate of 0.03 kg/s for a $2m^2$ PV-T collectors. On the other hand, no significant effect on the efficiency at higher flow rates because at higher flow rates, the time of contact with the back surface reduces, causing less heat removal, and hence, the overall thermal efficiency gets constant. The maximum energetic efficiencies of 13.36% and 11.92% respectively, obtained for the glazed and unglazed collectors with the corresponding mass flow rates of 0.0014 kg/s and 0.0049 kg/s.

Kim and Kim (2012) evaluate large reservoir combined with the highest flow velocity and an inlet water temperature, equivalent to the ambient temperature except for the smallest flow channel; yield a gain in the PV-T electrical efficiency. However, high velocities with smaller flow thickness, or low flow velocity with larger flow thickness, cool the PV module more effectively.

This confirmed that the thermal and electrical outputs increase with an increase in the absorber length, mass flow rate and packing factor, but decrease with an increased duct depth.

Herrando and Markides (2016) investigate completely covered hybrid PV-T system, providing electricity and hot water, can cover 51% and 36% of the electricity and hot water demand, for a flow rate of 20 L/h.

This literature review enables us to conclude the hybrid photovoltaic thermal system gives a better efficiency under limited mass flow rate with different output depend on the collector type and geometric configuration of the desired collector.

The electrical and thermal efficiencies of the PV-T system increase with an increase in the mass flow rate, but the dependent power consumption reduces the net electricity gain. The speed of the fluid increases with the increase in the tube diameter, but increasing the fluid velocity reduces the thermal output quality.

CHAPTER THREE

PHOTOVOLTAIC-THERMAL SYSTEM

3.1 Photovoltaic-Thermal Collector

A solar collector performs two important functions: -

- To absorb sunshine as much as possible and to transfer effectively the gained heat into a heat carrier medium and
- To lose little heat as possible through all device.

The conventional flat plate and concentrated type solar collector integrated with PV cells on the absorber, to produce both thermal and electrical energy is known as "**Photovoltaic-Thermal systems".** To achieve the above main point the energy from the sun can be used to produce thermal energy as well as electrical power as shown below by changing the collector types:

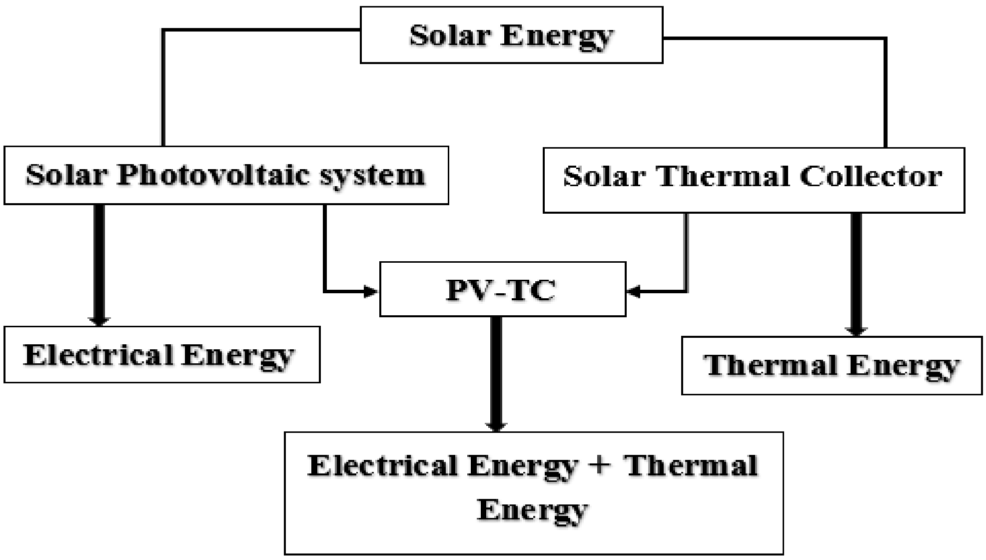

Figure 3. 1 Solar Energy Conversion Mechanism

Flat plate PV-T collectors collect direct and diffuse solar radiation without tracking systems. Although it has a large heat absorbing-surface, it produces less heat with low temperature compare with concentrating collectors. To warm up the water or air flat plate PV-T collector are suitable and less expensive than concentrator PV-T collectors.[24].

Table 3. 1 Types and application areas of PV-T System.

Collector	Type	Type based on working medium	Application area
PV-T Systems	Conventional flat plate PV-T System	PV-T/air	Space heating systems agricultural processes
		PV-T/water	Domestic/industrial water heating system Space heating system Water Distillation and Food processing systems
		PVT/ (air and water)	Industrial processes, space heating systems and agricultural processes

The PV module (used for combined purpose) temperature depends on the module encapsulating material, its thermal dissipation and absorption properties, irradiance level, ambient temperature, wind speed, and the installation conditions (the tilt angle and orientation of the collectors) [18], [24].

3.2 Types of PV-T collector Technology

The best observable classification of PV-T systems is based on the type of heat extraction medium, like air or water and based on the geometry of collector the PV-T divided into flat plate and concentrating PV-T collectors, but here only the flat plate PV-T collectors' types are listed and discuss in the following sections especially the liquid type flat plate collector in detail.

3.2.1 liquid-based PV-T collectors

The glazed PV-T water heating for public pool systems and large hot water demanding systems are the area of application, there is potential for further improvements with respect to the issues associated with high stagnation temperature, as well as the relatively large collector losses, due to both reflection and thermal losses in this kind of collector.

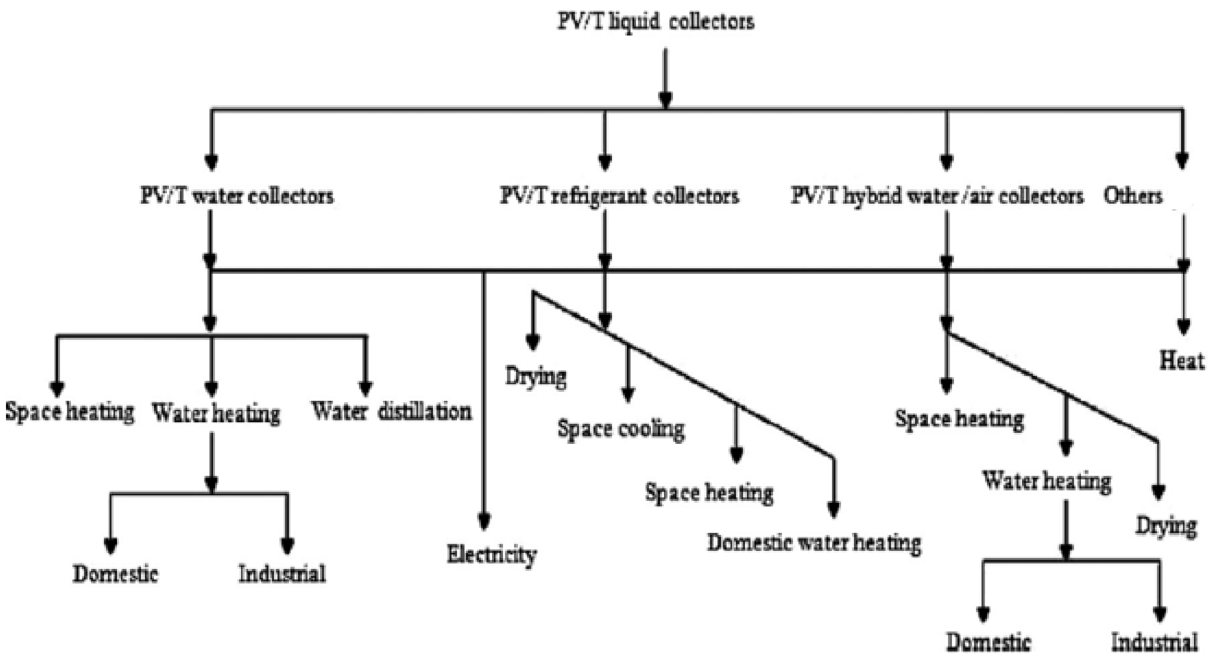

Figure 3. 2 liquid Type flat plate PV-T System with application area flow chart

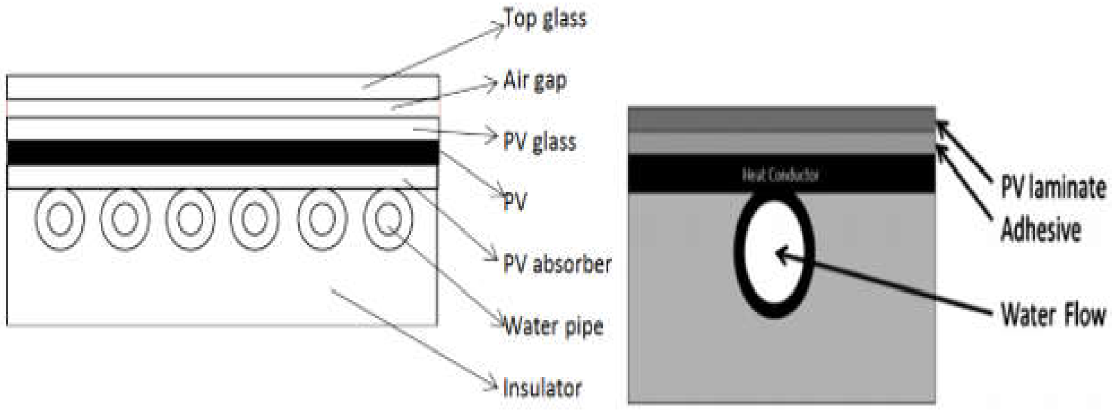

Figure 3. 3 Glazed and unglazed liquid-based PV-T/water collectors

The market for conventional unglazed liquid collectors consists primarily of pool heating applications which use liquid at low temperature as shown in the above figure.

The configurations of glazed and unglazed PV-T collectors are shown in figure 3.3 with all component arranged together.

3.2.2 Air-based PV-T Collector

The air-based PV-T collectors are similar to solar air heater, except that the black thermal absorber sheet is replaced by a solar PV module, under which air as the heat transfer fluid circulates through the duct[17].

Use air or gas as a working medium to transfer the heat with the advantages of no corrosion and air frost. The unique behaviour of this type collector is the difficulty to regulate and low heat storage capacity of air, which limits the practical application now a day.

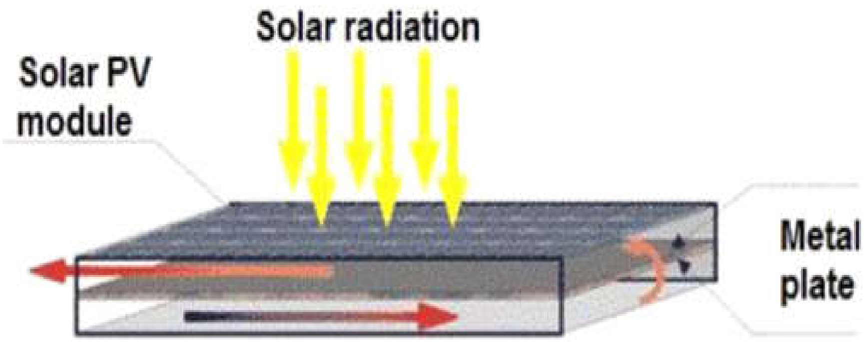

Figure 3. 4 Air-based flat plate PV-T Collector

3.3 Photovoltaic-thermal collector layers

The photovoltaic-thermal liquid-based collectors have glass cover, EVA, TEDLAR, PV, Absorber, etc. All of them discussed as follows:

3.3.1 Glass Cover

The glass in flat collectors has high penetrability to solar radiation and good insulation properties. Tempered and textured glass with high solar transmittance and low iron content used for photovoltaic module's top protective layer to facilitate the maximum solar radiation transmissibility of around 95% [17], which greatly affected, if the incident angle of solar radiation is greater than 40°.

Using double-glazing not suitable in PV-T collector due to the incoming radiation substantially weakened by passing two glasses, which can solve by using solar prismatic glass, it has microscopic ridges on its inner side that diffuse light and amend thus energy gains, especially when the sunshine comes from a low angle.

Table 3. 2 Input parameters for selected glass cover

Glass parameters	Symbol	Value
Thickness	δ_g	3mm
Density	ρ	2530kg/m^3
Specific heat capacity	Cp_g	880J/m k
Thermal conductivity	k_g	0.937W/m^{2}k
Absorpability	τ_g	0.066
Transmissivity	τ_g	0.94
Emissivity	ε_g	0.84

Source: https://www.uqgoptics.com/materials_commercial_sodalime.aspx

3.3.2 Photovoltaic Module

PV cells are made of semiconductor materials and major types of materials are crystalline and thin films, which vary from each other in terms of light absorption efficiency, energy conversion efficiency, manufacturing technology and cost of production.

Single-crystal silicon cells are the most common and uniform molecular structure. The higher a PV cell's conversion efficiency, the more electricity it generates for a given area of exposure to the sunlight. The conversion efficiency for single-silicon commercial modules ranges between 15-

20% [38]. Not only are they energy efficient, single-silicon modules are highly reliable for outdoor power applications.

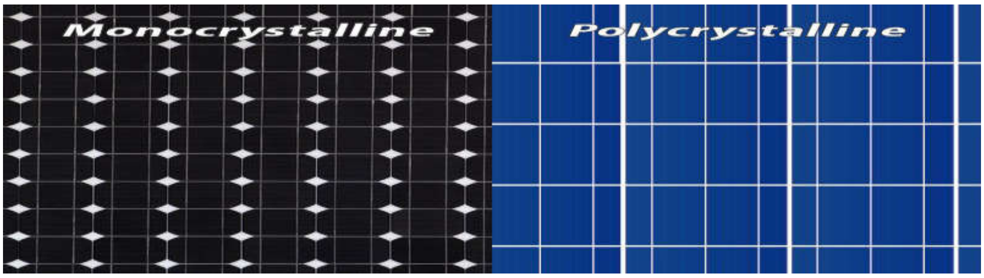

Figure 3. 5 Monocrystalline and polycrystalline solar panel:

Polycrystalline PV cells consists of small grains of single-crystal silicon, less energy efficient than single-crystalline silicon PV cells. The grain boundaries in polycrystalline silicon hinder the flow of electrons and reduce the power output of the cell. The energy conversion efficiency for a commercial module made of polycrystalline silicon ranges between 10 to 14%. Polycrystalline silicon material is stronger and cut into one-third the thickness of single-crystal material and it also has slightly lower wafer cost and less strict growth requirements.

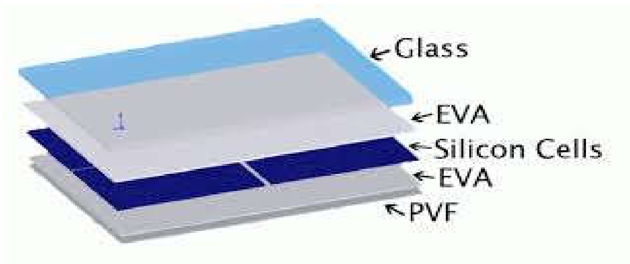

Figure 3. 6 PV Module layer

Ethylene Vinyl Acetate (EVA) is copolymer resin used in adhesives, sealants and coatings in photovoltaic cells. The main functions of EVA are Flexible even at low temperatures, tough at low and moderate temperatures, high Crack resistant and May be processed by conventional thermoplastic techniques or by conventional rubber processing techniques with Sensitive to heat in handling & shipping.

Highest thermal resistance layer in encapsulated solar cells; hence, filling it with thermal conductive materials enhances the thermal conductivity of the EVA, the PV efficiency, and heat dissipating ability of the solar cell effectively.

To obtain maximum efficiency in converting solar power into electricity, a solar panel that has a capacity of absorbing nearly every single photon of light, for every sun's position in the sky should accomplished by adequate antireflective coating utilization.

Poly Vinyl Fluoride polymer, commonly called as Tedlar, having excellent adhesion to EVA encapsulate and mainly used in the flammability lowering coatings of airplane interiors and photovoltaic module back sheets. It also used in raincoats and metal sheeting.

The adhesive layer with good thermal properties used to mechanically couple with PV module back surface and a thermal absorber, to increase the heat transfer. The presence of adhesive layer between the solar PV module and solar thermal conductor offers to transmit the heat generated in the PV module to the water tubes in an efficient manner.

Table 3. 3 Input parameters for selected PV module

PV parameters	**Symbol**	**Value**
Thickness	δ_{PV}	0.0035mm
Density	ρ_{PV}	2329kg/m^3
Specific heat capacity	Cp_{PV}	700J/k m
Thermal conductivity	k_{PV}	148W/m^{2}k
Absorptance	τ_{PV}	0.85
Emissivity	ε_{PV}	0.95
Packing factor	PF	0.97

Source https://www.el-cat.com/silicon-properties.htm

3.4 Pump

Pump is a mechanical machine used to move hot water or heat transfer fluid from the collector to the storage tank and which is selected according to the need for static and pressure head to provide the adequate flow rates at desire height. The drain-back and unpressurized systems require a high height pump to lift the water from the storage vessel to the collector and force the air out of the collector or collector array. Totally the pump selection depends on the following two parameters:

- Total head (static and pressure head) of the PV-T system
- The desired volume flow rates.

3.4.1 Total head (static and pressure head) of the PV-T system

The term pressure head includes the pressure drop along the flow line from the flow beginning up to the end the flow plus the desired static head. So, the pressure drops need the great attention in the flow is the following:

a) The pressure drops in the PV-T collector

The pressure drops in the PV-T collector depend on the shape pipe arrangement in the collector which includes the pressure drop in the pipe riser (ΔP_{rr}), header ($\boldsymbol{\Delta P_{bend}}$) and fitting ($\Delta P_{fit}$). The pressure drops through the oscillatory runner configuration type with no header than bent pipe is find by the following equation:

$$\boldsymbol{\Delta P_{rr}} = \frac{\boldsymbol{f*\rho*L_{rr}*V_w^2}}{\boldsymbol{2D_{irr}}} \quad \ldots 3.1$$

Where f is the friction factor of the flow inside the pipe, ρ is the density of the water at specified temperature, L_{rr} is the length of one runner, D_{irr} is the internal diameter of the runner and V is the mean velocity of the flowing fluid inside the runner.

$$\dot{Q_{rr}} = \frac{\dot{m}}{\rho}, \quad \text{is the volume flow rates through runner in PV} - \text{T collector}$$

$$\dot{Q}_{total} = n * \dot{Q_{rr}}, \quad \text{is the total volume flow rates through all runner}$$

$V_w = \frac{\dot{Q}_{total}}{A_{rr}}$, is the the mean fluid velocity flowing inside the runner

The pressure drop through bend pipe is also caused by the flow restriction at the curved circumferential area of the pipe and calculated with the following equations:

$$\Delta \boldsymbol{P}_{\boldsymbol{bend}} = \frac{f*\rho*L_{bend}*V_w^2}{2D_{irr}} \quad \text{.......} 3.2$$

Finally, the pressure drop in the fitting is the drop occurs due to some leakage in the mechanical fitting device.

$$\Delta \boldsymbol{P}_{\boldsymbol{fit}} = \frac{2*\rho*k_{fit}*V_w^2}{2} \quad \text{.......} 3.3$$

Where k_{fit} pressure loss factor (which is 0.9 most of the time in the desired application)

Therefore, the total pressure drops in PV-T collectors for oscillatory configurations runner arrangement from collector inlet up to collector outlet is calculate as the sum of the individuals pressure drop stated above:

$$\Delta \boldsymbol{P}_{\boldsymbol{PV-T}} = \Delta \boldsymbol{P}_{\boldsymbol{rr}} + \Delta \boldsymbol{P}_{\boldsymbol{bend}} + \Delta \boldsymbol{P}_{\boldsymbol{fit}} \quad \text{.......} 3.4$$

b) Pressure drop through the delivery or supply pipe (ΔP_{dp} *or* ΔP_{sp}) and return pipe (ΔP_{rp})

$$\Delta \boldsymbol{P}_{\boldsymbol{rp}} = \boldsymbol{f} * \boldsymbol{\rho} * \frac{L_{rp}}{D_{irp}} * \boldsymbol{V}_{\boldsymbol{w}}^{2} \quad \text{.......} 3.5$$

The pressure drops through the supply pipe

$$\Delta \boldsymbol{P}_{\boldsymbol{sp}} = \boldsymbol{f} * \boldsymbol{\rho} * \frac{L_{sp}}{D_{isp}} * \boldsymbol{V}_{\boldsymbol{w}}^{2} \quad \text{.......} 3.6$$

c) Pressure drop in the pipe bend

The pressure drops for any bend pipe transporting the fluid is calculated as follows:

$$\Delta \boldsymbol{P}_{\boldsymbol{b}} = \boldsymbol{\rho} * \boldsymbol{k}_{\boldsymbol{f}} * \frac{V_w^2}{2} \quad \text{.......} 3.7$$

d) The pressure drops due to elevation and inclination of the PV-T collector

For the collector tilted at appropriate inclination angle the pressure drop may be calculated by:

$$\Delta \boldsymbol{P}_{\boldsymbol{incl}} = \boldsymbol{\rho g L} \, \boldsymbol{sin} \, \boldsymbol{\beta} \quad \ldots 3.8$$

Finally, the overall pressure drop in the desire flow device should be the summation of pressure drop at each component in the system.

$$\Delta \boldsymbol{P}_{\boldsymbol{total}} = \Delta \boldsymbol{P}_{\boldsymbol{PV-T}} + \Delta \boldsymbol{P}_{\boldsymbol{b}} + \Delta \boldsymbol{P}_{\boldsymbol{sp}} + \Delta \boldsymbol{P}_{\boldsymbol{rp}} + \Delta \boldsymbol{P}_{\boldsymbol{incl}} \quad \ldots 3.9$$

The total pressure head (h_{head}) from total the pressure drop is calculated as:

$$\boldsymbol{h}_{\boldsymbol{head}} = \frac{\Delta P_{total}}{\rho * g} \quad \ldots 3.10$$

however, the total pumping head used for pump size selection is the summation of static head (determined by the required delivery height) and pressure head height which mathematically found as follows:

$$\boldsymbol{H}_{\boldsymbol{total}} = \boldsymbol{h}_{\boldsymbol{static}} + \boldsymbol{h}_{\boldsymbol{head}} \quad \ldots 3.11$$

3.4.2 Pump Application and specification

The SGR series [25]pump is selected to use for this application with the following manufacturer specifications: This kind of pump used to pump water supply from rain water tanks, Small drainage pits, Reservoirs, Emergency drainage of flooded areas, irrigation and residential cisterns applications with pumping head up to 30 meters and maximum volume flow rate up to 55litre/hr, maximum working pressure 8bar, fluid temperature up to 35˚C with operating options of manual and auto versions.

3.3 Control Element

A. Temperature controller

The temperature controllers used to maintain the temperature of the panels using the temperature difference in the working fluid.

B. Pump Control

The use of pump in thermal collection system increases the efficiency of the system by pumping the water as far as the temperature of the PV-T collectors rise.

3.4 Battery and Invertor

The total amount of electricity that a solar battery can store, measured in kilowatt-hours (kWh). Most home solar batteries are designed to be “stackable,” which means that you can include multiple batteries with your solar-plus-storage system to get extra capacity.

While capacity tells you how big your battery is, it doesn’t tell you how much electricity a battery can provide at a given moment. To get the full picture, you also need to consider the battery’s power rating. In the context of solar batteries, a power rating is the amount of electricity that a battery can deliver at one time. It is measured in kilowatts (kW). A battery with a high capacity and a low power rating would deliver a low amount of electricity (enough to run a few crucial appliances) for a long time. A battery with low capacity and a high-power rating could run your entire home, but only for a few hours with size given by manufacturers.[26]

3.6 Pipes and Cables

Pipes of the solar system must be fitted with thermal insulation e.g. of AEROFLEX type. It recommended realizing the whole piping of copper pipes connected by soldering. The connecting piping from collectors should be led the shortest way, for this reason the coil for balanced supply to collector fields thus made principally on the return piping to the collectors.

3.5 Advantages and Disadvantages of PV-T Technology

The PV-T technology has the following advantages

1) Reliability: - In harsh conditions the system has been shown to work.
2) Durability: - Most modules are guaranteed for 25years with production even after that.
3) Low maintenance cost: - Systems require periodic inspection and occasional maintenance.
4) No fuel cost: - No liquid fuel to deal with to produce power.

5) Reduced sound pollution: - Only sound produced is from the pump and tracking system if used.
6) Photovoltaic modularity: - Modules can be added to increase power.
7) Safety: - No fuel required to be stored or used.
8) Independence: - Based on the use, its system can be a standalone system with no grid tied components.
9) Electric grid decentralization: - For larger systems a small decentralized power station can reduce power outages.

And also, the Photovoltaic-Thermal system has the following drawbacks:

a) Initial Cost: - The cost of a PVT system generally has to be expended up front and benefits received over time.
b) Variability of solar radiation
c) Energy storage: If power is required outside daylight hours, then batteries generally needed. These batteries are high amp-hours, which Costly.
d) Efficiency improvements: - The use of solar power for home, office, barn, etc. Use first requires that energy conservation practiced.

CHAPTER FOUR

DIARY INDUSTRY ENERGY DEMAND

Currently, there are over 22 medium- and large-scale dairy processing companies in Ethiopia with nine of them operating in Addis Ababa, the rest in other major regional cities, but all of them use electricity/diesel generator as energy source. The figure 4.1 shows the SNNP (44%) and Oromia Regional (42%) states are leading state by dairy cows[5] as well as by dairy product, but almost all are the private sector. This commercial processors are adopting modern technology with the majority of their output being pasteurized milk in packs of 100, 250 and 500ml [27].

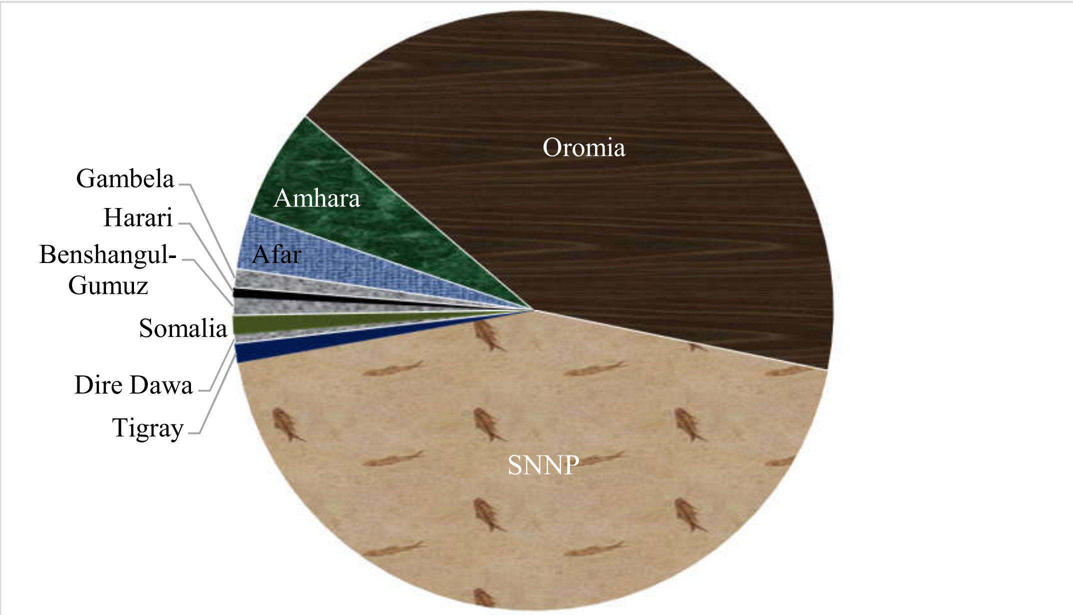

Figure 4. 1 Regional distribution of dairy cows for the year of 2011/12 G.C

4.1 Dairy process

The raw milk from local market pumped to a clarifier by means of the milk pump to the remove microscopic impurities then transported through pipe pass in flat plate heat exchange to reduce the temperature of processing milk at less than 6°C. Clarified milk (at specified temperature) sent to the cooler and then pumped to the storage tank. The milk preheated and pasteurized (patch or continues type) further heated by ultra -high temperature for sterilization purpose, the fatty ingredients homogenized in the homogenizer.

Finally, cooling achieved by means of chilled water to lower the temperature, after which the milk stored in the surge tank for filling into suitable containers for end use.

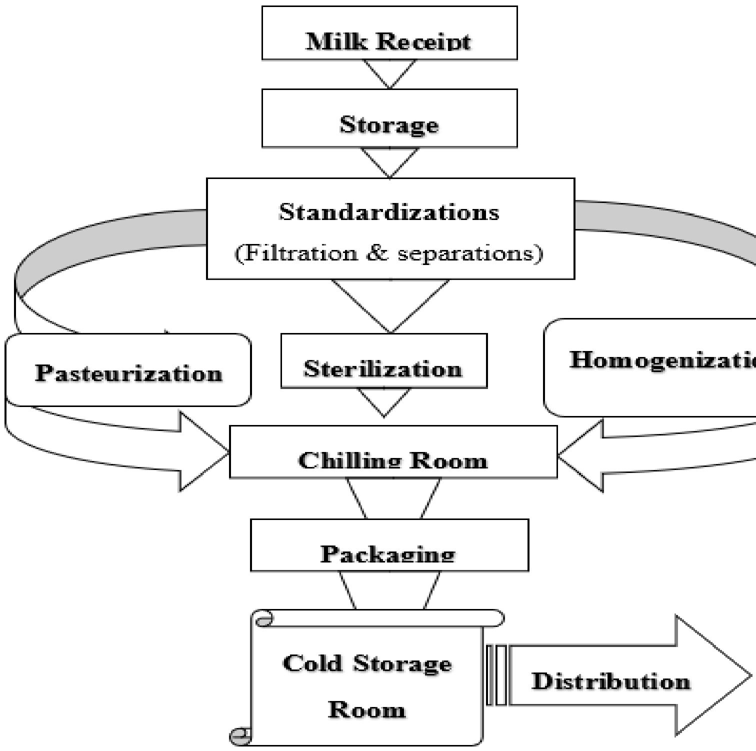

Figure 4. 2 The main milk processing flow chart

Some of those processes are list and defined as follows:

a) Pasteurization

Its head step in dairy processing by means of heating every particle of the milk or milk product at specific temperature for a specified period of time (63°C to 87°C).[27]

b) Standardization

Milk standardization means balancing the fat content in milk to the required percentage. Different milk products are needs different percentage of standardization.

c) Sterilization

Sterilization is the process and treatment used to produce long life milk products.

d) Homogenization

Homogenization is the process of reducing fat globules in size until the extent that no visible cream separation occurs in the processed milk and uniform composition or consistency without removing or adding any constituents. Homogenization increases the whiteness of milk, because the greater number of fat globules scatters light more effectively. Dairy products process temperature ranges are shown in table 4.1[28].

The raw material pass through the above process are raw milk, salt and coagulation enzyme. The raw milk and salt are available at local market while the coagulation enzymes have to be imported. The auxiliary materials required for packing materials like plastic bags and carton boxes available at local market and the processing temperature range given the Table 4.1.

Table 4. 1 Dairy processes with the utilized temperature range.

Industry	**Process**	**Temperature (℃)**
Dairy	Pasteurization	60-80
	Sterilization	100-120
	Drying	120-180
	Concentrates	60-80
	Boiler feed water	60-90

Those processing temperature range achieved from solar energy using the adequate technology for this temperature range as discussed early in this chapter three. The pasteurization temperature further varied based on the time required to kill all bacteria endanger human health. The following table shows the representing of various dairy processes along with different solar technologies that potentially used at specified temperature range[29].

Table 4. 2 Solar Technology and process temperature range in the dairy sector

Process	**Energy/Fuel being used**	**Application media**	**Temperature (℃)**	**Recommended solar technology**
Washing & cleaning	Electricity and Boiler fuels like furnace oil, rice husk	Hot water	40–60	FPC
Chilling/Cold storage	Electricity and diesel		< 5	Solar thermal systems, driving absorption chillier
Pasteurisation	Boiler fuels like furnace oil, rice husk	Process heat	70	FPC
Sterilisation/ Evaporation	Boiler fuels like furnace oil, rice husk	Process heat	100–120	ETC or solar concentrators
Spray drying	Boiler fuels like furnace oil, rice husk	Hot air	120	ETC/solar concentrators

4.2 Application of solar energy in dairy industry

Table 4. 3 Solar Energy applications area

Application Area	**Purpose**
Water Heating	washing, cleaning, sterilizing, pasteurizing, drying, cooking, hydrolysing, distillation, evaporation, extraction and polymerization.
Dairy Cooling	For preservations
Drying	To produce powder milk (35℃-80℃)[30]
Dairy Pumping	To pump hot water Chill water, milk and CIP
lightning Dairy offices	To light garden, road and chilling centre.

4.3 Challenges for Ethiopian dairy

A great challenge for the Ethiopian dairy sector is moderating the seasonality that affects both supply and demand. The seasonal mismatch between dairy supply (shortage in the months before the rainy season) and demand (drop during fasting months) strongly hurts the sector.

In the other hand, existing dairy industries in Ethiopia are operating in areas that are accessible to **transportation**, **electricity** and **markets**. This means that a substantial amount of milk does not reach the markets and a number of producers keep on producing at a subsistence level.

In general, the demand for milk products is increasing while supply is left-behind. Constrained by cows‟‟ nutrition, genetics and health, producers and energy need are not able to keep up with demand.[5] To satisfy the demand Ethiopia imports dairy products from abroad and must expand the dairy processing industries to urban centres by using alternative energy resources like solar energy.

The sufficient heat energy and electrical energy for milk processing operations investigated and designed by using the dairy industry energy consumption trends. This required energy is investigated in terms of hot water and electrical energy consumption as shown below.

4.4 Hot water consumption

In Ethiopian dairy, the amount of hot water required per day do not known, but from the monthly bill the average daily is known as 0.4-0.8litres water per litres of milk processed in some industry, however in many Ethiopian dairy the amount of water used in the milk processing was not specified because they use the water out of dairy processing with the one bill payment and the international experience at modern dairy processing plants **Bylund**, a water consumption rate of 1.3–2.5litres water/kg of milk intake is typical; however, 0.8–1.0litres water/kg of milk intake is possible.

Table 4. 4 Selected Ethiopian dairy industry daily processing capacity.

Company Name	**Location**	**Capacity (litre/day)**
Etete milk processing industry	Sendafa	12000-20000
Elemtu integrated milk industry	Sululta	10000-30000
Semit agro industry (modjo milk)	Modjo	2000-4000
Lame dairy processing	Addis Ababa	50,000-70,000
Family milk pant A	Addis Ababa	15000
Genesis farm	Bishoftu	2500-4000

Steam and thermal energy consumption in processing section and storage tank cleaning[31]

To achieve such low consumption requires not only advanced equipment, but for very good housekeeping and awareness among both employees and management, the design for new plant takes this numeric as a reference input in this thesis. The raw milk collected from the producers until 10:00am in the morning and the hot water high consumption profile starts after this hour. The performance of the solar water-heater is sensitive to the load timing and to the load day-to-day variability, as the temperature of the storage tank varies when a water draw-off event occurs.

The key parameters that define the profile of hot-water demand are the average daily volume, the yearly total demand, the draw-off flow rates and the distribution of the drawn hot water during the day.

Table 4. 5 Steam and thermal energy consumption in processing section and storage

Process	**Milk processed (L)**	**Amount of Steam consumed (Kg/m^3 milk)**	**Thermal Energy Consumption (GJ/1m^{3}milk)**
Milk pasteurization	121466.70	37.26	0.100
Cream pasteurization	2890.00	97.57	0.262
Milk pasteurizer cleaning		802.26	2.156
Cream pasteurizer cleaning		584.85	1.571
Raw milk storage tank cleaning		251.05	0.675
Silos cleaning		480.38	1.291
Cream tank cleaning		65.00	0.175
Pre- pack cleaning		556.02	1.494
Lassi culturing tank cleaning		81.86	0.220
Flavouring tank cleaning		27.29	0.073
Aging tank cleaning		43.66	0.117
Total		3027.2	8.134

4.5 Electricity Consumption

The energy consumed in any process depends on the processing temperature range. The concentration and drying of milk, whey or buttermilk are high energy consuming process. The production of market milk at the other extreme encompasses only some heat treatment and packaging, and therefore requires substantially less energy.

In Ethiopian dairy, the energy used at dairy processing plants for running process equipment, for heating, refrigeration, and for the generation of compressed air. Most of the time in Ethiopia electrical energy used to generate steam and hot water for evaporative and heating processes.

Table 4. 6 Specific energy consumption for various dairy products.

Product type	**Electricity Consumption (GJ/tonne)**	**Fuel consumption (GJ/tonne) of product**
Market milk/pasteurized	0.20	0.46
Cheese	0.76	4.34
Milk powder	1.43	20.60
Butter	0.71	3.53

Source: Joyce and Burgi, 1993(based on a survey of Australian dairy processors in 1981–82)

In Ethiopian dairy process, the substantial increases in electricity use have resulted from the trend towards automated plant with associated pumping costs and larger evaporators.

Table 4. 7 Energy Consumption for the selection of milk plants.

Type of plant	**Total energy (GJ/tonne) of product**
Modern plant with high-efficiency regenerative pasteuriser and modern boiler	0.34
Modern plant using hot water for processing	**0.50**
Old, steam-based plant	2.00
Range for most plants	0.5–1.2

Source: Joyce and Burgi, 1993 (based on a survey of Australian dairy processors in 1981–82)

Depending on the above data the amount of energy required to process milk in modern plant using hot-water is calculated and documented in the table 4.5.

Table 4. 8 Energy consumption range in selected dairy industry in Ethiopia

Industry name	**Location**	**Capacity (m^3/day)**	**Capacity (tonne)**	**Total energy (GJ/tonne)**
Etete Milk Processing Industry	Sendafa	12-20	12.36-20.6	6.13-10.3
Elemtu integrated milk industry	Sululta	10-30	10.3-30.9	5.15-15.45
Semit agro industry (modjo milk)	Modjo	2-4	2.06-4.12	1.03-2.06
Lame dairy processing	Addis Ababa	50-70	51.5-72.1	25.75-36.05
Family milk pant A	Addis Ababa	15	15.45	7.725
Genesis farm	Bishoftu	2-3	2.06-3.09	1.03-1.545

The net Specific total energy required in modern milk processing plants including CIP for one tonne of milk processed into liquid products in bottles having less than ten percent fat without added sweeter is 245kwh[32].

$$Q_{rth} = Q_{Oth} * V_{milk} \quad \ldots 4.1$$

Where Q_{rth} the required thermal energy to process the desired volume in to any product

Q_{Oth} total thermal energy required to process one metre cubic of milk

V_{milk} the total volume of milk being processed (m3)

So, based on the above calculations to process the maximum of Genesis farm or the average of Mojo milk (3000l) the amount of electrical energy required is 85.8KWh.

$$E_{total} = Q_{rth} + E_{rel} \quad \ldots 4.2.$$

CHAPTER FIVE

SOLAR ENERGY POTENTIAL ASSESSMENT

5.1 Estimation of Solar Energy Potential

The solar energy on the earth surface measured daily or monthly considered as the available solar energy at particular location. In many parties of Ethiopia, due to the lack of appropriate measuring technology, the exact available solar energy data is not recorded accurately. To overcome this problem and to have the strong data for design, empirical model is advisable to predict and estimate solar radiation by using geographical satellite data for particular location.

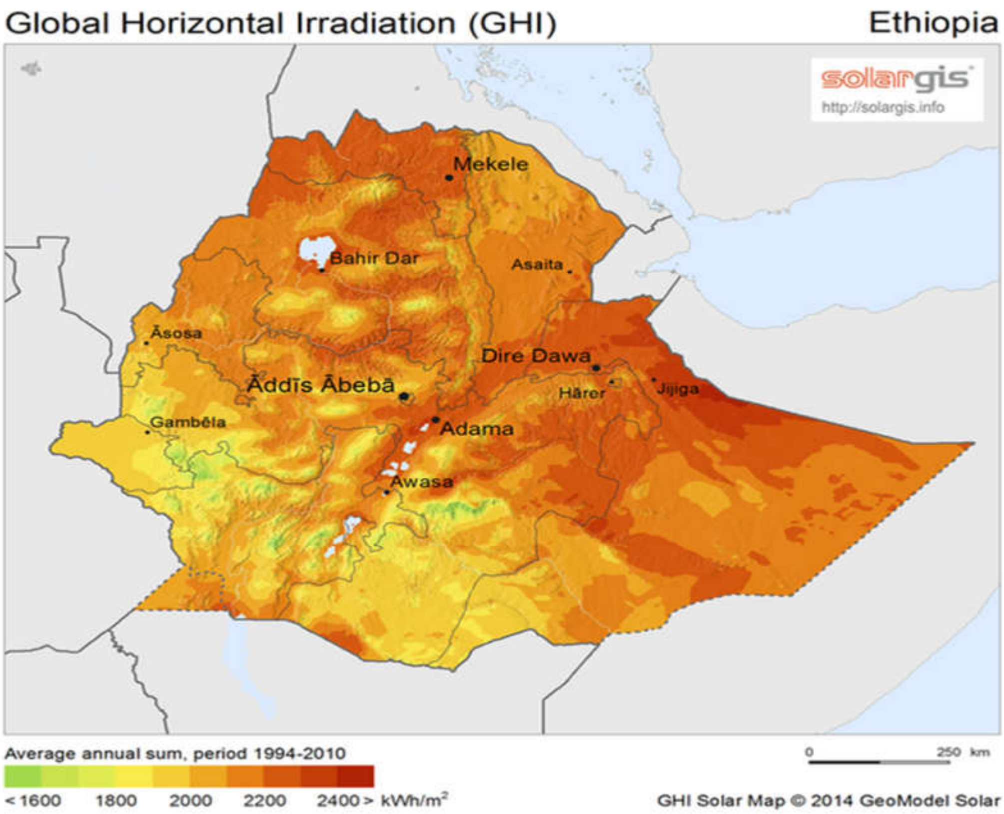

Figure 5. 1 Global Horizontal Solar Irradiation Resource Map in Ethiopia

5.1.1 Monthly Average Daily Global Radiation on Horizontal Surface

The empirical correlation proposed by Angstrom to estimate monthly average of daily global solar radiation on a horizontal surface is the well-known correlation for the numerical investigation to any solar system design **[8,9]**.

$$\frac{\overline{\mathrm{H}}}{\overline{\mathrm{H_O}}} = \mathrm{a} + \mathrm{b}\frac{\overline{\mathrm{n_s}}}{\overline{\mathrm{N_s}}} \ldots\ldots\ldots\ldots\ldots\ldots\ldots\ldots\ldots\ldots\ldots 4.1$$

Latitude (ϕ): is the angle between the radial line joining some particular location with the centre of the Earth, and its projection on the equatorial plane which is positive in northern hemisphere.

Hour angle (ω): This is the angle between projections of the Sun's rays (solar meridian) and the line running south–north through centre. The hour angle is the angular displacement of the Sun from the local meridian because of the Earth's rotation around its own axis.

Sunshine hour ($\overline{\mathrm{N_s}}$): The total duration in hours of the Sun's movement from sunrise to sunset (ω_s).

$$\overline{\mathrm{N_s}} = \left(\frac{2}{15}\right)\overline{\omega_s} \ldots\ldots\ldots\ldots\ldots\ldots\ldots\ldots\ldots\ldots\ldots 4.1a$$

$$\overline{\omega_\mathrm{s}} = \cos^{-1}(\tan\emptyset\tan\delta) \ldots\ldots\ldots\ldots\ldots\ldots\ldots\ldots\ldots\ldots\ldots 4.1\mathrm{b}$$

Declination (δ): is the angle between the line joining the centres of the Sun and the Earth, which also determines the direction of the direct rays coming from the Sun and their projection on the equatorial plane.

$$\delta = 23.45\sin\left(\frac{360}{365}(284 + N)\right) \ldots\ldots\ldots\ldots\ldots\ldots\ldots\ldots\ldots\ldots\ldots 4.1c$$

Regression constant

$$a = -0.11 + 0.235\cos\emptyset + 0.323\left(\frac{\overline{n_s}}{\overline{N_s}}\right) \ldots\ldots\ldots\ldots\ldots\ldots\ldots\ldots\ldots\ldots\ldots 4.1d$$

$$b = 1.449 - 0.533\cos\emptyset - 0.694\left(\frac{\overline{n_s}}{\overline{N_s}}\right) \ldots\ldots\ldots\ldots\ldots\ldots\ldots\ldots\ldots\ldots\ldots 4.1e$$

$$\overline{H_O} = \left(\frac{24 * 3600}{\pi}\right) I_{SC} \left\{\left[1 + 0.033 \cos\left(\frac{360 * N}{365}\right)\right]\left[\cos\emptyset \cos\delta \sin\overline{\omega_s} + \frac{\pi\overline{\omega_s}}{180} \sin\delta \sin\emptyset\right]\right. \quad \ldots 4.2$$

5.1.2 Monthly Average of Daily Diffuse Radiation on a Horizontal Surface

From equation 4.1 and recorded sunshine hours, the monthly average daily diffuse radiation on a horizontal surface $\overline{H}_d$ calculated.

$$\frac{\overline{H}_d}{\overline{H}} = 0.931 - 0.814\left(\frac{\overline{n_s}}{\overline{N_s}}\right) \quad \ldots 4.3$$

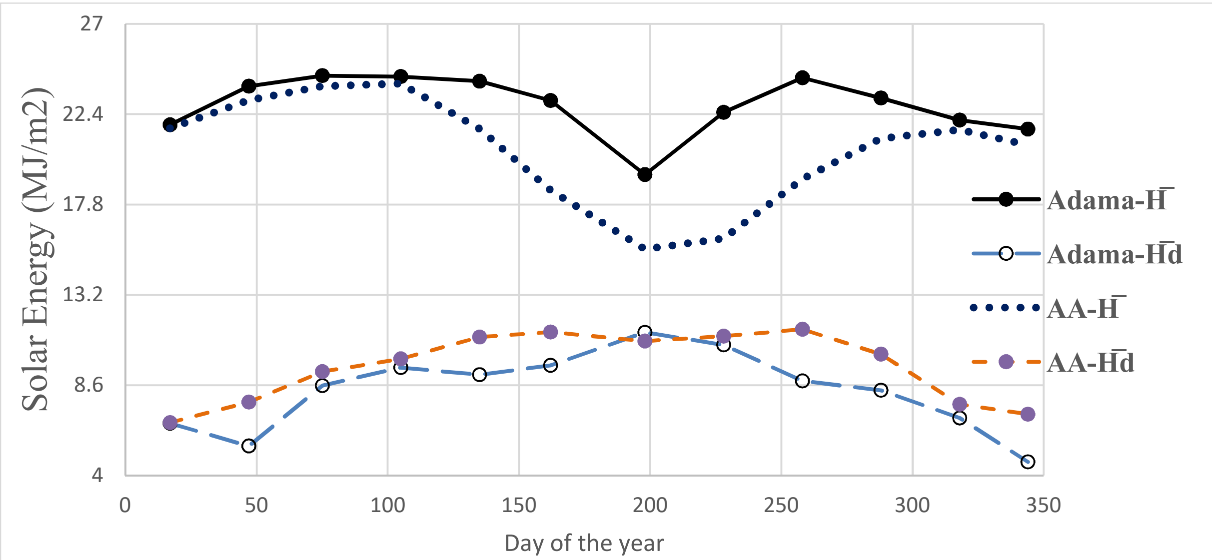

Figure 5. 2 Adama and Addis Ababa monthly average daily global and daily diffuse radiation on horizontal surface

As shown in the figure 5.3 monthly average daily global radiation on extra-terrestrial surface of both locations differ only by latitude, so the solar energy available almost the same. The Addis Ababa daily bright sunshine hour is less than Adama bright sunshine hour throughout the year.

5.1.3 Monthly Average of Hourly Global Radiation on a Horizontal Surface

The monthly average hourly global radiation on a horizontal surface calculated from monthly average daily global radiation on a horizontal surface**[8, 9]**.

$$\frac{\bar{I}}{\bar{H}} = (a + b\cos\omega) \qquad 4.4$$

$$a = 0.409 + 0.5016\sin(\varpi_s - 60) \qquad 4.4a$$

$$b = 0.6609 - 0.4767\sin(\varpi_s - 60) \qquad 4.4b$$

Based on the above equations the monthly average of hourly global radiation on a horizontal surface for both Adama and Addis Ababa calculated and plotted in the following figure respectively.

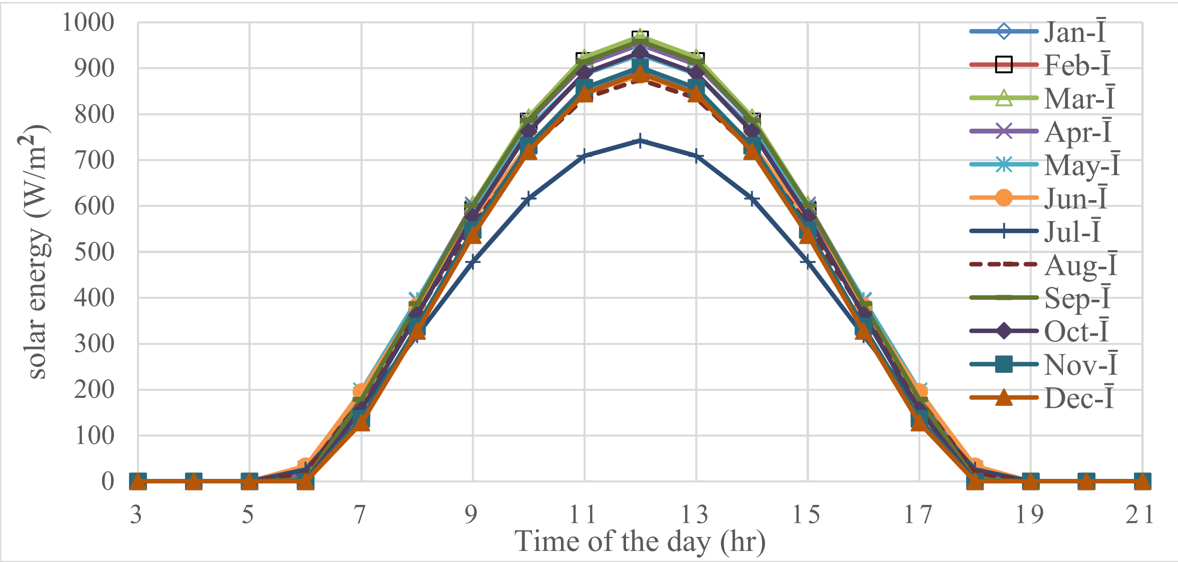

Figure 5. 3 Adama Monthly Average of Hourly Global Radiation on a Horizontal Surface

The minimum monthly average hourly global radiation at Adama and Addis Ababa obtained in July (742.56MJ/m^2, 595.6MJ/m2 respectively) month and the maximum in February (963.63, 936.6MJ/m^2).

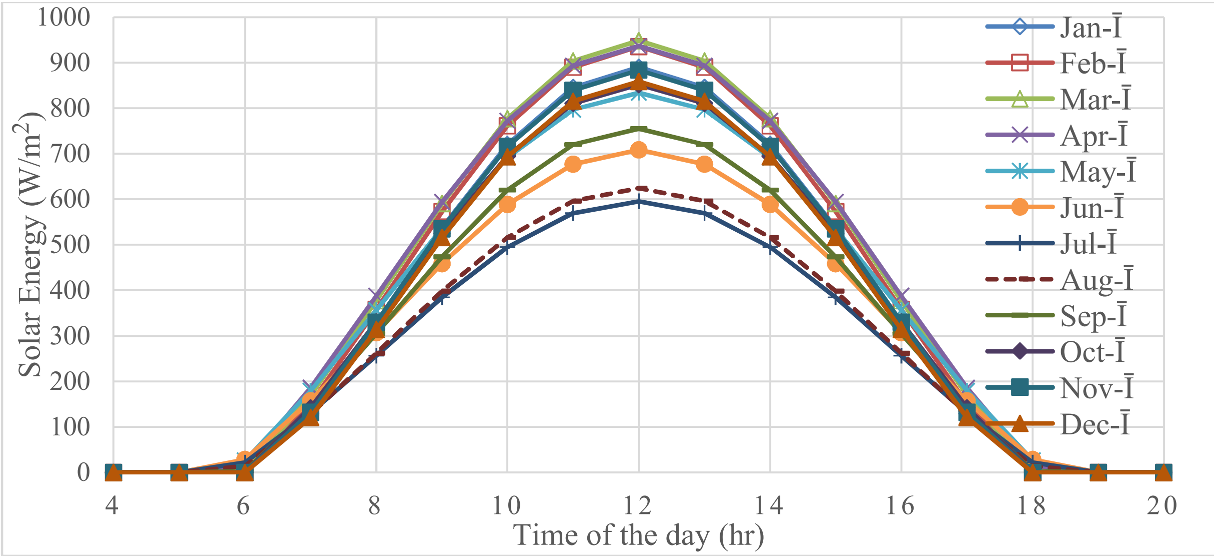

Figure 5. 4 Addis Ababa Monthly Average of Hourly Global Radiation on horizontal surface

5.1.4 Monthly Average of Hourly Diffuse Radiation on a Horizontal Surface

Similarly, the monthly average hourly diffuse radiation on a horizontal surface calculated from the monthly average daily diffuse radiation on a horizontal surface

$$\frac{\bar{I}_d}{\bar{H}_d} = \frac{\pi}{24}\left(\frac{\cos\omega - \cos\bar{\omega}_s}{\sin\bar{\omega}_s - \frac{\pi}{180}\bar{\omega}_s\cos\bar{\omega}_s}\right) \quad \ldots\ldots 4.5$$

Using equation 4.5 the monthly average hourly diffuse radiation is plotted as follows for Adama and Addis Ababa, the overall analysis of this energy potential discussed under section 5.5 in detail regarding to the comparison of those two areas, the Adama diffuse radiations for each is less than Addis Ababa corresponding month of the diffuse radiations calculated as shown in the next two graphs.

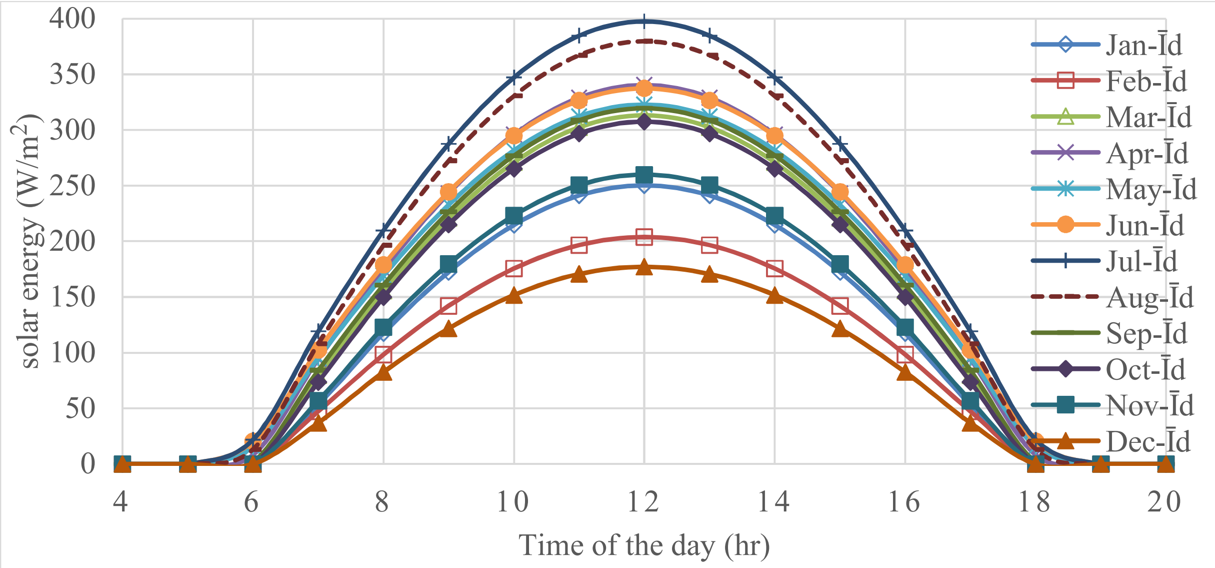

Figure 5. 5 Adama Monthly Average of Hourly Diffuse Radiation on a Horizontal Surface

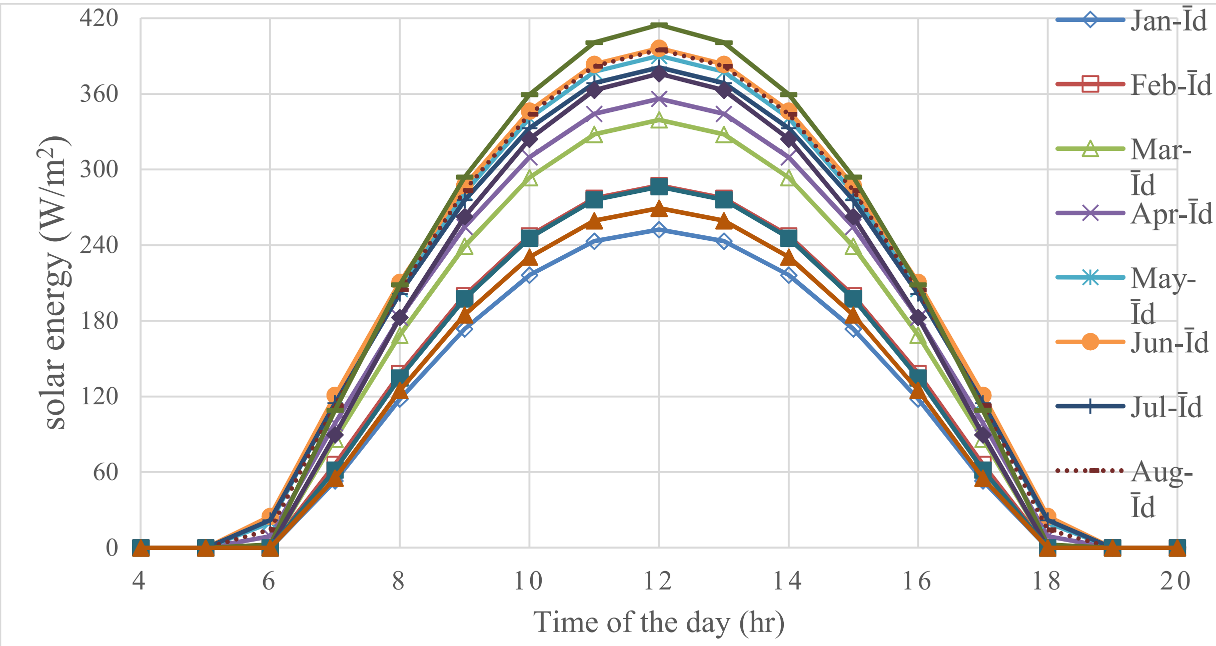

Figure 5. 6 Addis Ababa Monthly Average of Hourly Diffuse Radiation on a Horizontal Surface

5.1.5 Total Solar Radiation on an Inclined/Tilted Surface

The solar radiation energy incident on the collector surface which is inclined at an angle of β to the horizontal, defined in terms of the global radiation (G_r), the diffuse radiation (D_r), the beam radiation factor (R_b) and the ground reflectivity factor (ρ) for any inclined surface estimated using the following relation:[24]

$$I_T = I_b R_b + R_d I_d + \rho R_r (I_b + I_d) \ldots\ldots\ldots 4.6$$

Diffuse radiation conversion factor (R_d)

$$R_d = \frac{1 + \cos\beta}{2} \ldots\ldots\ldots 4.6a$$

Reflective radiation conversion factor (R_r)

$$R_r = \frac{1 - \cos\beta}{2} \ldots\ldots\ldots 4.6a$$

Slope (β): This is the angle between the plane surface under consideration and the horizontal surface (tangential plane at observer) and Its numerical value is considered positive for slope toward the south and negative for slope toward the north.

Beam radiation conversion factor (R_b)

$$R_b = \frac{\cos\theta_i}{\cos\theta_Z} \ldots\ldots\ldots 4.6a$$

Angle of incidence ($\boldsymbol{\theta_i}$): The angle made between normal to the inclined surface and the solar beam radiation falling on the inclined surface.

$$\boldsymbol{\cos\theta_i = (\cos\emptyset\cos\beta + \sin\emptyset\sin\beta\cos\gamma)\cos\delta\cos\omega + \cos\delta\sin\omega\sin\beta\sin\gamma + (\sin\emptyset\cos\beta - \cos\emptyset\sin\beta\cos\gamma)}$$

Zenith ($\boldsymbol{\theta_Z}$): The angle between Sun's rays and the line perpendicular to a horizontal plane.

$$\cos\theta_Z = \cos\delta\cos\emptyset\cos\overline{\omega} + \sin\delta\sin\emptyset \ldots\ldots\ldots\ldots\ldots\ldots\ldots\ldots\ldots 4.6d$$

Surface azimuth angle (γ): The angle made between the line due south and the projection of normal to the inclined surface on the horizontal plane (tangential plane at observer on the surface of the Earth. Since the desired collector is Sloped towards the south γ is zero.

It's the amount of solar energy converted in to heat at a unit time, considering the without considering dust effect and shading effect on the desired collector surface is given by:

$$\dot{q}_{ab} = \alpha\tau I_T(t) \ldots\ldots\ldots\ldots\ldots\ldots\ldots\ldots\ldots\ldots\ldots\ldots\ldots\ldots\ldots\ldots\ldots\ldots\ldots\ldots 4.7$$

5.2 Ambient Temperature Hourly Variation

The ambient temperatures hourly variation estimated by De Wit et al. (1978) from the daily maximum and daily minimum temperatures using a truncated cosine wave by subroutine that divides the day into two segments from sunrise to 14:00hr and from 14:00hr to sunrise of the next day. The method assumes T_{max}at 14:00hr and T_{min} at sunrise, and the intervening temperatures are calculated from the following equations for the mentioned segments[33].

5.2.1 Ambient Temperature Hourly Variation for daylight hours

For the first segment hsr $\leq h \leq 14hr$

$$T(t) = \frac{(T_{max} + T_{min})}{2} - \frac{(T_{max} - T_{min})}{2}(\cos(\frac{\pi(h - hsr)}{14 - hsr}) \ldots\ldots\ldots\ldots\ldots\ldots\ldots\ldots 4.8a$$

Where

- T(t) is the temperature at any hour of the day or night period.
- h time of the day in hour
- hsr sunrise hour in hour
- h' is constants used to join the equations for $h < hsr, h' = h + 10$ and $h' = 14$ for $h > 14{:}00h$

5.2.1 Ambient Temperature Hourly Variation for Night hours

For the second segments $0 \leq h \leq$ hsr and $14{:}00 \leq$ h $\leq 24{:}00$hr

$$T(hr) = \frac{(T_{max} + T_{min})}{2} + \frac{(T_{max} - T_{min})}{2}(COS(\frac{\pi h'}{10 + hsr}) \ldots\ldots\ldots\ldots\ldots\ldots\ldots\ldots 4.8b$$

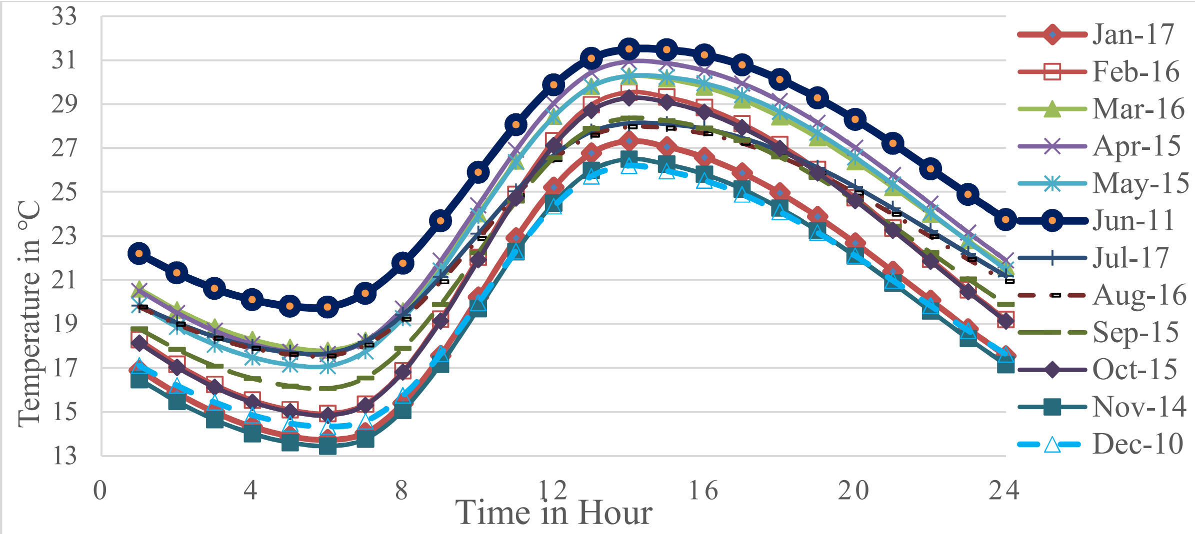

Figure 5. 7 Adama Ambient Temperature Hourly Variation

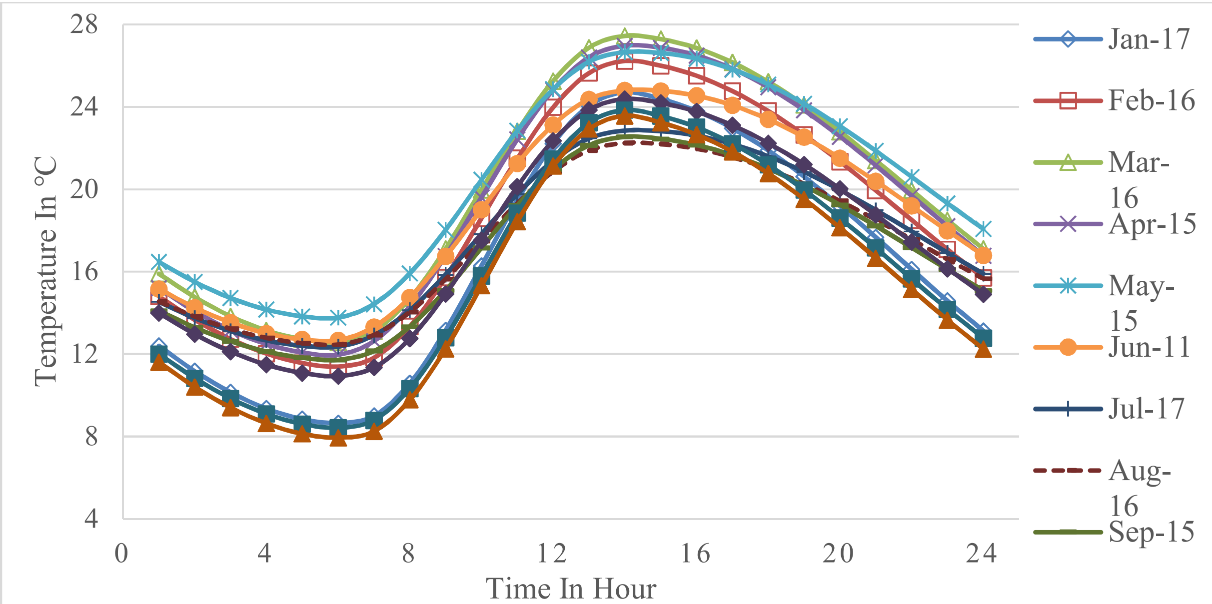

Figure 5. 8 Addis Ababa Hourly Temperature Variation

5.3 Total Solar Energy Gain

The monthly average hourly solar energy collected per square metre and hourly ambient temperature variations for Addis Ababa and Adama locations are plotted by using metrological season for representative days of the months. In both location the solar energy available for each month of Spring, Summer, Autumn and Winter season are compared to select better solar energy resource locations for dairy plant applications.

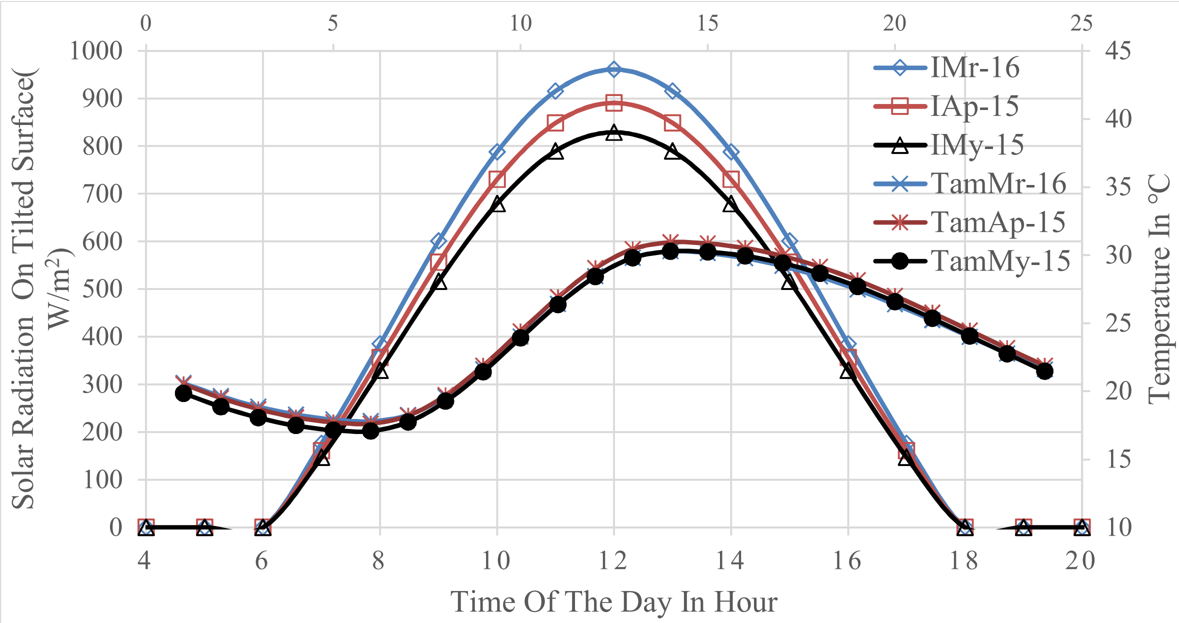

Figure 5. 9 Adama Spring season Monthly Average hourly solar radiations with corresponding ambient temperature

Based on the metrological season the maximum available solar energy in all three spring months are 960.93, 890.35 and 829.17W/m2 obtained from the mathematical manipulations of Adama solar data for March, April and May month respectively as plotted in figure 8.1. In the same manner from Addis Ababa solar data the Spring month maximum 939.13, 877.41 and 754.84W/m2 for March, April and May respectively obtain as plotted in figure 8.2. The maximum solar energy occurs for both locations in March month and minimum in May month. From these two graphs Adama spring season energy available is greater than Addis Ababa spring season solar energy available.

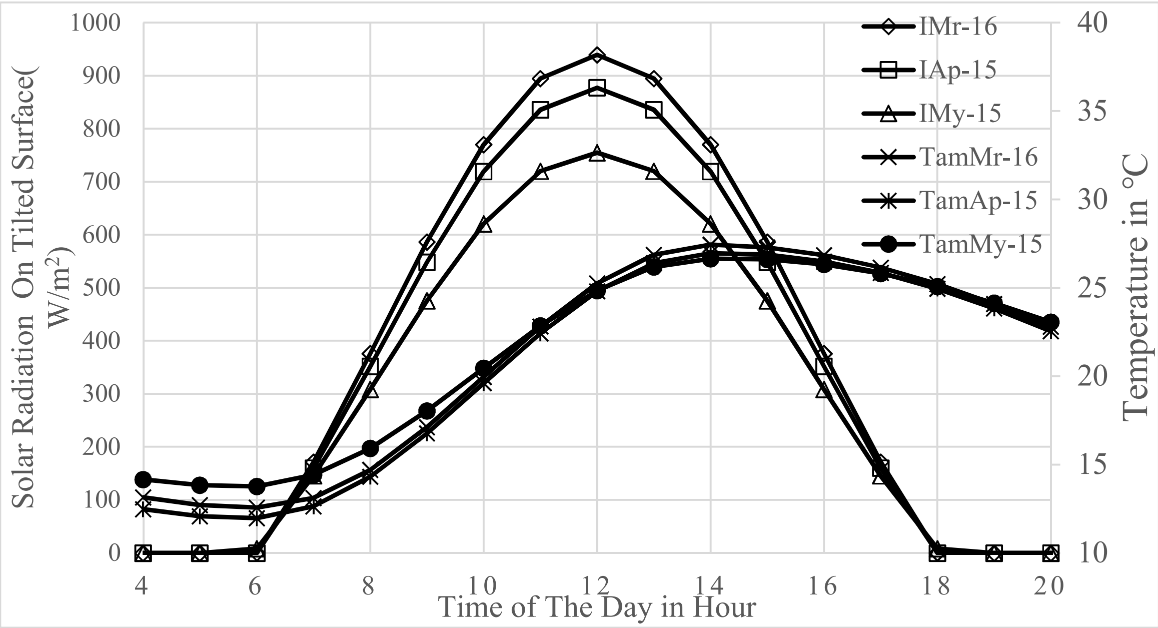

Figure 5. 10 Addis Ababa Spring season Monthly Average hourly solar radiations with corresponding ambient temperature

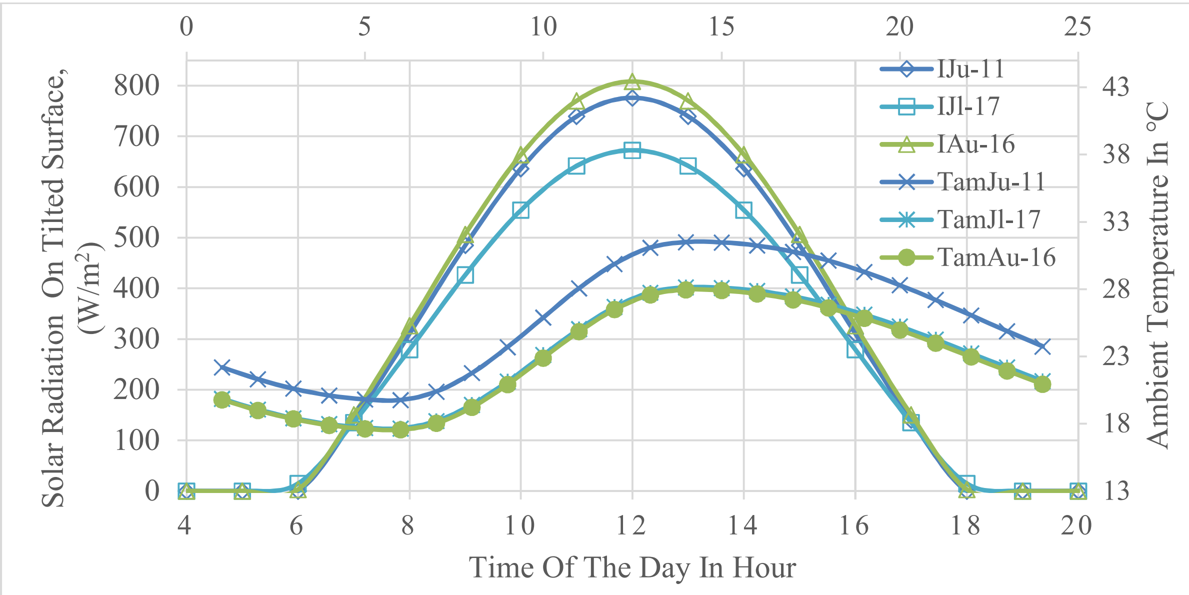

Figure 5. 11 Adama Summer season Monthly Average hourly solar radiations with corresponding ambient temperature

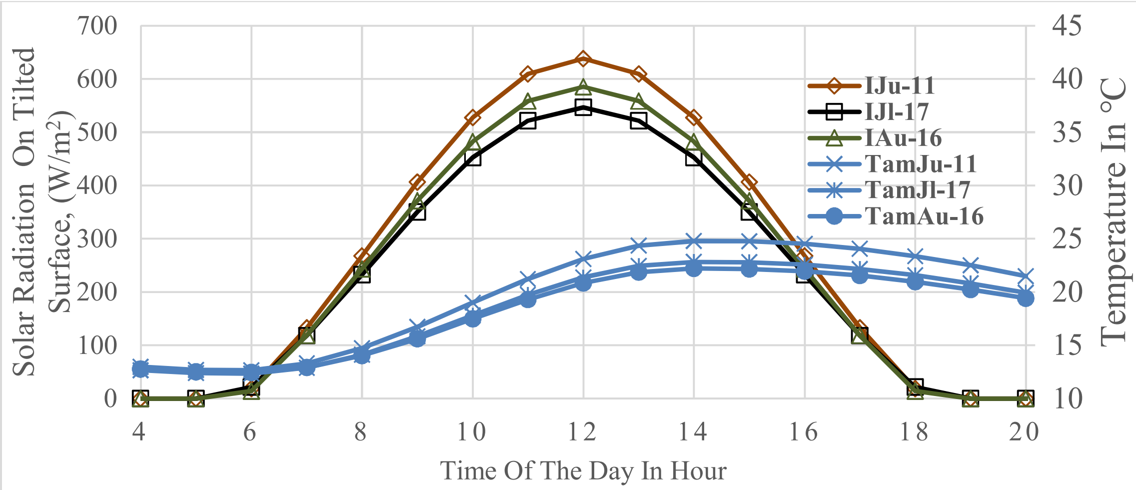

Figure 5. 12 Addis Ababa Summer season Monthly Average hourly solar radiations with corresponding ambient temperature

In summer season the maximum and minimum solar energy occurs in August and July month at Adama and Addis Ababa summer season the maximum occurs in June and minimum in July.

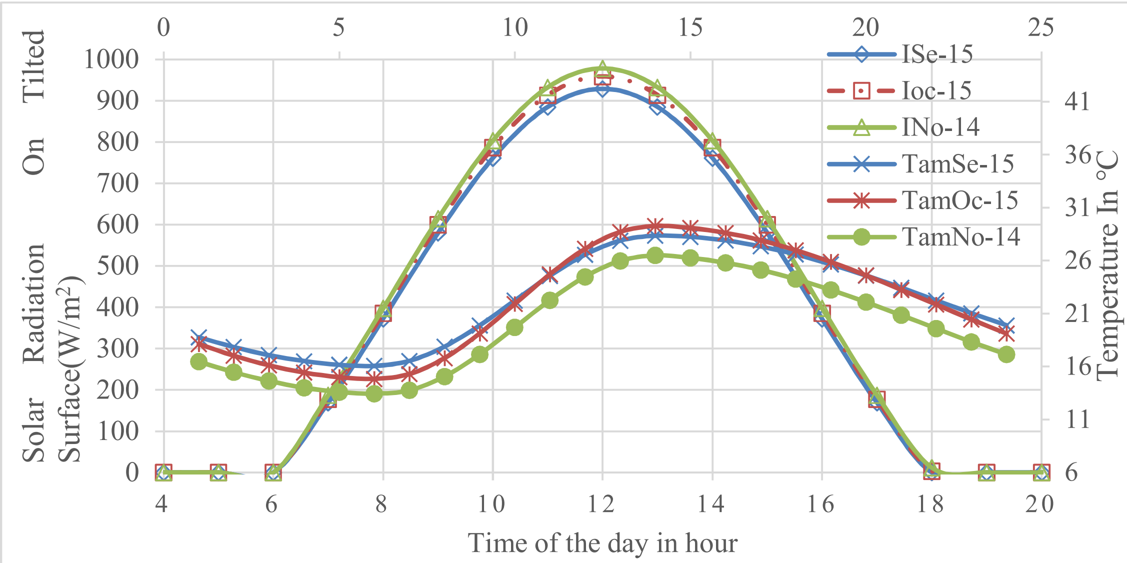

Figure 5. 13 Adama Autumn Season Monthly Hourly Solar Radiations with Corresponding Ambient Temperature

In Adama and Addis Ababa Autumn season the maximum energy gained in November but with different numerical value as shown in above and below figure respectively and the minimum in

September.

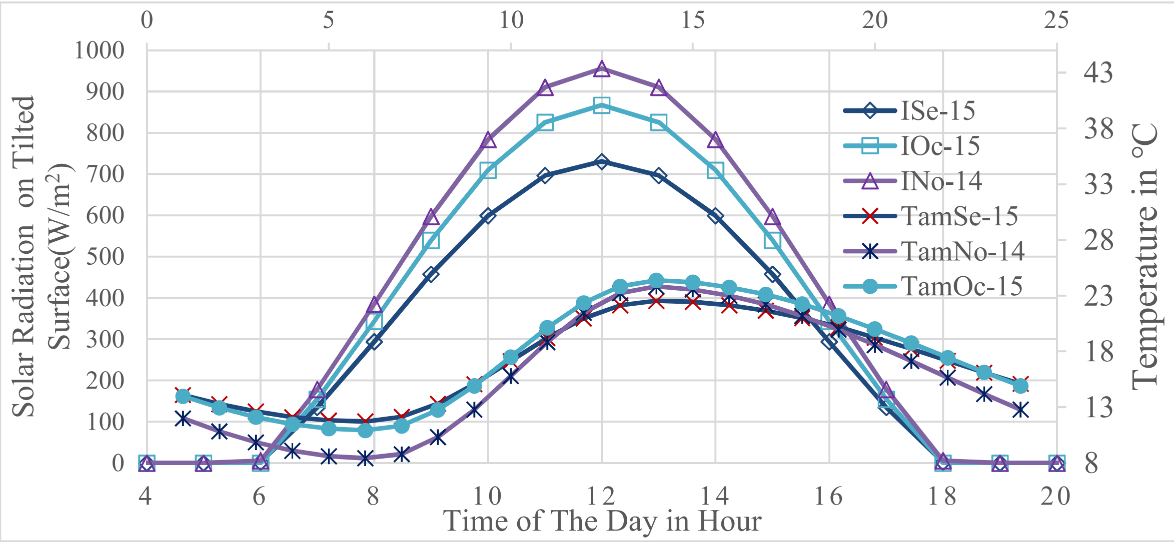

Figure 5. 14 Addis Ababa Autumn season Monthly Average hourly solar radiations with corresponding ambient temperature

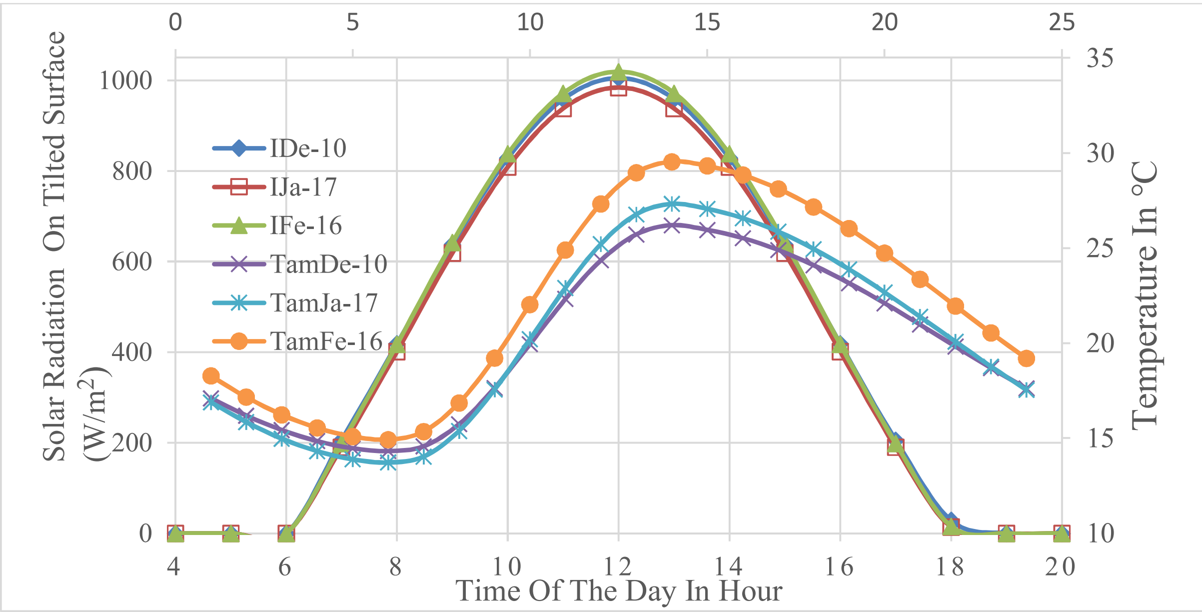

Figure 5. 15 Winter Season Monthly Average Hourly Solar Radiations with Corresponding Ambient Temperature

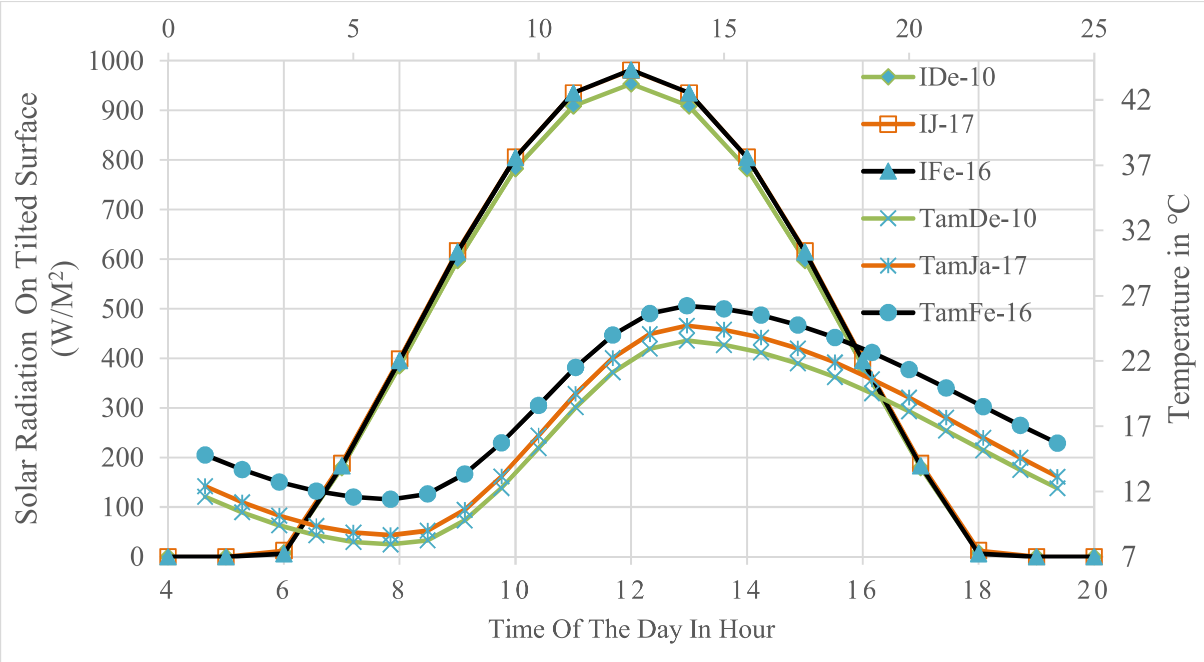

Figure 5. 16 Addis Ababa Winter season Monthly Average hourly solar radiations with corresponding ambient temperature

CHAPTER SIX

PHOTOVOLTAIC-THERMAL COLLECTOR PERFORMANCE PARAMETERS

Solar Radiation required for any system design calculation is the solar radiation energy incident on the collector surface which is inclined at any angle to the horizontal, that defined in terms of the global radiation, diffuse, beam radiation factor and the ground reflectivity factors are determined by material properties.

6.1 Optical modelling

6.1.1 Reflection of The Glass Cover

For any smooth surfaces, the Fresnel expressions used to calculate the reflection of un-polarized radiation on passing from medium one with a refractive index one to medium two with a refractive index two by using Fresnel formulas:

$$\tau_r = \frac{1-r}{1+r} \quad \text{...6. 1}$$

$$r = \frac{1}{2}\left[\frac{\sin 2\,(\theta_2-\theta_1)}{\sin 2\,(\theta_2-\theta_1)} + \frac{\tan 2\ (\theta_2-\theta_1)}{\tan 2\ (\theta_2-\theta_1)}\right] \quad \text{...6. 2}$$

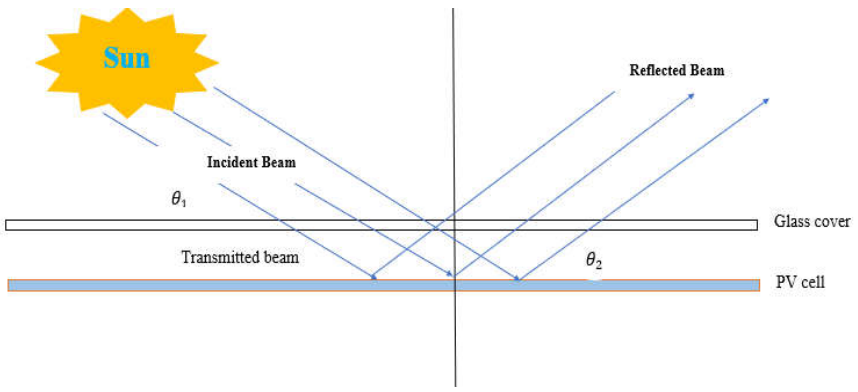

Figure 6. 1 Simple diagram for Reflection of solar ray through the medium

Where r is the glass reflection coefficient, θ_1 is angle of incidence, θ_2 is the refraction angle

As shown in figure 6.2 the transmissivity of the glass decreases as the angle of incidence increase, finally transmissivity become zero when the beam radiation is perpendicular to the collector surface.

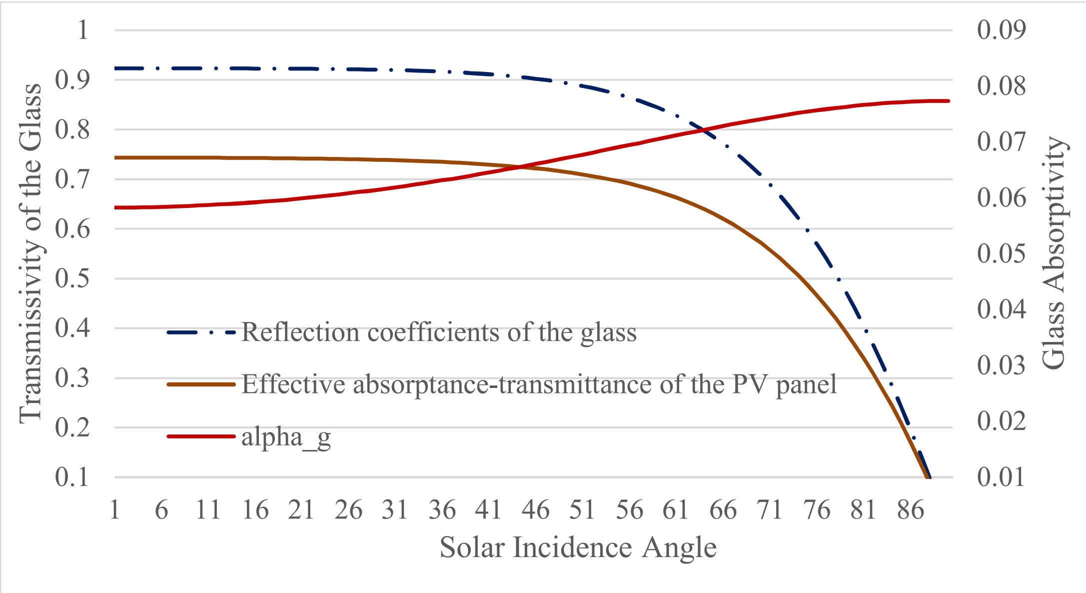

Figure 6. 2 Optical properties of glass cover versus Incidence angle

6.1.2 Absorption of The Glass Cover

The absorption of radiation in a partially transparent medium described by Bouguer’s law, which is based on the assumption that the absorbed radiation is proportional to the local intensity in the medium and the distance the radiation has travelled in the medium as shown in the following equation:

Where ℵ the extinction coefficient of the glass , v_n the refraction index of the glass

$$\boldsymbol{\alpha_g = 1 - \tau_g} \quad \text{……6. 3}$$

$$\boldsymbol{\tau_g = e^{\frac{-\aleph\delta_g}{\cos\theta_2}}} \quad \text{……6. 4}$$

$$\boldsymbol{\theta_2} = \frac{\boldsymbol{sin\theta_1}}{\boldsymbol{v_n}} \quad \text{………}6.5$$

6.1.3 Optical properties of cover systems

The transmittance, reflectance and absorptance of a single cover, allowing for both reflection and absorption losses are plotted as with the refraction angle, θ_2.

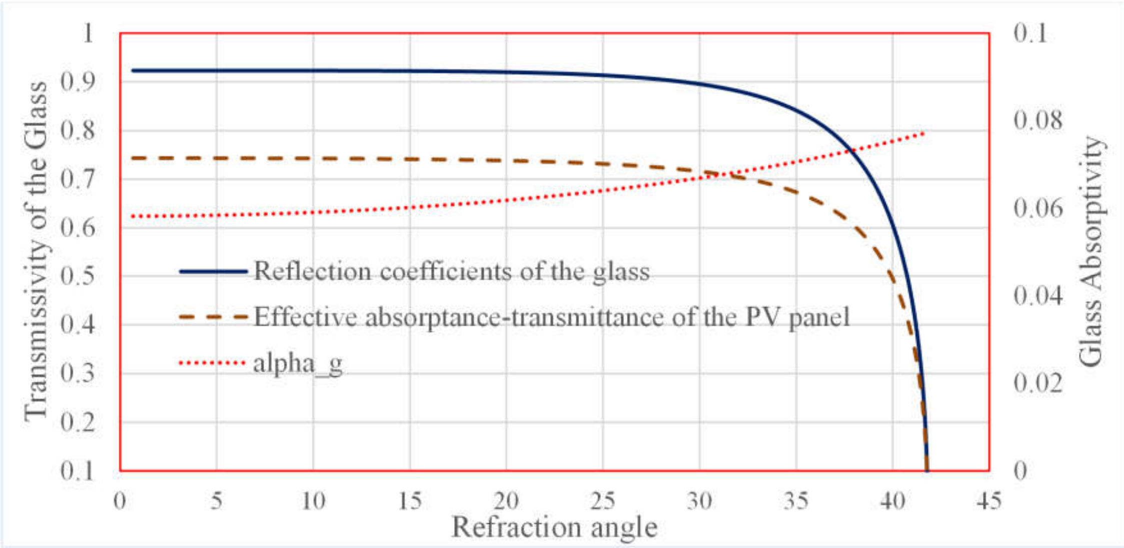

Figure 5. 17 Optical properties of glass cover versus Refraction angle

6.1.4 Equivalent angles of incidence for diffuse and ground-reflected radiation

The preceding analysis applies only to the beam component of solar radiation. Radiation incident on a collector also consists of scattered solar radiation from the sky and reflected solar radiation from the ground. The calculation simplified by defining an equivalent angle for beam radiation that gives the same transmittance as for diffuse and ground-reflected radiation. If the diffuse radiation from the sky and the radiation reflected from the ground are both isotropic, then the transmittance of the glazing systems found by integrating the beam transmittance over the appropriate incidence angles.

6.1.5 Transmittance-Absorptance product

Some of the radiation passing through the cover system reflected back to the cover system while the remainder is absorbed at the plate. In turn, the reflected radiation from the plate partially reflected at the cover system and back to the plate. It assumed that the reflection from the absorber plate is diffuse and unpolarized as shown on above figure.

6.2 PV-T Collector Heat loss and Efficiency Factor

The heat losses from any solar systems take the three modes of heat transfer: radiation, convection and conduction.

The **conduction** heat losses occur from sides and the back of the collector plate.

The **convection** heat losses take place from the absorber plate to the glazing cover, which reduced by evacuating the space between the absorber plate and the glazing cover and by optimizing the gap between them.

The **radiation** losses occur from the absorber plate due to the plate temperature. The heat losses from the transparent cover to the ambient air are due to radiate and convective exchanges, which affected by the wind velocity, ground, and surrounding condition and by long wave radiation from the sky. They can be considerably reduced by selective black coatings which have high solar absorptivity and low long wave emissivity.

6.2.1 PV-T Collector Overall Heat Loss

The overall heat loss is the amount of solar energy dissipated through photovoltaic-thermal collector in the form of heat by radiation, convection and conduction mode to the environment in top side, bottom and edge side of the collector.

6.2.2 Top Heat Loss coefficient

The conductive heat transfer coefficient between PV cell and absorber plate

$$h_{PV,abs} = (\frac{\delta_{EVA}}{k_{EVA}} + \frac{\delta_{Tedlar}}{k_{Tedlar}} + \frac{\delta_{Glue}}{k_{Glue}})^{-1} \quad \ldots 6.1$$

Finally, the net heat transfer coefficient on the top side of the photovoltaic-thermal collector by radiation and convection:

$$h_1 = h_{1c} + h_{1r} \quad and \quad h_2 = h_{2conv} + h_{2rad} \quad \ldots 6.2$$

The overall top loss coefficient by conduction, convection and radiation:

$$U_{top} = (\frac{1}{h_1} + \frac{1}{h_2} + \frac{1}{h_{PV,abs}})^{-1} \quad \ldots 6.3$$

6.2.3 Sky Temperature

In the solar energy system design the temperature of sky may be calculated from the ambient air temperature as shown in equation 5.8.

$$T_{sky} = T_{am} - 6 \quad \ldots 6.4$$

6.2.4 Radiated Heat Transfer Coefficient

a) Radiation heat transfer coefficient From the PV cell to the glass cover

$$h_{1r} = \varepsilon_{eff}\sigma \left\{ \frac{(T_{pV}+273)^4 - (T_g+273)^4}{T_{pV} - T_g} \right\} \quad \ldots 6.5$$

$$\varepsilon_{eff} = \left(\frac{1}{\varepsilon_p} + \frac{1}{\varepsilon_g} - 1\right)^{-1} \quad \ldots 6.6$$

b) Radiation heat transfer coefficient From the Glazing Cover to the ambient

$$h_{2r} = \varepsilon_g\sigma \left\{ \frac{(T_g+273)^4 - (T_{sky}+273)^4}{T_g - T_{am}} \right\} \quad \ldots 6.7$$

6.2.5 Convection Heat Loss Coefficient

The heat transfer coefficients to the ambient synchronize free and forced convection at specified wind speed.

$$h_{2c} = h_{wind} = 5.7 + 3.8V \quad \ldots\ldots 6.8$$

And also, the natural convection heat loss coefficient between glass cover and PV cell will be [24]calculate:

a) Heat transfer coefficient from PV cell to the glass cover

$$h_{1conv} = \frac{N_u k_{air}}{L} \quad \ldots\ldots 6.9$$

$$R_a = \frac{g\beta_V \Delta T L^3}{v\alpha} \quad \ldots\ldots 6.10$$

$$P_r = \frac{v}{\alpha} \quad \ldots\ldots 6.11$$

$$N_u = 1 + 1.44\left[1 - \frac{1708\, sin(1.8\beta)^{1.6}}{R_a \cos\beta}\right]\left[1 - \frac{1708}{R_a \cos\beta}\right]^* + \left[\left(\frac{R_a \cos\beta}{5830}\right)^{1/3} - 1\right]^* \quad \ldots\ldots 6.12$$

- "*" exponent means only the positive value of the term in square bracket is to be considered.
- Zero used for negative values.

6.2.7 Back and edge heat loss

The energy loss through the edge and back of the collector is the result of the conduction through the back insulation and the convection and radiation heat transfer from the back of the collector to the ambient.

Side loss is not included in simulation for one dimensional heat analysis because the is assumed as well insulated in the edge side/ adiabatic/, but the side loss coefficient is calculated by equation 5.17.

$$U_s = \frac{pd_e}{A_C}\frac{k_i}{\delta_e} \quad \ldots\ldots 6.13$$

6.2.8 Overall heat loss coefficient

Finally, the total heat loss from the solar collector found iteratively for average solar insolation by using steady state equations derived by energy balance on the layers of the PV-T collector.

$$U_L = U_t + U_b + U_e \ldots\ldots\ldots\ldots 6.14$$

The edge loss almost negligible, but its numerical value calculated and used in the iterations to obtain the over all heat loss coefficient plotted in the following figure.

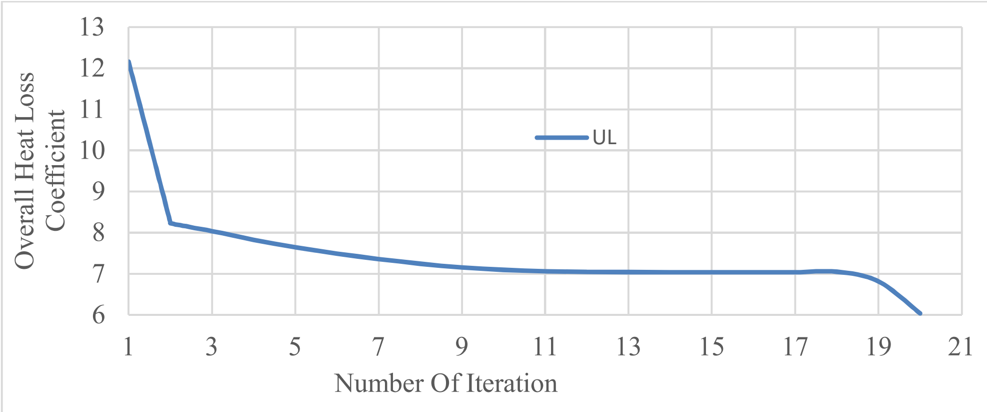

Figure 6. 3 PV-T Collector Overall heat loss coefficient

The absorber plate immerged under PV panel that is a complicated function of temperature distribution of plate, bond conductivity, heat transfer inside of tubes with the following different geometric configuration.

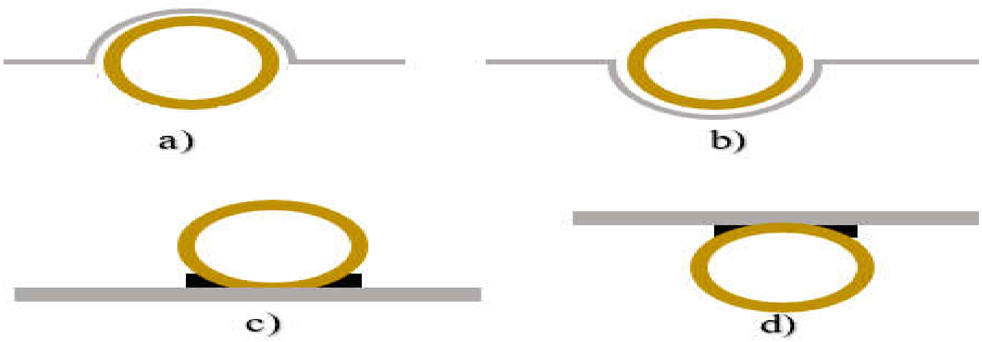

Figure 6. 4 Absorber plate and tube bonding alternative configurations

These factors determine the absorber plate temperature and the heat loss, the collector efficiency factor and the heat removal factor introduce in the system at all. The figure 5.5d configuration is the simplest and easy to interprets the properties between the sheet plate and tubes, simple to manufacture. The most common absorber plate in this technology are copper, aluminium and stainless steel.

6.2.9 Collector Efficiency Factor

The region between the centre line separating the tubes and the tube bond base considered as a fin. The absorber sheet has a thickness of δ_P. Because the sheet material is a good conductor, the temperature gradient through the thickness of sheet is negligible. The quantity of heat transferred through the fin is parameterized by **fin-efficiency factor**. Therefore, the rate of heat conducted toward the tube by conduction due to fin per unit length written as:

$$\boldsymbol{F} = \frac{tanh\frac{m(W-D_o)}{2}}{\frac{m(W-D_o)}{2}} \quad \ldots 6.15$$

$$\boldsymbol{m^2} = \frac{U_L}{\delta_P k_p + \delta_{pv} k_{pv}} \quad \ldots 6.16$$

Where W is the tube pitch (m); b is the bond breadth (m); and L_t is the length of tube, which is also known as a “riser” (m).

The flat plate collector–efficiency factor F' defined as the ratio of the actual rate of useful heat collection to the rate of useful heat collection when the collector’s absorbing plate is at the local fluid temperature.

The following assumptions made to determineF':

- The incident solar radiation is absorbed only by the absorber plate
- The bottom surface of the absorber plate and tubes are perfectly insulated
- The heat loss occurs only from the top surface of the plate
- The tubes are brazed onto the plate as shown in Figure below
- The bond has thermal conductivity, which also accounts for the effects of a poor joint
- The thermal inertia effect neglected for steady-state conditions.

Therefore, collector-efficiency factor equation given by:

$$F' = \frac{\frac{1}{U_L}}{W\left[\frac{1}{U_L[(W-b)F+b]} + \frac{1}{\left(\frac{bk_b}{\delta_b}\right)} + \frac{1}{\pi A_{mw}\, {k_t}/{\delta_t}} + \frac{1}{\pi D_i h_s} + \frac{1}{\pi D_i h_f}\right]} \quad or$$

$$\boldsymbol{F' = \{\frac{1}{F_t} + \frac{U_L}{h_{gp}} + (U_L W)/(\pi D_O h_t)\}} \quad \ldots\ldots 6.17$$

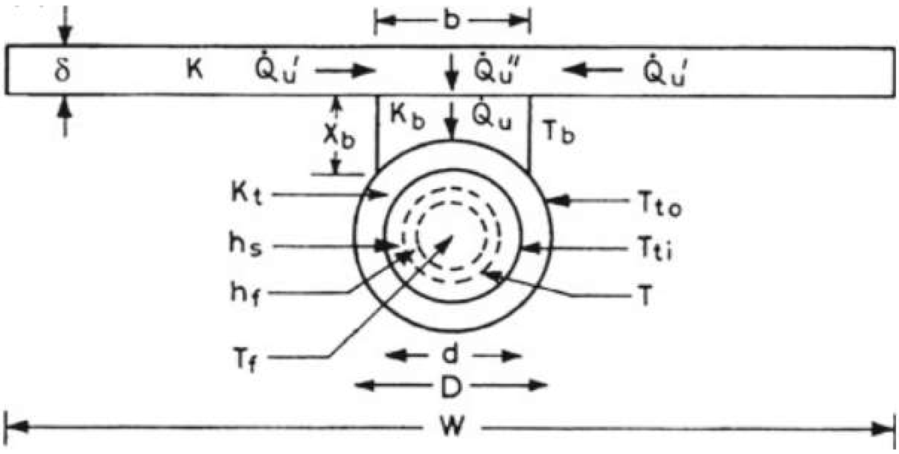

Figure 5. 18 Schematic representation of section through finned tube.

a) Collector Heat Removal Factor

The flat-plate heat removal factor (F_R) defined as the ratio of the rate actual useful energy gain to the rate of useful energy gain if the entire collector were at the fluid-inlet temperature in a forced circulation mode. Mathematically expressed as:

$$\boldsymbol{F_R = \frac{\dot{m}c}{A_c U_L}\left(1 - exp\left(-\frac{A_c U_L F'}{\dot{m}c}\right)\right)} \quad \ldots\ldots 6.18$$

$$\boldsymbol{F_R = \frac{\dot{Q}_u}{A_c(\dot{q}_{ab} - U_L(T_{fi} - T_{am}))}} \quad \ldots\ldots 6.19$$

b) Collector flow factor

It is the ratio of collector heat removal to collector efficiency factor.

$$F_t = \left(1 - \frac{D_O}{W}\right) F + \frac{D_O}{W} \quad \text{......6. 20}$$

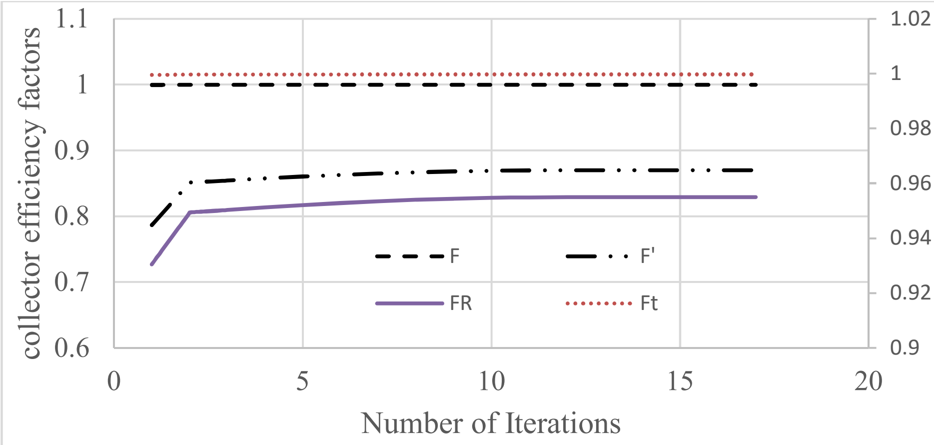

Figure 6. 5 Collector Efficiency Factors

6.3 The Electrical Performance Effect

As mentioned in the literature review the efficiency of uncovered PV-T collector commonly greater than a PV laminate collector. However, for a covered PV-T collector, the electrical efficiency reduced due to reflection at the top cover and the high temperatures to which the PV exposed depending on the solar fraction of the system.

The thermal shock may happen after a period of stagnation, which the PV-T collector switched and cold-water flows through the very hot collector. Thermal shock leads to the formation of steam and sudden and non-uniform thermal contraction of the absorber.

6.4 Thermal Performance effect

The Shading of the absorber plate by the sidewalls of the collector increases the collector spacing and decreases the electrical energy. The shading effect is high in the early morning and late evening times and has three percent solar absorption effect on the collector.

In the cause of heat extraction from the desired thermal systems, the extraction fails leads to stagnation which occurs due to pump failure or the thermal storage capacity exceeded. In that cause, the absorber releases the absorbed heat through convection and radiation to the environmental. Whereas for an unglazed PV-T this phenomenon leads to normal PV-temperatures of up to 80°C [11,14] for glazed PV-T collectors much higher temperatures may be found. Such high temperatures are very demanding for most encapsulation techniques, including the commonly used EVA, and specific attention should take to prevent delamination or Yellowing of the encapsulant. The same is done for plastic superstrare materials.

6.5 Design parameter effects

6.5.1 Number glass covers

As the number of tubes increases, the tube-to-tube spacing decreases and the collector heat removal factor increases. Thus, the instantaneous efficiency improves with the increase of the number of tubes discussed in the numerical calculation in the results and discuss with good improvement decreases and the optimum number of tubes for the collector.

6.5.2 Collector tilt angle

Collector tilt angle is the angle between the collector and the local horizontal which is approximately latitude that tilted at some angle. The optimum inclination angle of solar collector for better energy gain achieved by whether manually or automatically by tracking the sun positions in the sky. For flat plate solar collector in the northern hemisphere facing due to south is latitude plus 15 degree in winter month and latitude minus 15 degree in summer month when the collector operates under adverse conditions (due to lower ambient temperature) and load is greatest**.**

Liu and Jordan have suggested that the collector in the northern hemisphere, sloped towards the equator, the equation for beam radiation conversion factor (Rb) is given as discussed previously **[2,3].**

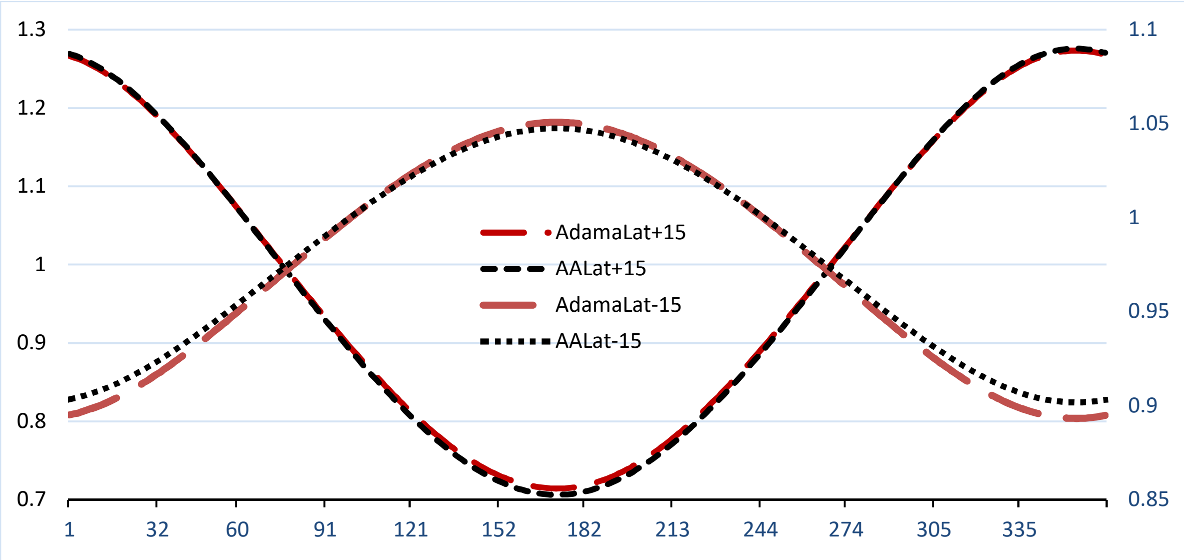

Figure 6. 6 Adama and Addis Ababa Beam radiation conversion factor

6.5.3 Collector Azimuth angle

The azimuth angle is the angle the collector faces relative to south. The maximum performance of the flat plate collector occurred at azimuth of zero degree. [2]

CHAPTER SEVEN

THERMAL STORAGE TANK DESIGN

The most common technique to heat a water, increasing its temperature, then storing the heat as internal energy within the desired material without phase change is known as **sensible heat storage** which is directly proportional to specific heat capacity, mass of the water and change in temperature.

7.1Thermal Storage Tank

The main function of thermal storage tank is to provide hot water at some adequate temperature which realize the desired thermal energy, If the stratification is maintained in the storage by avoiding the mixing of the cold and hot water.

7.2 Storage Tank Size and Storing Capacity

Depend upon the amount energy planned to store in the tank become big or small. The height to diameter ratio (aspect ratio) of the storage tank is no specified in know mathematical relations, but the diameter always assumed to found the height of the storage tank from the desired volume assigned to hold by tank.

$$V_S = \frac{\pi H D^2}{4} \quad \text{……6. 6}$$

Assume $H = 2D_o$, for good thermal startifications.

$$\mathrm{V_S} = \frac{\pi * 2 * \mathrm{D}^3}{4} = 4.2\mathrm{m}^3,\ \ \mathrm{D} = 1.388\mathrm{m}, \mathrm{H} = 2\mathrm{D} = 2.776\mathrm{m}\text{ , which is the best option size}$$

7.3 Storage Tank Insulation Thickness Determination

The heat dissipations through storage tank surface have great effect on the economic utilization of the storage and the storage insulation determined by serious design considerations as one of the storage tank design. The insulation thickness is taken as utilizable parameter and then determined by considering the economic benefits between the cost of the added insulation and the benefit gained from the saved energy or by calculating the insulation thickness is as follows:

The overall heat transfer coefficient U across the storage tank is assumed first. Then, the thickness of the insulation is determined. The determination of the required insulation thickness for some assumed value of the overall heat transfer coefficient U by neglecting the effect of the storage tank material on heat transfer, the temperature difference across the insulation is taken as ΔT. The rate of heat loss from the tank is then given by:

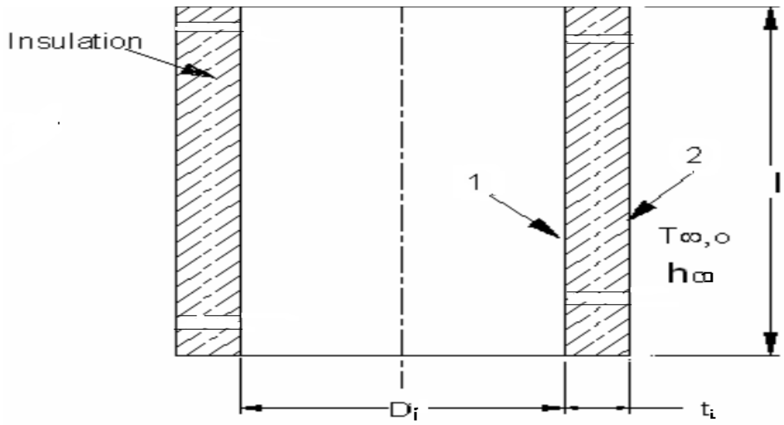

Figure 7. 1 Side insulation Cross-sectional view of storage tank

The heat transfer through the storage and rate of heat transfer from the inside of the storage to the environment are given by:

$$\dot{Q} = UA\Delta T \qquad 7.7$$

$$\dot{Q} = \frac{2\pi l(T_1 - T_{am})}{\frac{2}{D_o h_o} + \frac{1}{k_{ins} \ln D_o/D_i}} \qquad 7.8$$

Assuming the change in temperature in equation 6.2 and 6.3 the thickness calculated as:

$$\frac{2\pi l}{\frac{2}{D_o h_o} + \frac{1}{k_{ins} \ln D_o/D_i}} = U\pi D_o l \qquad 7.9$$

After rearrangement:

$$\mathrm{D_o} = \mathrm{D_i} \exp\left(\frac{2\mathrm{k}}{\mathrm{D_o}}\left(\frac{1}{\mathrm{U}} - \frac{1}{\mathrm{h_o}}\right)\right) \quad \text{7.10}$$

But, D_o the outer diameter of the storage tank is the summation of the plate thickness, inner diameter and insulation thickness that given by the following mathematical countenance:

$$\mathrm{D_o} = \mathrm{D_i} + 2\mathrm{t_{plate}} + 2\mathrm{t_{ins}} \quad \text{7.11}$$

7.4 Energy in Storage Tank

The transient heat energy balance in the storage tank for the model shown in the figure 7.1 is given by the following expression:

$$(\rho \mathrm{V_S C_P})_{\mathrm{w}} \frac{\mathrm{dT_S}}{\mathrm{dt}} = \dot{\mathrm{Q}}_{\mathrm{U}} - \dot{\mathrm{Q}}_{\mathrm{l}} - \dot{\mathrm{Q}}_{\mathrm{loss}} \quad \text{7.12}$$

$$\dot{\mathrm{Q}}_{\mathrm{U}} = \dot{\mathrm{m}}\mathrm{C_p}(\mathrm{T_{wo}} - \mathrm{T_{win}}) \quad \text{7.13}$$

$$\dot{\mathrm{Q}}_{\mathrm{loss}} = \mathrm{A_{Sh}}\mathrm{U_{sl}}(\mathrm{T_S} - \mathrm{T_{am}}) \quad \text{7.14}$$

$$\dot{\mathrm{Q}}_{\mathrm{l}} = (\rho \mathrm{c})_{\mathrm{w}}\mathrm{D_{total}}\mathrm{D_{fraction}}(\mathrm{T_S} - \mathrm{T_{ws}}) \quad \text{7.15}$$

Where

T_S The storage tank temperature
T_{ws} The supply water temperature
A_{Sh} Heat transfer area of the storage
U_{Ls} Storage Heat transfer coefficient
D_{fraction} Fraction of daily consumption
δ_{ins} the storage insulation thickness
δ_{ins} storage tank thickness
k_{ins} insulation thermal conductivity
$\dot{Q}_U$ Rate of useful heat
$\dot{\mathrm{Q}}_{\mathrm{loss}}$ Storage heat loss
$\dot{Q}_l$ supplied energy to the daily process
D_{total} water daily consumption
k_s Storage thermal conductivity
h_s storage tank heat loss coefficient

The total loss from the storage to the surrounding is given as:

$$U_{sl} = \frac{1}{R_{tot}} = \frac{\ln{}^{D_O}/_{D_i}}{2\pi k_{in}} + \frac{1}{\pi D_o H} \dots\dots\dots 7.16$$

Finally, the storage tank temperature at any time is calculated from the previous time value which is guessed given by the following equations:

$$T_{SO}^{P+1} = T_{SO}^{P} + \left(\frac{\Delta t}{\rho V_S C_P}\right)\{\dot{m}C_p(T_{wo}^{p} - T_{wi}^{p}) - A_{Sh}U_{sl}(T_{so}^{p} - T_{am}^{p}) - (\rho c)_w D_{total} D_{fraction}(T_{so}^{p} - T_{sw}^{p})\} \dots\dots\dots 7.17$$

7.5 Storage Tank Modelling

To model the temperature in the storage tank with diameter, D_s and height, H_s divided into number of layers (assume as10) used to store the thermal energy from the collector for transient analysis:

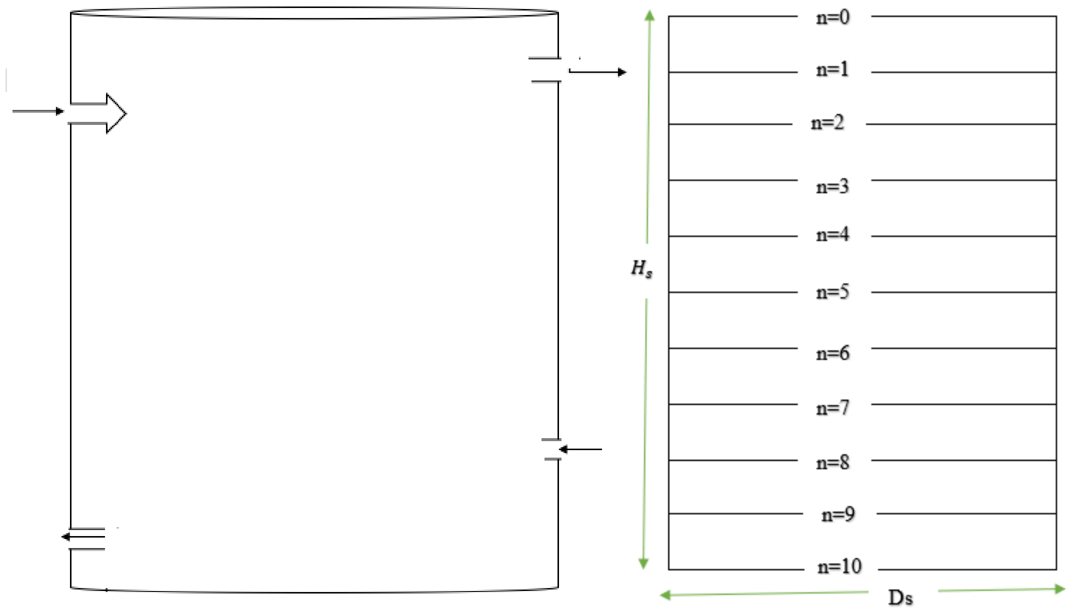

Figure 7. 2 Storage Tank Diagram with Discretised Node

Apply the finite difference method to each individual nodes of the storage tank to obtain the matrix equation to demonstrate the temperature distribution at every node inside the storage and the circumferential and longitudinal area of the storage tank calculated by the next equation respectively for vertical cylinder shown on figure 7.1.

$$A_{sd} = \frac{\pi D_s^2}{4} \quad \ldots 7.18$$

$$A_{sh} = \pi D_s H_s \quad \ldots 7.19$$

At top node (n=1) the energy balance equation to this layer is given by:

$$\frac{1}{10} V_s \rho_w C_w \frac{\partial T_1}{\partial t} = \dot{m}_w C_w (T_0 - T_1) + 10 \frac{k_w}{h_s} A_{sd} (T_2 - T_1) + h_{am-s} \left(A_{sd} + \frac{A_{sh}}{10}\right) (T_{am} - T_1) \ldots 7.20$$

for the time step (p) the storage temperature at interior node one is given as:

$$\frac{1}{10} V_s \rho_w C_w \left(\frac{T_1^{p+1} - T_1^p}{\Delta t}\right) = \dot{m}_w C_w ({T_0}^p - {T_1}^p) + 10 \frac{k_w}{h_s} A_{sd} ({T_2}^p - {T_1}^p) + h_{am-s} \left(A_{sd} + \frac{A_{sh}}{10}\right) ({T_{am}}^p - {T_1}^p) \ldots 7.21$$

By collecting some term in one side the equation become:

$${T_1}^{p+1} = \frac{10\Delta t}{V_s \rho_w C_w} \dot{m}_w C_w {T_0}^p + \left\{1 - \left(\dot{m}_w C_w + 10 \frac{k_w}{h_s} A_{sd} + h_{am-s} \left(A_{sd} + \frac{A_{sh}}{10}\right)\right) \frac{10\Delta t}{V_s \rho_w C_w}\right\} {T_1}^p + \frac{10\Delta t}{V_s \rho_w C_w} \left(10 \frac{k_w}{h_s} A_{sd} {T_2}^p\right) + h_{am-s} \left(A_{sd} + \frac{A_{sh}}{10}\right) \frac{10\Delta t}{V_s \rho_w C_w} {T_{am}}^p \ldots 7.22$$

$${T_1}^{p+1} = a_{11} {T_1}^p + a_{12} {T_2}^p + a_0 {T_0}^p + b_0 {T_{am}}^p \ldots 7.23$$

Where

- V_s volume of the storage tank
- $\dot{m}_w$ mass flow rate through the tube
- k_w thermal conductivity of water
- k_s thermal conductivity of storage
- C_w specific heat capacity of water
- C_s specific heat capacity of storage
- ρ_w density of water
- ρ_s density of storage tank material
- Δt time step
- p variable assigned for time step
- T Fluid temperature at any particular node
- T_{am} ambient temperature
- T_o PV-T collector fluid outlet temperature

At bottom node (n=10) the energy balance equation to this layer is given by:

$$\frac{1}{10}V_s\rho_sC_s\frac{\partial T_{10}}{\partial t} = \dot{m}_wC_s(T_9 - T_{10}) + 10\frac{k_s}{h_s}A_{sd}(T_9 - T_{10}) + h_{am-s}\left(A_{sd} + \frac{A_{sh}}{10}\right)(T_{am} - T_{10}) \quad 7.24$$

After some rearrangement the bottom node temperature at any time t is:

$$T_{10}{}^{p+1} = \frac{10\Delta t}{V_s\rho_sC_s}h_{am-s}\left(A_{sd} + \frac{A_{sh}}{10}\right)T_{am}{}^{p} + \left\{1 - \left(\dot{m}_wC_s + 10\frac{k_s}{h_s}A_{sd} + h_{am-s}\left(A_{sd} + \frac{A_{sh}}{10}\right)\right)\frac{10\Delta t}{V_s\rho_sC_s}\right\}T_{10}{}^{p} + \frac{10\Delta t}{V_s\rho_sC_s}\left(\dot{m}_wC_s + 10\frac{k_s}{h_s}A_{sd}\right)T_9{}^{p} \quad 7.25$$

$$T_{10}{}^{p+1} = a_{109}T_9{}^{p} + a_{1010}T_{10}{}^{p} + b_{10}T_{am}{}^{p} \quad 7.26$$

The energy balance for the interior 2 up to 9 calculated by assigning each layer by j:

$$\frac{1}{10}(V\rho C)_s\frac{\partial T_j}{\partial t} = \dot{m}_wC_s(T_{j-1} - T_j) + 10\frac{k_s}{h_s}A_{sd}(T_{j-1} - T_j) + 10\frac{k_w}{h_s}A_{sd}(T_{j-1} - T_j) + h_{am-s}\left(\frac{A_{sh}}{10}\right)(T_{am} - T_{10}) \quad 7.27$$

Finally, the matrix equations for interior node are:

$$T_j{}^{p+1} = \frac{10\Delta t}{V_s\rho_sC_s}h_{am-s}\left(\frac{A_{sh}}{10}\right)T_{am}{}^{p} + \left\{1 - \left(\dot{m}_wC_s + 10\frac{k_s}{h_s}A_{sd}\right)\frac{10\Delta t}{V_s\rho_sC_s}\right\}T_j{}^{p} + \frac{10\Delta t}{V_s\rho_sC_s}\left(\dot{m}_wC_s + 10\frac{k_s}{h_s}A_{sd}\right)T_{j-1}{}^{p} + \frac{10\Delta t}{V_s\rho_sC_s}\left(10\frac{k_w}{h_s}A_{sd}\right)T_{j+1}{}^{p} \quad 7.28$$

$$T_j{}^{p+1} = a_{jj-1}T_{j-1}{}^{p} + a_{jj}T_j{}^{p} + a_{jj+1}T_{j+1}{}^{p} + b_jT_{am}{}^{p} \quad 7.29$$

Therefor the all matrix equation for ten nodes arranged as:

$$T_1{}^{p+1} = a_{11}T_1{}^{p} + a_{12}T_2{}^{p} + a_0T_0{}^{p} + b_1T_{am}{}^{p} \quad 7.12\text{ a}$$

$$T_2{}^{p+1} = a_{21}T_1{}^{p} + a_{22}T_2{}^{p} + a_{23}T_3{}^{p} + b_2T_{am}{}^{p} \quad 7.12\text{ b}$$

$$T_3{}^{p+1} = a_{32}T_2{}^{p} + a_3T_3{}^{p} + a_{34}T_4{}^{p} + b_3T_{am}{}^{p} \quad 7.12\text{ c}$$

$$T_4{}^{p+1} = a_{43}T_3{}^{p} + a_{44}T_4{}^{p} + a_{45}T_5{}^{p} + b_4T_{am}{}^{p} \quad 7.12\text{ d}$$

$$T_5{}^{p+1} = a_{54}T_4{}^{p} + a_{55}T_5{}^{p} + a_{56}T_6{}^{p} + b_5T_{am}{}^{p} \quad 7.12\text{ e}$$

$$T_6{}^{p+1} = a_{65}T_5{}^p + a_{66}T_6{}^p + a_{67}T_7{}^p + b_6T_{am}{}^p \quad \ldots\ldots 7.12\text{ f}$$

$$T_7{}^{p+1} = a_{76}T_6{}^p + a_{77}T_7{}^p + a_{78}T_8{}^p + b_7T_{am}{}^p \quad \ldots\ldots 7.12\text{ g}$$

$$T_8{}^{p+1} = a_{87}T_7{}^p + a_{88}T_8{}^p + a_{89}T_9{}^p + b_8T_{am}{}^p \quad \ldots\ldots 7.12\text{ h}$$

$$T_9{}^{p+1} = a_{98}T_8{}^p + a_{99}T_9{}^p + a_{910}T_{10}{}^p + b_9T_{am}{}^p \quad \ldots\ldots 7.12\text{ i}$$

$$T_{10}{}^{p+1} = a_{109}T_9{}^p + a_{1010}T_{10}{}^p + b_{10}T_{am}{}^p \quad \ldots\ldots 7.12\text{ j}$$

General the equation 7.12(a-j) is written as a matrix for as shown equation 7.13 and used in steady state temperature distribution in the storage tank.

$$T_j^{P+1} = AT_j^P \quad \ldots\ldots 7.30$$

Where A is assigned for previous time temperature coefficient in matrix form.

CHAPTER EIGHT

MODELLING AND SIMULATION OF PV-T SYSTEM

The modelling of the solar energy system is grounded on two important conditions for the actual PV and PV-T for its equivalent circuit to show the net profit between these two collectors.

8.1 Modelling of PV Cell Collector

As the solar energy (solar radiation) strikes the solar panels the electron and proton start movement to made the paired p-n junction by living their place without back falling due to electric field produced in photovoltaic materials. This paired carries the photon current that proportional to the insolation which is called **Photocurrent** (electric current induced by the action of light) generated.

In solar cell modelling there are two important points used to define the electrical meaning in mathematical formulas. Those two important points are short circuit current and open circuit voltage. Short circuit current (I_{sc}) is the highest current that exist when there is no current fall through actual diode which implies the diode voltage (V_d) is zero and the open circuit voltage (V_{oc}) is the voltage when the leads left open. There is no voltage drop in the diode.

$$I_{Ph} = \left[I_{sc} + \beta_i\left(T_{pv} - T_{ref}\right)\right]\left(\frac{I_T}{1000}\right) \quad \text{8.1. 1}$$

Module reverse saturation current I_{rs}:

$$I_{rs} = \frac{I_{sc}}{\left[exp\left(\frac{qV_{OC}}{N_S kbT_{ref}}\right)\right]} \quad \text{8.1. 2}$$

Where,

I_{Ph} is the photo-current(A);
T_{ref} Refence temperature, 25°C,
T_{pv} cell operating temperature (K);
I_{sc} the short circuit current (A)?
I_{rs} reverse saturation current (A)
q electron charge ($1.6x10^{-19}C$)
V_{OC} open circuit voltage
N_s Number of cells connected in series
b Idealistic factor of the diode,
k Boltzmann's cons. ($1.3805x10^{-23}J/K$).

I_T Solar irradiation(w/m2)

β_i short-circuit current temperature coefficient

The module diode saturation current I_d varies with the cell temperature, which is given by:

$$I_d(T) = I_{rs}\left[\frac{T_{pv}}{T_{ref}}\right]^3 exp\left[\frac{qE_g}{bK}\left(\frac{1}{T_{pv}} - \frac{1}{T_{ref}}\right)\right] \ldots\ldots 8.1.3$$

$\boldsymbol{T_{ref}}$ is nominal temperature =298.15K; $\boldsymbol{E_{go}}$ is band gap energy of the semiconductor, =1.12Ev; the short circuit current, open circuit voltage and load current of the PV module as a function of temperature and insolation is given by the following mathematical relation.

The band energy gap of any material at any temperature[24] is given by:

$$E_g = E_{g,ref}\left(1 - c\left(T_{pv} - T_{ref}\right)\right) \ldots\ldots 8.1.4$$

Where

$$\mathrm{E_{g,ref}} = 1.12\mathrm{eV\ or\ } 1.794 * 10^{-19} \mathrm{\ and\ c} = 0.0002677 \mathrm{\ for\ silicon\ material}$$

$$I_{sc}(T, I_T) = I_{sc}(1 + \beta_i\left(T_{pv} - T_{ref}\right) * \frac{I_T}{I_{ref}} \ldots\ldots 8.1.5$$

$$V_{oc}(T, I_T) = \left(V_{oc} - \beta_V\left(T_{pv} - T_{ref}\right)\right) * \frac{I_T}{I_{ref}} \ldots\ldots 8.1.6$$

Finally, the current delivered as a load current *I* from the module connected in both series and parallel alternatives.

$$I = N_P I_{Ph} - N_P I_O\left[exp\left(\frac{V/_{N_S} + I^{R_S}/_{N_P}}{bV_t}\right) - 1\right] - I_{sh} \ldots\ldots 8.1.7$$

$$V_t = \frac{kT_{pv}}{q} \ldots\ldots 8.1.8$$

$$I_{sh} = \frac{VxN_P/_{N_S} + IxR_S}{R_{Sh}} \ldots\ldots 8.1.9$$

Here N_P number of PV modules connected in parallel; R_s is series resistance (Ω); $R_{sh}$is the shunt resistance (Ω), V diode thermal voltage (V).

The reverse saturation current I_O of a diode is constant under constant temperature and can be determined by displaying the open-circuit conditions as shown in figure below:

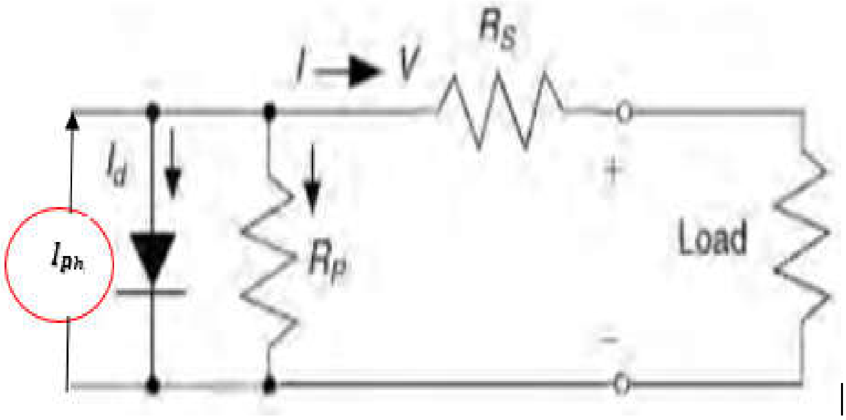

Figure 8. 1 General equivalent circuit for PV cell

8.1.1 PV Module Temperature with Insolation

The cell temperature at any ambient temperature[24] is calculated by using the normal operating Cell temperature (NOCT) which is give by PV module manufacturer at any ambient temperation and solar insolation as shown below:

$$T_{PV} = T_{am} + \left(\frac{I_T}{I_{T,NOCT}}\right)\left(\frac{U_{L,NOCT}}{U_L}\right)\left(T_{NOCT} - T_{am,NOCT}\right)\left(1 - \frac{\eta_{ref}}{\alpha\tau}\right) \ldots\ldots\ldots\ldots 8.1.10$$

The value of $\alpha\tau$ determined from the module propreties but using 0.9 without serious error and the ratio of $\frac{\eta_{ref}}{\alpha\tau}$ is very small compared to the unity so its removed from the equations (A.Q.Jakhrami et al).

$$T_{PV} = T_{am} + \left(\frac{I_T}{I_{T,NOCT}}\right)\left(\frac{9.5}{5.7+3.8V_w}\right)\left(T_{NOCT} - T_{am,NOCT}\right) \ldots\ldots\ldots\ldots 8.1.11$$

The wind speed assumed to be 1m/s then the module cell temperature can found by:

$$T_{PV} = T_{am} + \left(\frac{I_T}{I_{T,NOCT}}\right)(T_{NOCT} - T_{am,NOCT}) \ldots \ldots \ldots \ldots \ldots \ldots \ldots \ldots \ldots \ldots \ldots \ldots \ldots \ldots \ldots \ldots \ldots \ldots \ldots 8.1.12$$

Finally the PV module efficiency and PV-T collector efficiency as a function of their corresponding temperature found from the following expression:

$$\eta_{PV} = \eta_{ref}(1 - \beta_0(T_{PV} - T_{ref}) \ldots \ldots \ldots \ldots \ldots \ldots \ldots \ldots \ldots \ldots \ldots \ldots \ldots \ldots \ldots \ldots \ldots \ldots \ldots 8.1.13$$

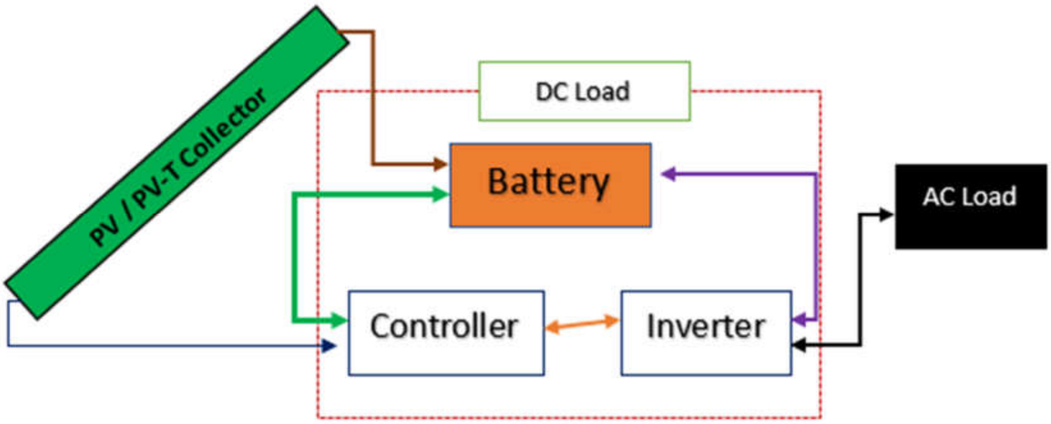

Figure 8. 2 Overall PV module with complete component assembly

8.2 Modelling of Flat Plate PV-T Solar Collectors

The component of flat plate PV-T solar collector are glass cover, PV module, and absorber plate for incident solar radiation, parallel tubes attached to the plates and edge and back insulation are modelling and analysis for this type of collector configuration is performed by setting some reasonable assumption to reduce the complexity of the decretive equations and the model thermal equation of PV-T system develops based on the following assumptions:

- The flow was fully developed in the tubes.
- The optical properties constant for desired materials
- The header covers/bent tube/ a small area of the collector and its effect on the temperature distribution on the absorber neglected.
- The incident irradiance (I), (V) the wind speeds and $T_{am}$the ambient temperature uniform boundary conditions at the surface of the PV-T collector.

- The fluid inlet temperature assumed to be constant (controlled by heat recovery) to identify the energy variations for that particular location's due ambient temperature and solar irradiance.
- Water flow-rate evenly distributed between the pipes, the thermal losses and mixing effects at the inlet and outlet manifolds are negligible.
- The temperature profile between two adjacent pipes is symmetrical, and the temperature has a maximum on the symmetry axis.
- The fluid temperature in the flow direction is assumed across the tube due to high velocity of the flowing fluid and the short tube length.
- After pasteurization and sterilization processes the working fluid having high temperature directly stored in the storage tank.
- One dimensional heat transfer modelling is used for steady state analysis to determine the required parameter and dimensions of the collector.
- And also, 1D heat transfer is assumed in simulation

Therefor the transient heat flow equations used to determine electrical and heat gain by simulating the heating system inputting climatic data and design parameters for selected particular area.

8.2.1 Marching Equation

The dynamic energy modelling for the desired collector is derived at each node which solved at 2D in the logic that the collector segmented along the flow direction (y-direction) and the set of equation developed by energy balance on each layer in Z -directions (Duffy and Beckman, 1991).

The main challenge in the two dimension al modelling the system become little bit complex and difficult to manage, without any considerable error the system can be modelled in one dimensional in the x-directions under the stated assumptions.

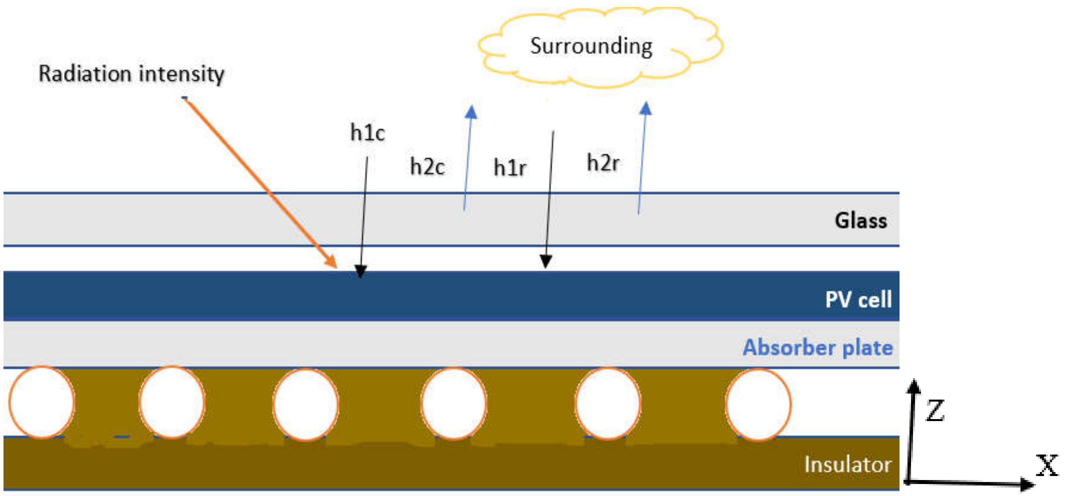

Figure 8. 3 One dimensional heat transfer coefficient for energy balance

The temperature distribution modelling is performed along x axis as shown in the 3D view ("numerical investigation and modelling of solar photovoltaic / thermal systems afroza nahar institute of graduate studies" 2017) of figure 7.4

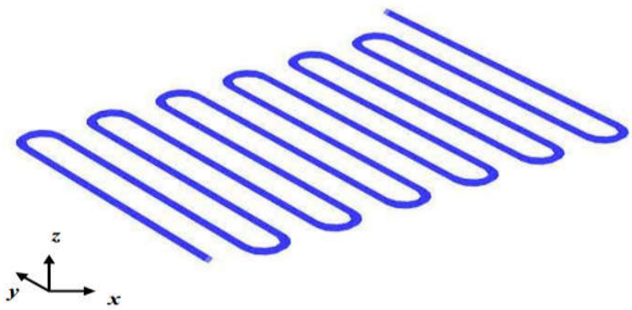

Figure 8. 4 Serpentine flow pipe 3D view

The thermal model based on the energy balance in the various layer of the PVT collector as discussed in chapter five will be modelled as follows:

8.2.1.1 Energy Balance on Glass cover

The amount of solar energy deliver to the glass cover is the summation of solar energy stored over a time, solar radiation absorbed by glass, internal and external solar energy loss from the glass cover is calculated as:

$$\delta_g \rho_g C_g \frac{\partial T_g}{\partial t} = \alpha_g I_T + \delta_g k_g \frac{\partial^2 T_g}{\partial x^2} + \delta_g k_g \frac{\partial^2 T_g}{\partial y^2} - \varepsilon_g \sigma\left(T_g^4 - T_{sky}^4\right) - h_{am}\left(T_g - T_{am}\right) + \sigma\left(\frac{\varepsilon_g \varepsilon_{PV}}{\varepsilon_g + \varepsilon_{PV} - \varepsilon_g \varepsilon_{PV}}\right)\left(T_{PV}^4 - T_g^4\right) + \frac{1}{R_{gap}}\left(T_{PV} - T_g\right) \quad \text{8.2. 1}$$

$$h_{am} = \sqrt[3]{h_w^3 + h_{free}^3} \quad \text{8.2.1 a}$$

The free stream convection on the surface is assumed to be zero and the only convection coefficient involves on the top surface of the glass cove is purely due to wind velocity.

$$R_{C,PV-P} = R_c = \frac{\delta_{eva}}{K_{eva}} + \frac{\delta_{glue}}{K_{glue}} + \frac{\delta_{PVF}}{K_{PVF}} \quad \text{8.2.1 b}$$

R_c the conduction thermal resistance between PV cell and absorber plate

$$\frac{1}{R_{gap}} = \frac{\delta_{eva}}{k_{eva}} + \frac{\delta_g}{k_g} + \frac{\delta_{PV}}{2k_{PV}} + \frac{\delta_g}{2k_g} + \frac{1}{h_{gap}} \quad \text{8.2.1 c}$$

$$h_{gap} = \frac{K_{air} Nu_{air}}{\delta_{air}} \quad \text{8.2.1 d}$$

$$\varepsilon_{eff} = \left(\frac{\varepsilon_g \varepsilon_{PV}}{\varepsilon_g + \varepsilon_{PV} - \varepsilon_g \varepsilon_{PV}}\right) \quad \text{8.2.1 e}$$

Nu_{air} is the Nusselt number that already defined in chapter 5.

$$\delta_g \rho_g C_{pg} \frac{\partial T_g}{\partial t} = \alpha_g I_T - \varepsilon_g \sigma\left(T_g^4 - T_{sky}^4\right) - h_{am}\left(T_g - T_{am}\right) + \sigma\left(\frac{\varepsilon_g \varepsilon_{PV}}{\varepsilon_g + \varepsilon_{PV} - \varepsilon_g \varepsilon_{PV}}\right)\left(T_{PV}^4 - T_g^4\right) + \frac{1}{R_{gap}}\left(T_{PV} - T_g\right) \quad \text{8.2. 1}$$

Or

$$\delta_g \rho_g C_{pg} \frac{\partial T_g}{\partial t} = \alpha_g I_T + h_w\left(T_{am} - T_g\right) + h_{r,g-sky}\left(T_{sky} - T_g\right) + h_{c,pv-g}\left(T_{pv} - T_g\right) + h_{r,pv-g}\left(T_{pv} - T_g\right) \quad \text{8.2. 2}$$

The discetized of the glass layers as afunction of time at (p+1) which is determined from the previous time value is given by:

$$T_g^{\,p+1} = T_g^{\,p} + \Delta t\{\alpha_g I_T - \varepsilon_g\sigma\left({T_g^4}^P - {T_{sky}^4}^P\right) - h_{am}\left(T_g^p - T_{am}^p\right) + \sigma\varepsilon_{eff}\left({T_{PV}^4}^P - {T^4}_g^P\right) + \frac{1}{R_{gap}}\left({T_{PV}}^P - {T_g}^P\right)\}/\delta_g\rho_g C_{pg} \;\ldots\ldots 8.2.3$$

Where the heat transfer coefficient $h_{r,g-sky}$, $h_{c,pv-g}$, $h_{r,pv-g}$ *and* h_w are discussed in chapter 5 from equation 5.9 up to 5.16 and p is the time step for the discretised equation.

$$T_g^{\,p+1} = \left\{1 - \frac{\Delta t}{mc_g}\left(\varepsilon_g + \varepsilon_{eff}\right)\sigma T_g^3 + h_{am} + \frac{1}{R_{gap}}\right\}T_g^{\,p} + \frac{\Delta t}{mc_g}\left\{\varepsilon_g\sigma T_{sky}^4 + h_{am}T_{am} + \left(\varepsilon_{eff}\sigma T_{PV}^3 + \frac{1}{R_{gap}}\right)T_{PV}^P\right\} \;\ldots\ldots 8.2.4$$

8.2.1.2 Energy Balance on PV cell energy balance

The net solar energy stored over time in PV cell is the total solar radiation pass through glass cover minus the amount of solar radiation converted into electrical energy and loss from the PV cell is calculated as:

$$\delta_{PV}\rho_{PV}C_{pPV}\frac{\partial T_{PV}}{\partial t} = (\tau\alpha)_{PV}I_T - Q_{el} + \delta_{PV}k_{PV}\frac{\partial^2 T_{PV}}{\partial x^2} + \delta_{PV}k_{PV}\frac{\partial^2 T_{PV}}{\partial y^2} - \sigma\left(\frac{\varepsilon_g\varepsilon_{PV}}{\varepsilon_g+\varepsilon_{PV}-\varepsilon_g\varepsilon_{PV}}\right)\left(T_{PV}^4 - T_g^4\right) - \frac{1}{R_{gap}}\left(T_{PV} - T_g\right) - \frac{1}{R_C}\left(T_{PV} - T_P\right) \;\ldots\ldots 8.2.5$$

$$\frac{\partial T_{PV}}{\partial t} = \frac{\left\{(\tau\alpha)_{PV}I_T - (\tau\alpha)_{PV}\,\eta_{el}I_T - \sigma\left(\frac{\varepsilon_g\varepsilon_{PV}}{\varepsilon_g+\varepsilon_{PV}-\varepsilon_g\varepsilon_{PV}}\right)\left(T_{PV}^4 - T_g^4\right) - \frac{1}{R_{gap}}\left(T_{PV}-T_g\right) - \frac{1}{R_C}\left(T_{PV}-T_P\right)\right\}}{\delta_{PV}\rho_{PV}C_{pPV}} \;\ldots\ldots 8.2.6$$

or

$$\frac{\partial T_{pv}}{\partial t} = \frac{\{(\tau\alpha)_{PV}I_T + \boldsymbol{h}_{c,pv-p}\left(T_p - T_{pv}\right) + \boldsymbol{h}_{r,pv-\boldsymbol{g}}\left(T_{\boldsymbol{g}} - T_{pv}\right) + \boldsymbol{h}_{co,pv-\boldsymbol{g}}\left(T_{\boldsymbol{g}} - T_{pv}\right) - (\tau\alpha)_{PV}\,\eta_{el}I_T\}}{\delta_{pv}\rho_{pv}C_{ppv}} \;\ldots\ldots 8.2.7$$

The equation used as input for the transient analysis in for PV layer if the following:

$$T_{PV}^{P+1} = T_{PV}^P + \frac{\Delta t\left\{(\tau\alpha)_{PV}I_T - Q_{el} - \sigma\varepsilon_{eff}\left({T_{PV}^4}^P - {T_g^4}^P\right) - \frac{1}{R_{gap}}\left({T_{PV}}^P - {T_g}^P\right) - \frac{1}{R_C}\left({T_{PV}}^P - {T_P}^P\right)\right\}}{\delta_{PV}\rho_{PV}C_{pPV}} \;\ldots\ldots 8.2.8$$

The electrical energy generated by the hybrid collector is given as a function of the PV cell temperature:

$$Q_{el} = \eta_O(1-\beta_O(T_{PV}-T_O)\tau_g I_T \ldots \ldots \ldots 8.2.9$$

$$T_{PV}^{P+1} = (1-\eta_o(1+\beta_O T_O))((\tau\alpha)_{PV} I_T)\frac{\Delta t}{mC_{pv}} + \{1+\frac{\Delta t}{mC_{pv}}[(\tau\alpha)_{PV}\eta_O I_T - \sigma\varepsilon_{eff}T_{PV}^3 - \frac{1}{R_{gap}} - \frac{1}{R_C}]\}T_{PV}^P + \frac{\Delta t}{mC_{pv}}\{(\sigma\varepsilon_{eff}T_g^3 + \frac{1}{R_{gap}})T_g^p + \frac{1}{R_C}T_P^p\} \ldots \ldots 8.2.10$$

8.2.1.3 Energy Balance on Absorber plate

The heat energy balance on the absorber plate is calculated by using the following formulas:

$$\delta_P\rho_P C_{pP}\frac{\partial T_P}{\partial t} = \delta_P k_P\frac{\partial^2 T_{PV}}{\partial x^2} + \delta_P k_P\frac{\partial^2 T_{PV}}{\partial y^2} + \frac{T_{PV}-T_p}{R_{C,PV-P}} - \frac{1}{R_f}(T_P - T_f) - \frac{1}{R_{loss}}(T_P - T_{am}) \ldots \ldots 8.2.11$$

$$R_{loss} = \frac{\delta_i}{k_i} + \frac{1}{h_{free}} \ldots \ldots 8.2.1\ f$$

$$\delta_p\rho_p C_{pp}\frac{\partial T_p}{\partial t} = h_{c,pv-p}(T_{pv}-T_p) - h_f(T_P - T_f) - h_{loss}(T_P - T_{am}) \ldots \ldots 8.2.12$$

$$T_P^{p+1} = T_P^p + \frac{\Delta t\{h_{c,pv-p}(T_{PV}^p - T_P^p) - h_f(T_P^p - T_f^p) - h_{loss}(T_P^p - T_{am}^p)\}}{\delta_p\rho_p C_{pp}} \ldots \ldots 8.2.13$$

$$h_f = 4.36\frac{k_w}{d_h} \qquad for\ Re < 2300,\ which\ is\ laminar\ flow$$

$$h_f = 0.023\frac{k_w}{d_h}Re_w^{0.8}Pr_w^{0.4} \qquad for\ Re > 2300,\ which\ is\ turbulent\ flow$$

$$T_P^{p+1} = \{1-\left(\frac{\Delta t}{m_w C_w}\right)(h_C + h_f + h_{loss})\}T_P^p + \frac{\Delta t}{m_w C_w}\left(\frac{T_{PV}^p}{R_C} + \frac{T_f^p}{R_f} + \frac{T_{am}^p}{R_{loss}}\right) \ldots \ldots 8.2.14$$

8.2.1.4 Energy Balance on Oscillatory Tube

The Oscillating tubes are attached to the absorber plate with good thermal conductor material by welding to made the metal to metal contact, which is good for heat transfer more than any mechanical bonding. So that, the heat flux through the tube and plate is assumed to be constant and the temperature distribution in the tube combine through the thermal resistance to reduce the complexity of the overall equation.

8.2.1.5 Energy Balance on Water in the tube

$$m_w C_w \frac{\partial T_{wo}}{\partial t} = -\dot{m} C_w (T_{in} - T_{wO}) + \pi D_i \Delta x h_f (T_p - T_{mw}) \text{......................} 8.2.\,15$$

The transient fluid equations from inlet up to outlet is given by:

$$T_{wo}^{p+1} = T_{wo}^{p} + \Delta t\{-\dot{m} C_w (T_{wi}^{p} - T_{wo}^{p}) + \pi D_i \Delta x h_f (T_p^{p} - 0.5(T_{wo}^{p} + T_{wi}^{p}))\} / \, m_w C_w \dots\dots\dots 8.2.\,16$$

$$T_{wo}^{p+1} = \left\{1 - \left(\frac{\Delta t}{m_w C_w}\right)\left(\dot{m} C_w + 0.5\pi D_i \Delta x h_f\right)\right\} T_{wo}^{p} + \frac{\Delta t}{m_w C_w}\{\left(\dot{m} C_w - 0.5\pi D_i \Delta x h_f\right) T_{wi}^{p} + \pi D_i \Delta x h_f T_p^{p}\} \dots\dots\dots 8.2.\,17$$

But the mean water temperature (T_{mw}) is the sum average of inlet (T_{wi}) and outlet water temperature (T_{wo})

$$T_{mw} = \frac{T_{wo} + T_{wi}}{2} \dots\dots\dots 8.2.1\text{ g}$$

Finally, the equation 8.2.4,8.2.10,8.2.14 & 8.2.17 are used to simulate the temperature distribution in the above component with time.

The water in the storage tank is allowed to pass through the inlet of the FPCs, and the flow of cold water from the insulated storage tank to the inlet of the collector is maintained by thermostat device or temperature controller. The useful energy balance under forced mode given by the following mathematical relation.

$$\dot{Q}_u = M_w C_w \frac{dT_w}{dt} + (UA)_t (T_w - T_{am}) + \dot{M} C_w (T_w - T_{am}) \dots\dots\dots 8.\,2$$

8.3 Simulation flow chart

The iterations start by initial guesses at each layer of the PV-T collectors and water in the tank. The initial and boundary conditions of the component temperature, ambient temperature, wind speed and water temperature obtained from the literature review and metrological data then begins the calculations as follows by Assigning the mass flow rate, material property data and assume the geometry of the system.

i. Assume initial temperature of absorber plate and average solar insolation.

ii. Find overall heat loss coefficient

iii. Find the new value of absorber plate temperature.

iv. Find the overall loss coefficient and if the UL >>8, reduce radiation heat transfer coefficient by 10%, increase or decrease the air gap to manage the convection loss.

v. Repeat the calculations until the consecutive overall heat loss coefficient difference approaches to <1%.

Transient analysis algorithms:

a. Assign all data into the simulation's tools and determine the boundary conditions.
b. Assign the initial value for glass cover, PV cell, plate, water and storage temperature.
c. Assign the time steps (Δt)and space step Δx size, start the calculations.
d. Combine and interpret the simulations.
e. Justify the simulation result with appropriate evidence and give the conclusions.

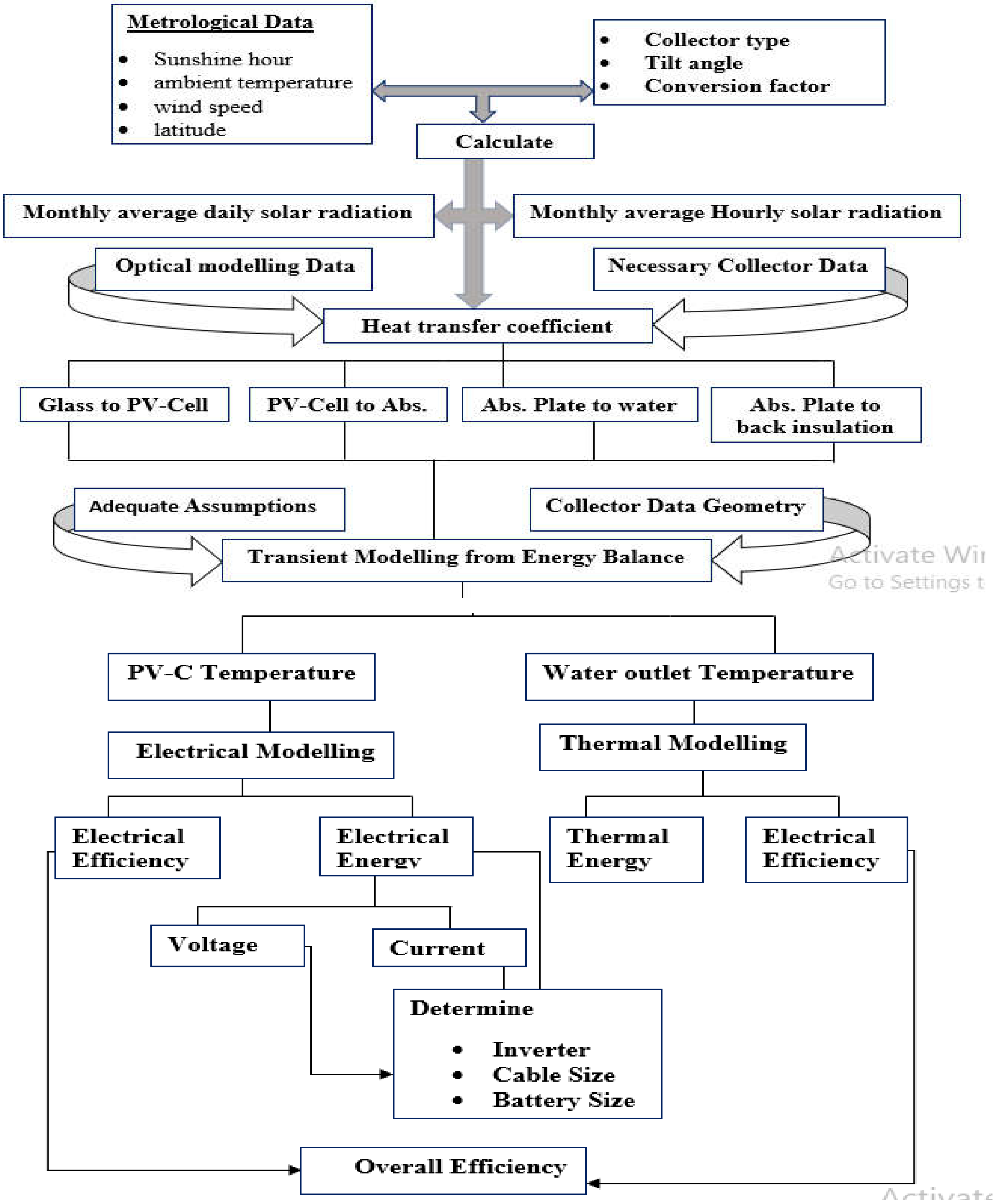

Figure 8. 5 PV-T Collector Simulation Flow Chart

CHAPTER NINE

RESULT AND DISCUSSION

9.1 System Temperature profile

By using the hourly solar energy gain and discussed in chapter five the PV module temperature is calculated as descried in chapter eight and the temperature of PV cell in Photovoltaic thermal collector calculated from the transient equations developed and discussed for each PV-T collector layer.

9.1.1 PV Module Temperature

The PV module temperature are plotted by season, to compare the temperature at the same module data for different locations and to show the solar energy increment causes PV temperature increment as mentioned in literature review, the PV module temperature vary with ambient temperature and insolation's as discussed in section 8.1.1.

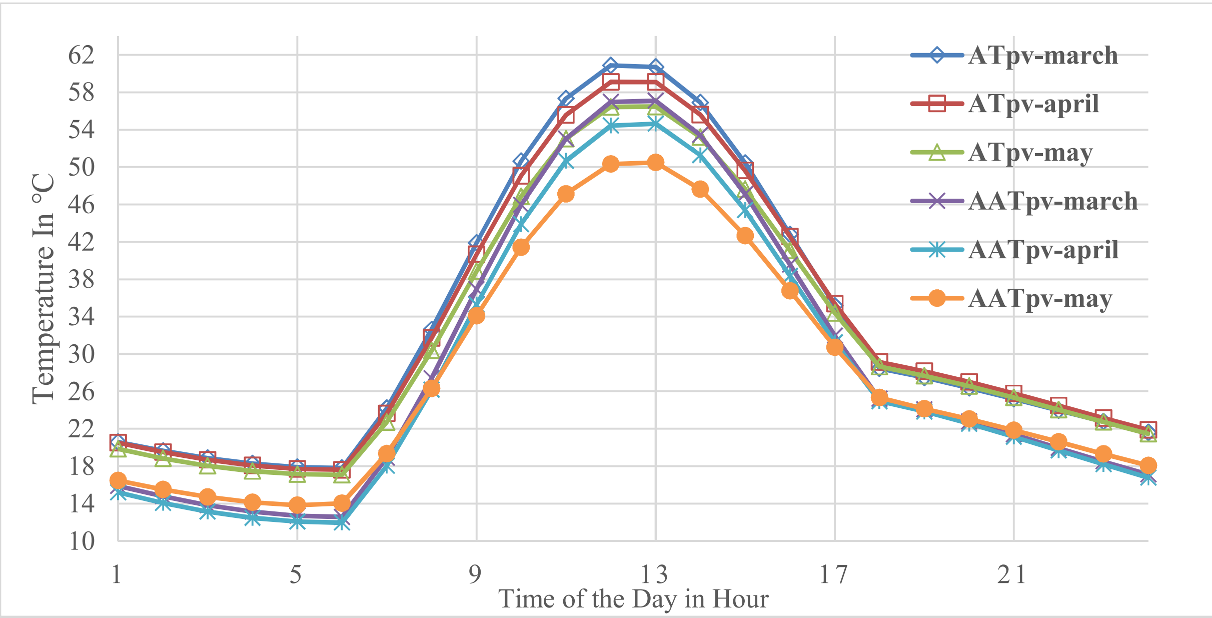

Figure 9. 1 PV Module Temperature in Spring Season of Adama And Addis Ababa

AT_{pv} denoted for Adama PV temperature and AAT_{pv} denoted for Addis Ababa PV temperature.

The adama March month temperature is greater than Addis Ababa march month maximum temperature by more than 5℃. This temperature difference achieved for the same technical data. The temperature during night time almost approaches to normal operating module temperature checked at standard data.

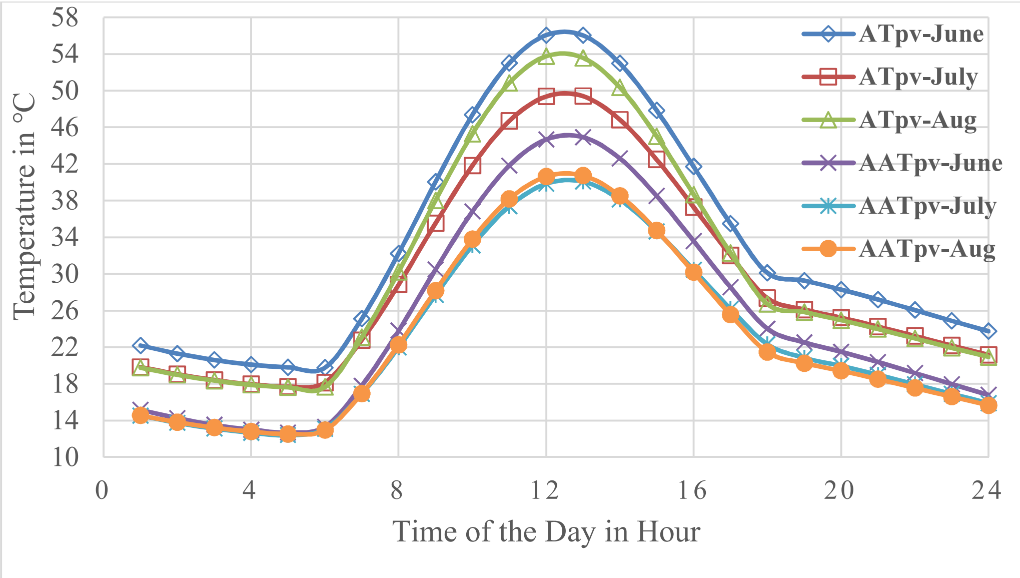

Figure 9. 2 PV Module Temperature in Summer Season of Adama And Addis Ababa

In summer season the temperature difference for the same month of both location shows greater than 9℃ and still PV module temperture in summer season of Adama is greater than corresponding season of Addis Ababa due to ambient temperature and insolation.

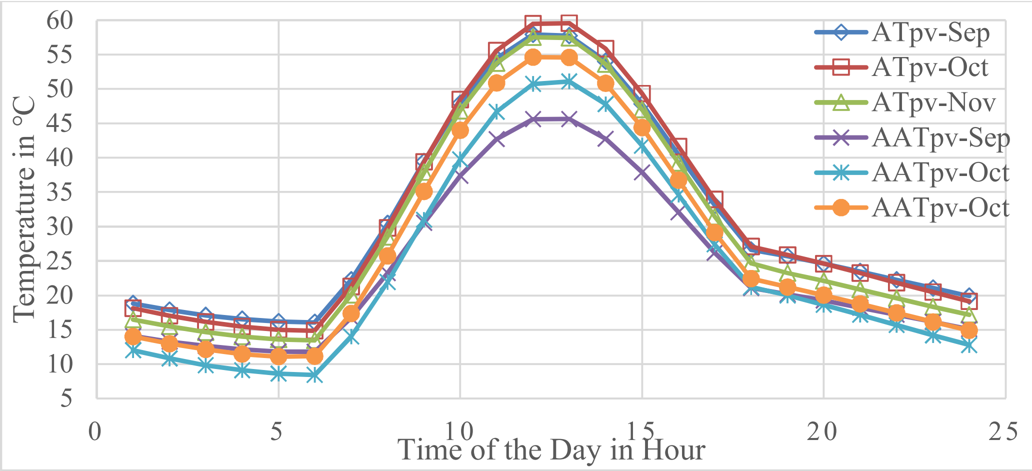

Figure 9. 3 PV Module Temperature in Autumn Season of Adama And Addis Ababa

The module temperature in winter month in of both locations temperature difference not depart like others three season.

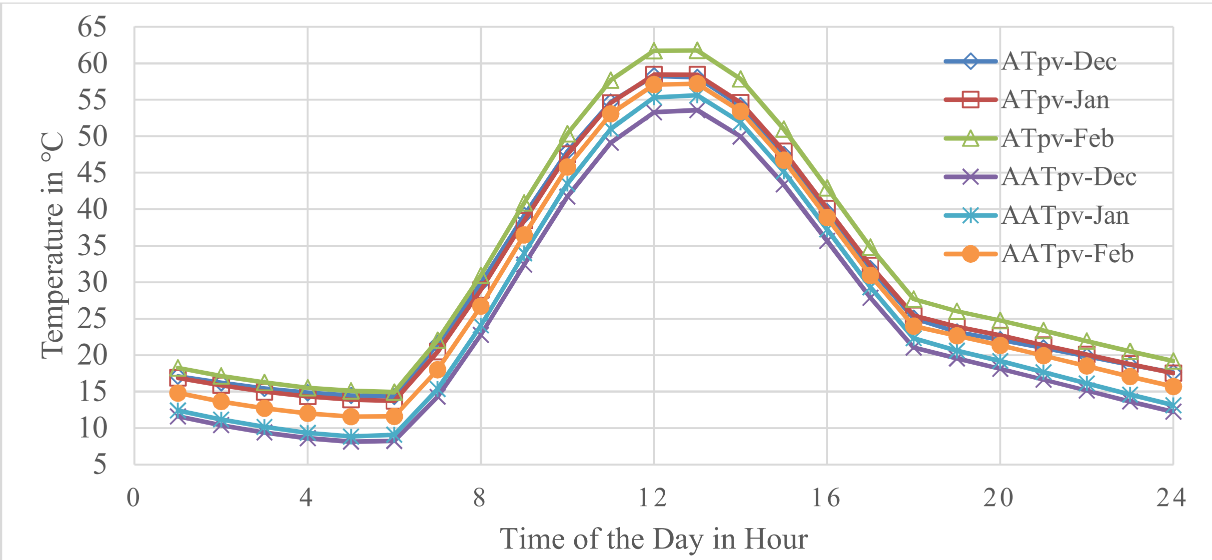

Figure 9. 4 PV Module Temperature in Winter Season of Adama And Addis Ababa

9.1.2 PV-T Temperature

The photovoltaic thermal collector temperature is plotted by season to compare the temperature at the same device with different data to analyse and show the difference. As mentioned in literature review the amount of solar energy cases the rise of PV temperature is absorbed in the form of heat to decrease the electrical efficiency of PV module is clearly understood from the following temperature and efficiency graphs. The graph profile almost similar, due storage tank temperature in the night the PV-T collector temperature increase then decrease up to 6:00Am finally increase with sun rise.

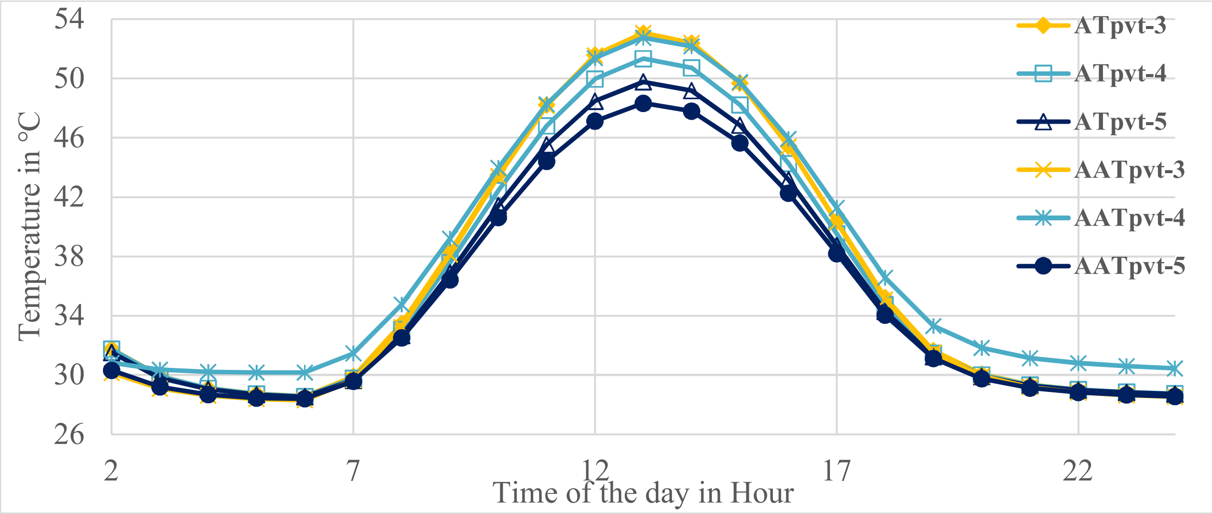

Figure 9. 5 PV-T Collector Temperature in spring Season of Adama And Addis Ababa

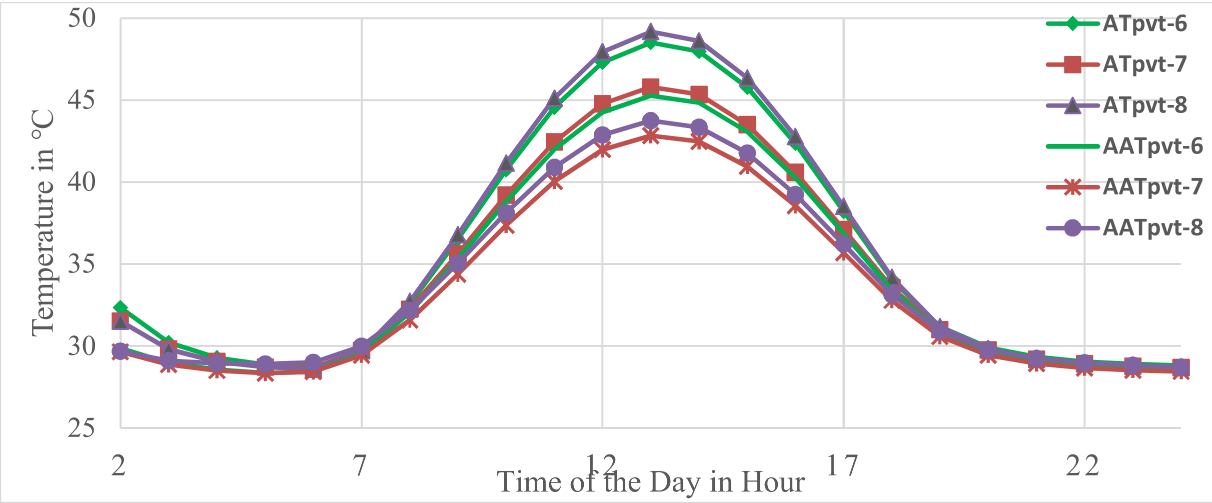

Figure 9. 6 PV-T Temperature in Summer Season of Adama And Addis Ababa

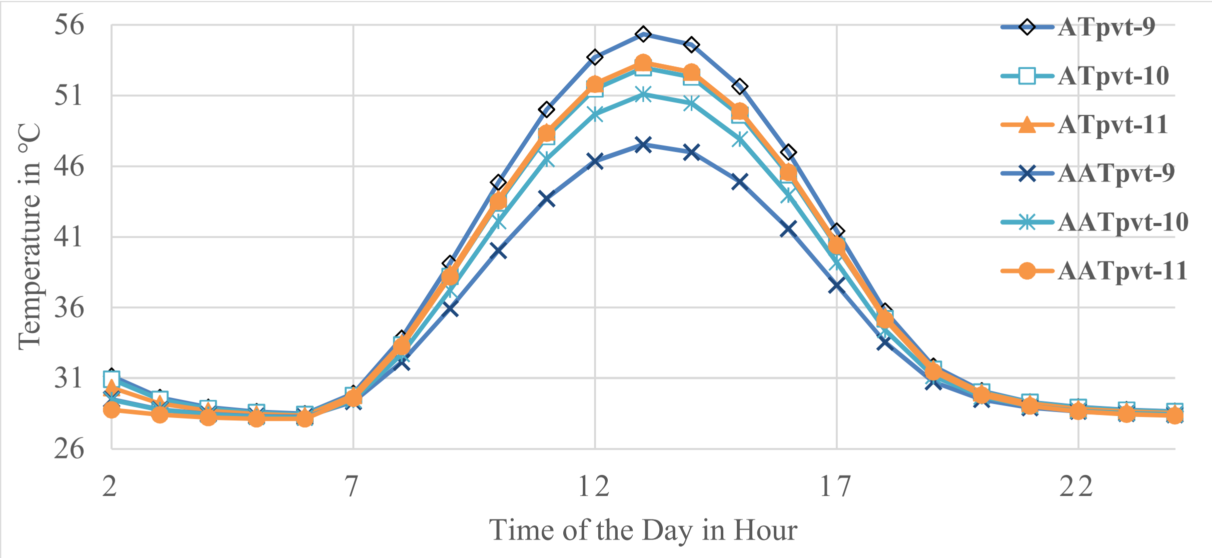

Figure 9. 7 PV-T Module Temperature in Autumn Season of Adama and Addis Ababa

In the night time the PV-T collector temperature distribution doesn't lower than 27°C due to the fluid temperature initial assumed which is controlled by thermostat for better electrical energy generation.

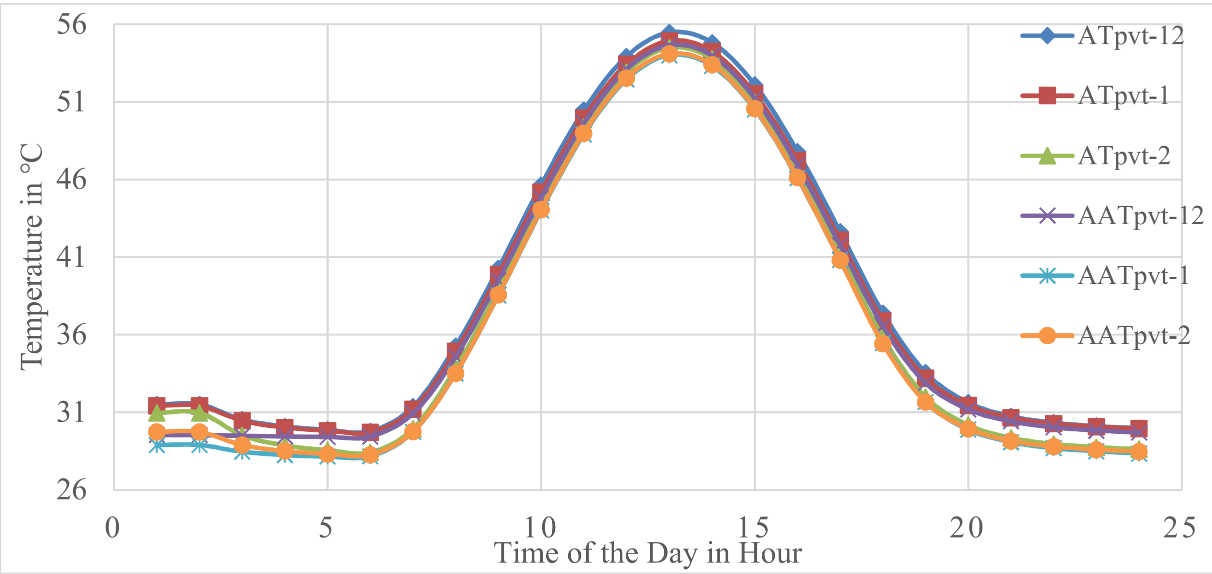

Figure 9. 8 PV-T Module Temperature in Winter Season of Adama And Addis Ababa

9.1.3 Combined PV and PV-T Temperature profile

In this section the temperature difference without cooling and with cooling is plotted as shown in figure below, which indicates due to cooling the maximum temperature of PV-T collect is less than 53℃ whereas the module temperature rises up to 61℃ in march month.

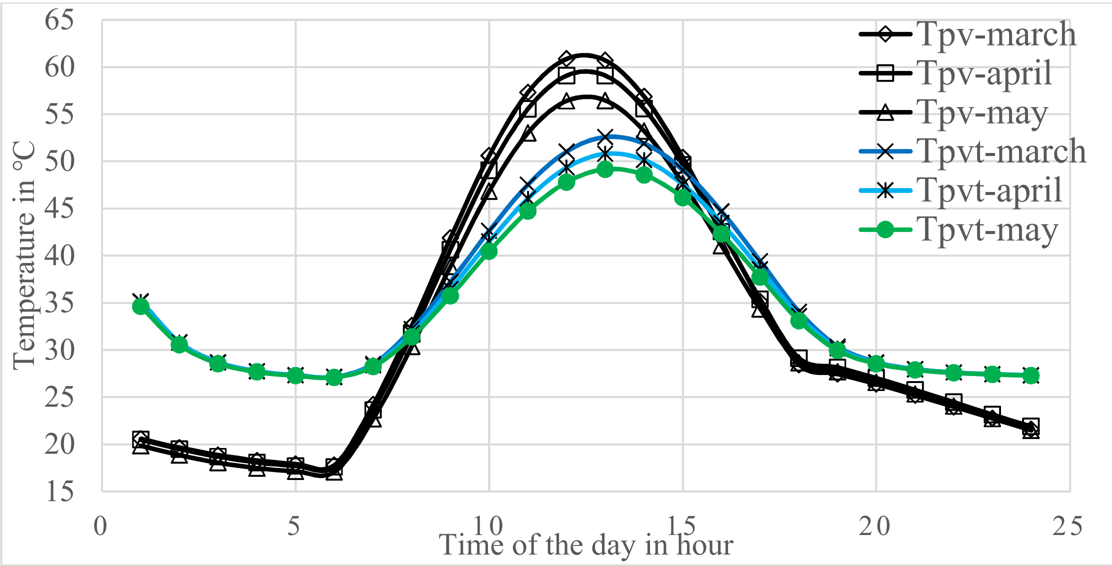

Figure 9. 9 Adama Spring Season PV-Module and PV-T Collector Cell Temperature

The PV module and PV-T collector PV cell temperature suddenly increase after 6:00am and decrease after 12:00am as shown in figure 8.17, but due to the cooling medium in PV-T collector the PV cell temperature remain below module temperature in the range of sunshine hours and remain above during non-sunshine hours due to the working fluid starts cooling (flow through module) when the PV temperature become more than reference temperature and normal operating temperature for better efficiency as discussed in the previous chapter. For the spring season three months, the PV module temperature rise more than 55℃ and only maximum 53℃ occur in April for PV-T collector which is good achievement in temperature reduction. This reduced PV-T collector temperature on the other hand used to increase the current, voltage and electrical power output or save the amount of energy lost due to temperature rise.

As shown in figure 9.11 the maximum PV-T collector PV cell temperature is less than 49℃ which is occur in August month and the PV module maximum temperature is more than 53℃ for both August and June, 49℃ for July which implies the lowest PV module temperature in the season as well as in the year.

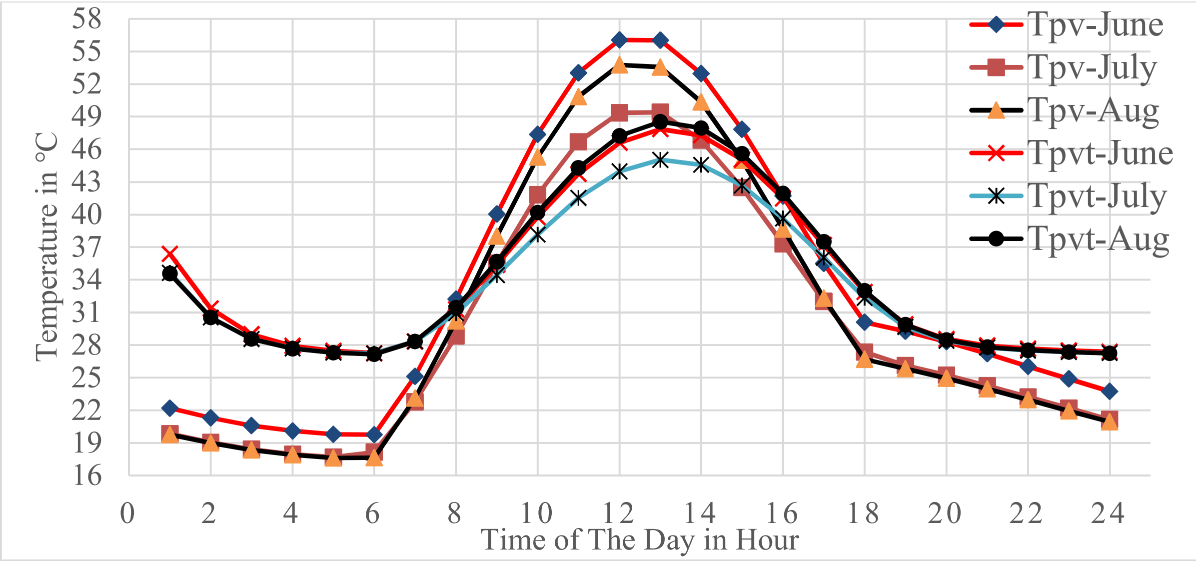

Figure 9. 10 Adama Summer Season PV-Module and PV-T Collector Cell Temperature

During the night time there is solar radiation, but the of photovoltaic thermal collector shows higher temperature than PV module collector. The temperature difference between Photovoltaic thermal collector and PV module is the effect of fluid temperature in the storage tank which makes the PV-T collector to rise more than separately installed PV module.

The PV module and PV-T collector temperature is high in Autumn season as referred from the above figure due to the corresponding solar radiation and ambient temperature in occur in this season. The PV module temperature is greater than 57℃ through the month of this season and the PV-T collector PV cell temperature is less the 55℃.

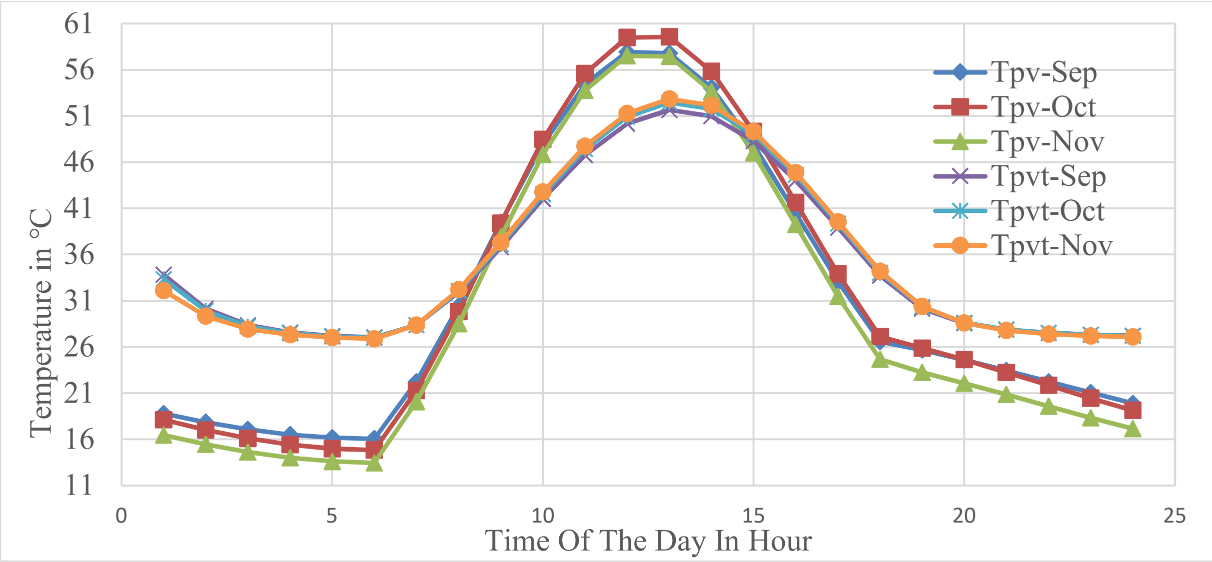

Figure 9. 11 Adama Autumn Season PV-Module and PV-T Collector Cell Temperature

In the winter season due to relatively high solar radiation and ambient temperature in the Adama the module temperature rises more than 58℃ and also the PV-T cell temperature reaches 54℃.

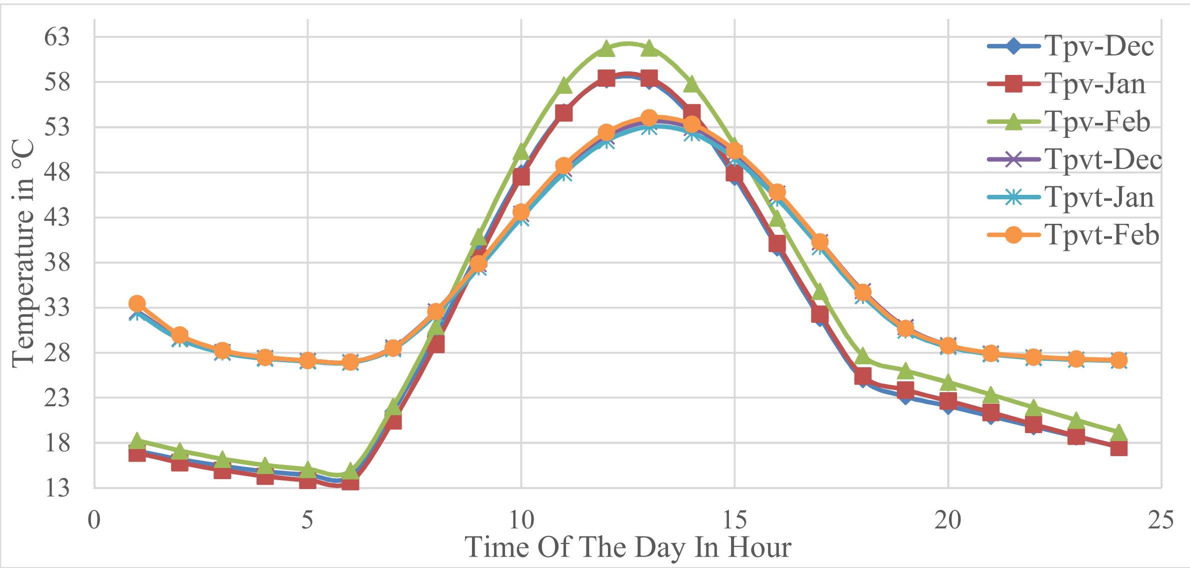

Figure 9. 12 Adama Winter Season PV-Module and PV-T Collector Cell Temperature

9.1.3 Absorber Plate Temperature

The aluminium sheet heat absorber plate is extracting the excess heat in the PV layer results good transfer heat to water. For both Adama and Addis Ababa the temperature distribution on the sheet absorber shown in figure 9.13 and 9.14 respectively. The observer plate in Adama weather conditions give the temperature greater than 46℃ for the period of 11 month through the year except July.

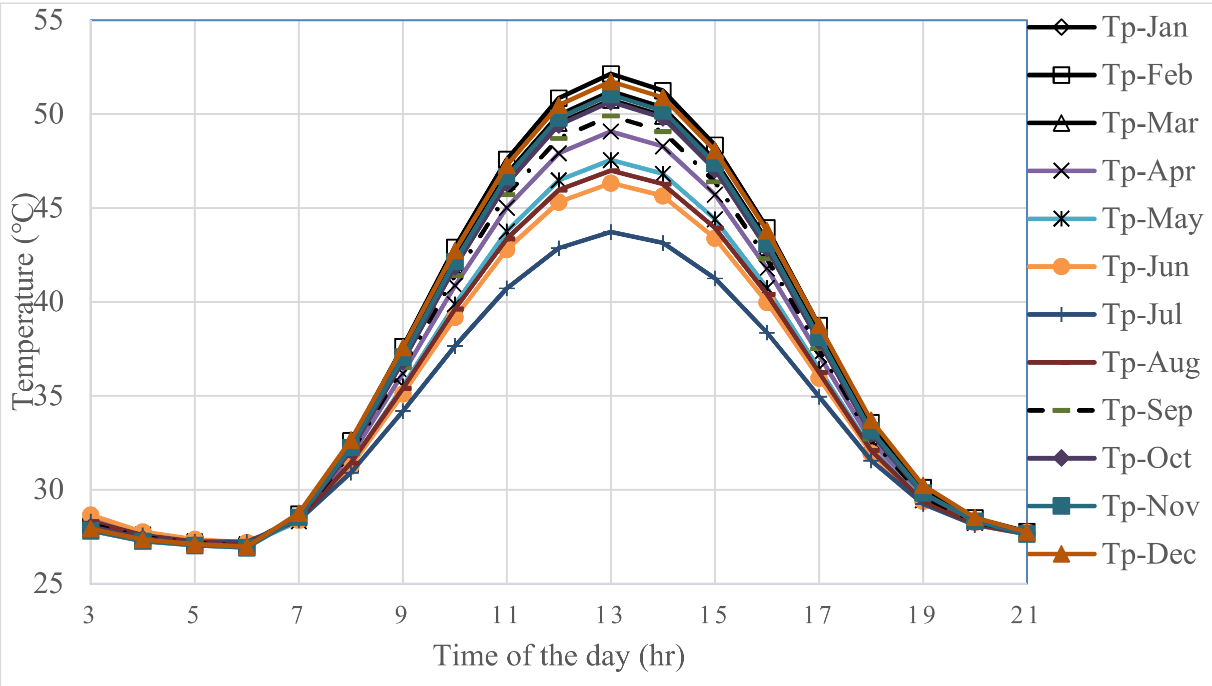

Figure 9. 13 Adama Absorber Plate Temperature

The absorber plate temperature increasement or decrement affect the module temperature as well as cooling fluid temperature which implies that the amount solar insolation on the absorber plate is the energy that mainly contribute for fluid temperature. As previously explained the temperature of absorber plate in the night become higher by extracting heat from the working fluid from the storage tank.

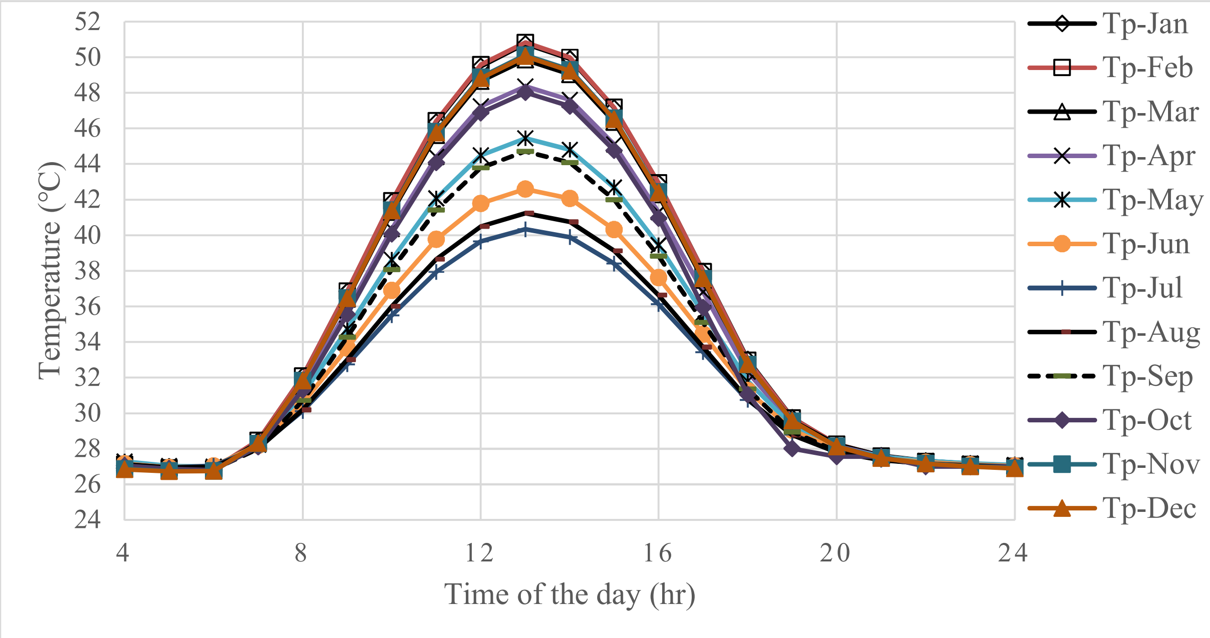

Figure 9. 14 Addis Ababa Absorber Plate Temperature

9.1.4 Storage Tank Temperature

After calculating the useful energy gain, total loss and daily load energy the transient fluid temperature in the storage is calculated and the results plotted in the figure 9.15 and figure 9.16 for Adama and Addis Ababa respectively for comparison.

Table 9. 1 Adama storage tank steady state temperature distribution for daily maximum

Node	Jan	Feb	Mar	Apr	May	Jun	Jul	Aug	Sep	Oct	Nov	Dec
0	59.1	61.5	62.01	62.27	61.29	62.29	58.4	58.96	59.93	60.917	58.284	58.175
1	56.1	58.49	59.01	59.27	58.29	59.28	55.39	55.957	56.927	57.714	55.181	55.172
2	53.1	55.5	56.01	56.28	55.3	56.29	52.4	52.962	53.932	54.519	52.085	52.176
3	50.1	52.5	53.01	53.28	52.3	53.29	49.4	49.962	50.932	51.319	48.985	49.176
4	47.1	49.5	50.01	50.28	49.3	50.29	46.4	46.962	47.932	48.119	45.885	46.176
5	44.1	46.5	47.01	47.28	46.3	47.29	43.4	43.962	44.932	44.919	42.785	43.176
6	41.1	43.5	44.01	44.28	43.3	44.29	40.4	40.962	41.932	41.719	39.685	40.176
7	38.1	40.5	41.01	41.28	40.3	41.29	37.4	37.962	38.932	38.519	36.585	37.176
8	35.1	37.5	38.01	38.28	37.3	38.29	34.4	34.962	35.932	35.319	33.485	34.176
9	32.1	34.5	35.01	35.28	34.3	35.29	31.4	31.962	32.932	32.119	30.386	31.177
10	27	27	27	27	27	27	27	27	27	27	27	27

The storage tank temperature distribution under steady state from daily maximum transient temperature result used to calculate the temperature distributions in each nodes of the storage tank by using Gauss iteration method and the temperature distribution on each layer of the storage tank coloured by using excel conditional formal as shown in table 9.1 and table 9.2 for Adama and Addis Ababa respectively.

The following graph show the transient temperature distributions of the storage tank.

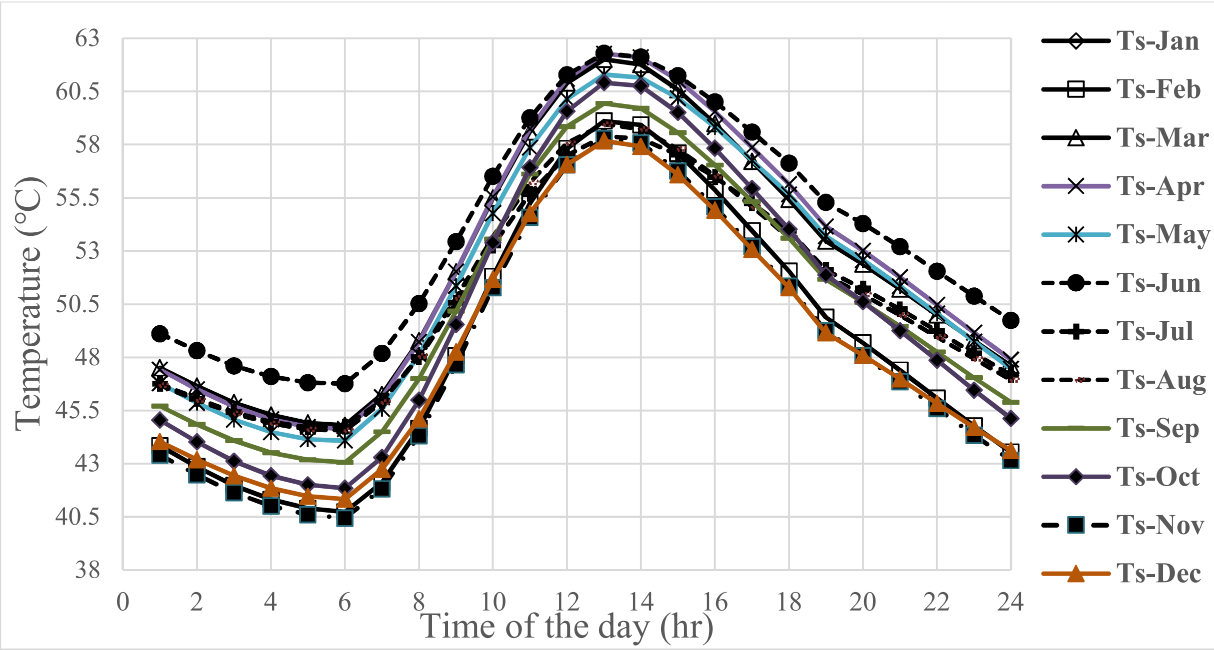

Figure 9. 15 Storage Tank Temperature Distributions for Adama

The resulted colour in the thermal storage tank shows the well stratified tank temperature distributions due to initially assumed height to diameter ratio.

Table 9. 2 Addis Ababa Storage tank steady state temperature distribution

Node	Jan	Feb	Mar	Apr	May	Jun	Jul	Aug	Sep	Oct	Nov	Dec
0	59.7	61.32	62.18	61.17	59.9	57.03	54.31	54.07	55.6	58.52	58.68	58.36
1	56.7	58.32	58.68	57.666	56.7	53.92	51.31	51.12	52.8	55.52	55.73	55.31
2	53.7	55.33	55.19	54.171	53.5	50.83	48.31	48.17	50.1	52.52	52.78	52.26
3	50.7	52.33	51.69	50.671	50.3	47.73	45.31	45.22	47.4	49.52	49.83	49.21
4	47.7	49.33	48.19	47.171	47.1	44.63	42.31	42.27	44.6	46.52	46.88	46.16
5	44.7	46.33	44.69	43.671	43.9	41.53	39.31	39.32	41.9	43.52	43.93	43.11
6	41.7	43.33	41.19	40.171	40.7	38.43	36.31	36.37	39.1	40.52	40.98	40.06
7	38.7	40.33	37.69	36.671	37.5	35.33	33.31	33.42	36.4	37.52	38.03	37.01
8	35.7	37.33	34.19	33.171	34.3	32.23	30.31	30.47	33.6	34.52	35.08	33.96
9	32.7	34.33	30.69	29.671	31.1	29.13	27.31	27.52	30.9	31.52	32.13	30.92
10	27	27	27	27	27	27	27	27	27	27	27	27

The temperature distribution shows more than 32℃ for 7 month and for Addis Ababa only 4 months generate more than this temperature.

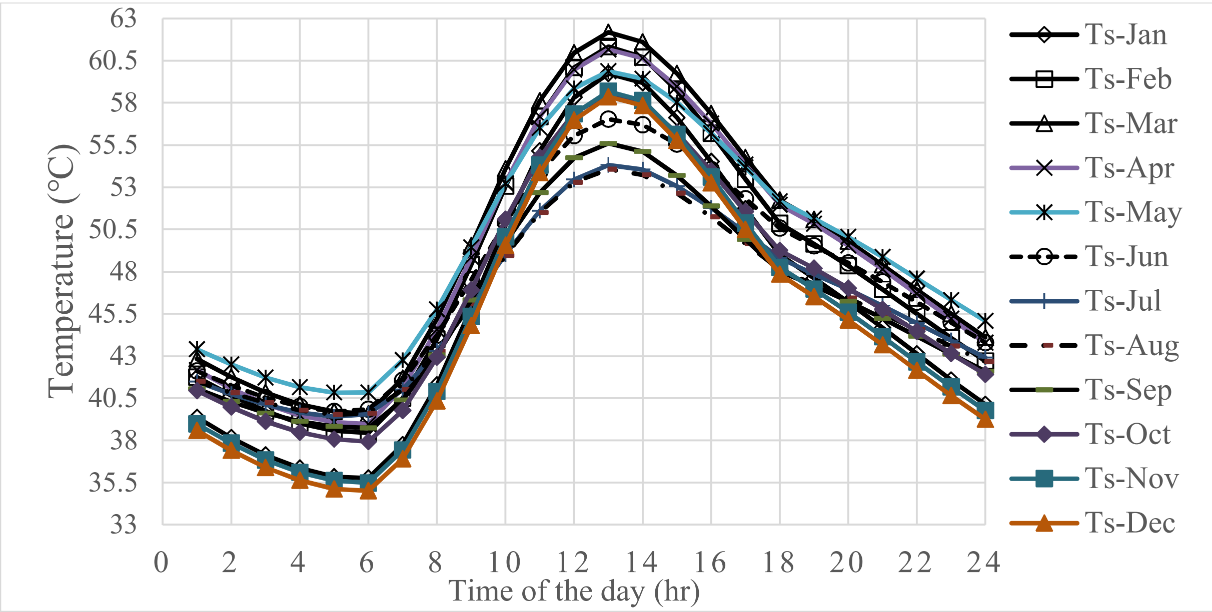

Figure 9. 16 Storage Tank Temperature Distributions for Addis Ababa

The working fluid (water) temperature in the storage tank decrease in the night time and increase in the day because the storage charging is done in only the day time.

9.2 System Electrical Energy and Efficiency curve

9.2.1 Efficiency of PV Module

In this section the module efficiency of PV module plotted for corresponding temperature discussed in section 9.1.1. The efficiency drops in PV module reach up to 0.7% for maximum year PV module temperature as in the next for graph.

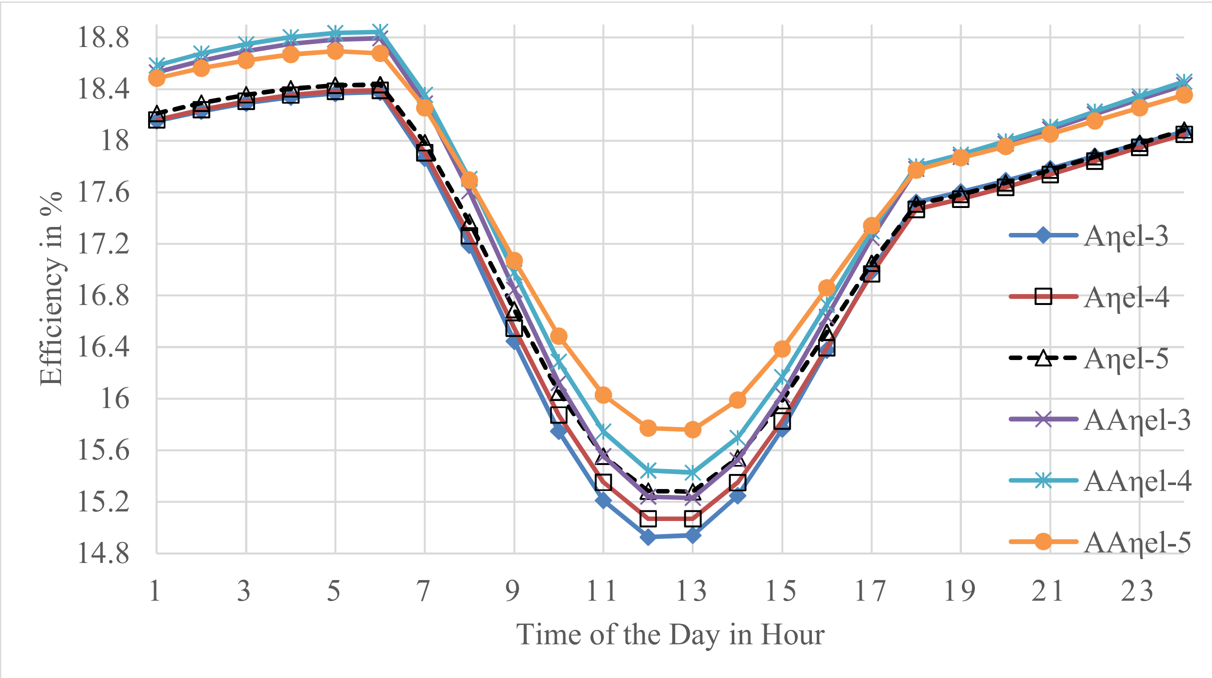

Figure 9. 17 Spring Season PV Module Efficiency

The maximum spring and summer season efficiency drop for the temperature rise in PV module is 2.86% and2.49% for the June in Addis Ababa, respectively, 2.6 % and 1.6% in Adama for July month.

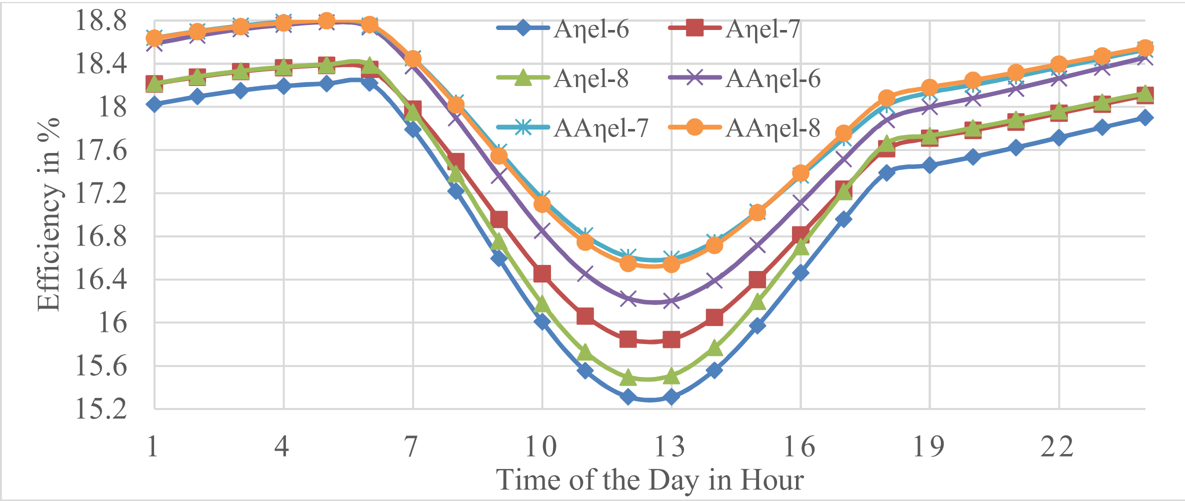

Figure 9. 18 Summer Season PV Module Efficiency

For the same PV module, the electrical efficiency of the device is higher in Addis Ababa due to the lower ambient and insolation in the site in all metrological season.

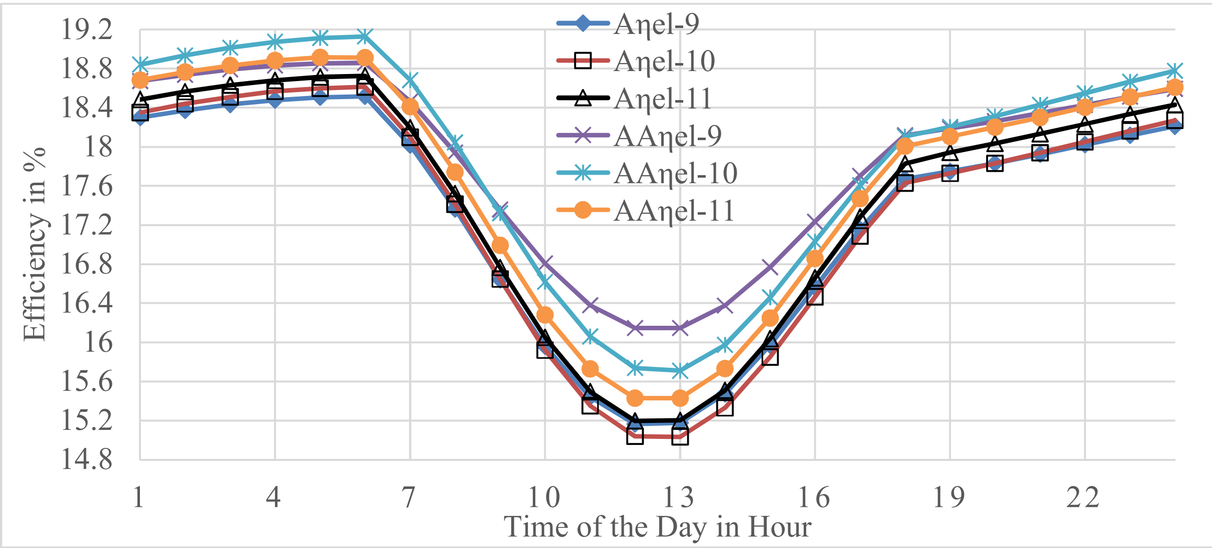

Figure 9. 19 Autumn Season PV Module Efficiency

Note: $A\eta_{el}$ and $AA\eta_{el}$ represents Adama and Addis Ababa electrical efficiency respectively and the number from 1 up to 12 repersents months of the year

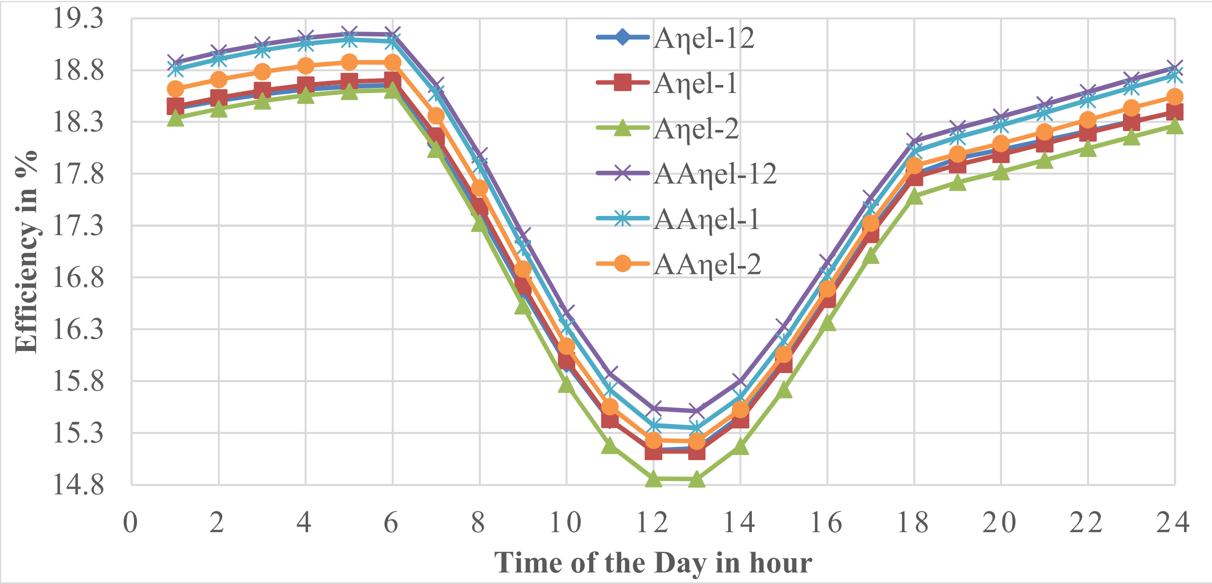

Figure 9. 20 Winter Season PV Module Efficiency

8.3.2 Efficiency PV-T Collector

The collector temperature profile shown in the next four graphs determined by the temperature in the storage and solar radiation.

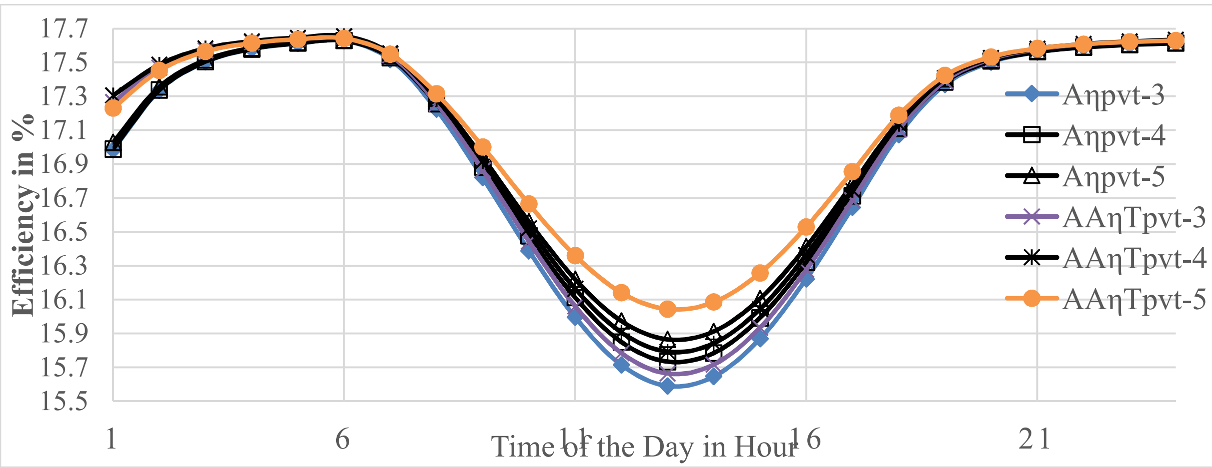

Figure 9. 21 Spring Season PV-T Collector Efficiency

Specially in the night time significant efficiency variation happens due to the working fluid temperature from the storage circulating through the collector.

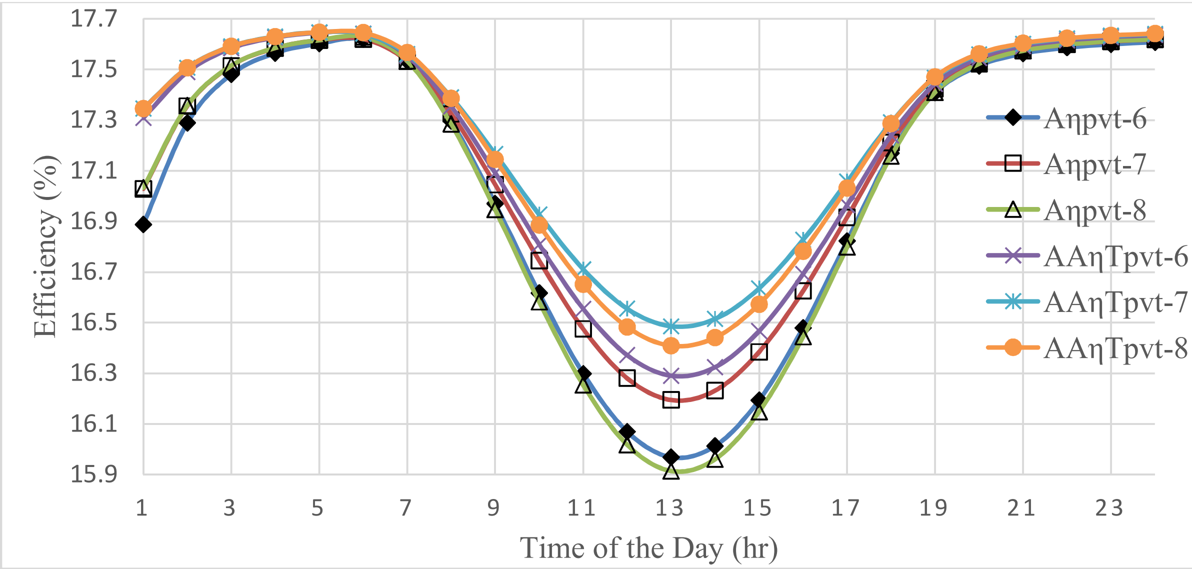

Figure 9. 22 Summer Season PV-T Collector Efficiency

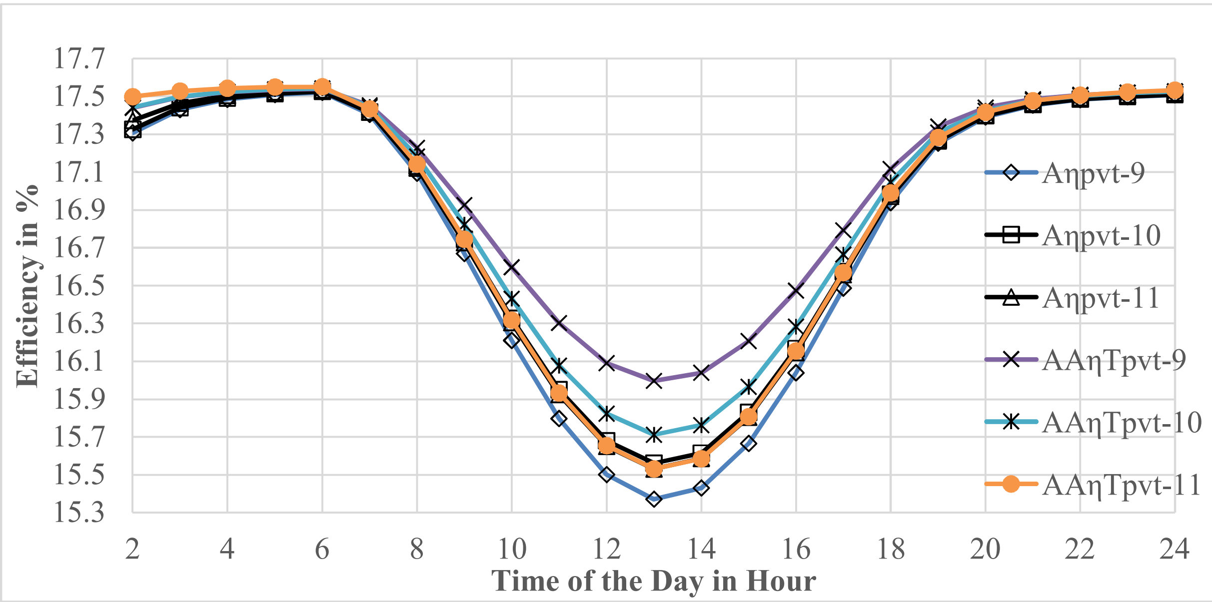

Figure 9. 23 Autumn Season PV-T Collector Efficiency

In all season during the night time the collector efficiency almost uniform and constant for both Adama and Addis Ababa.

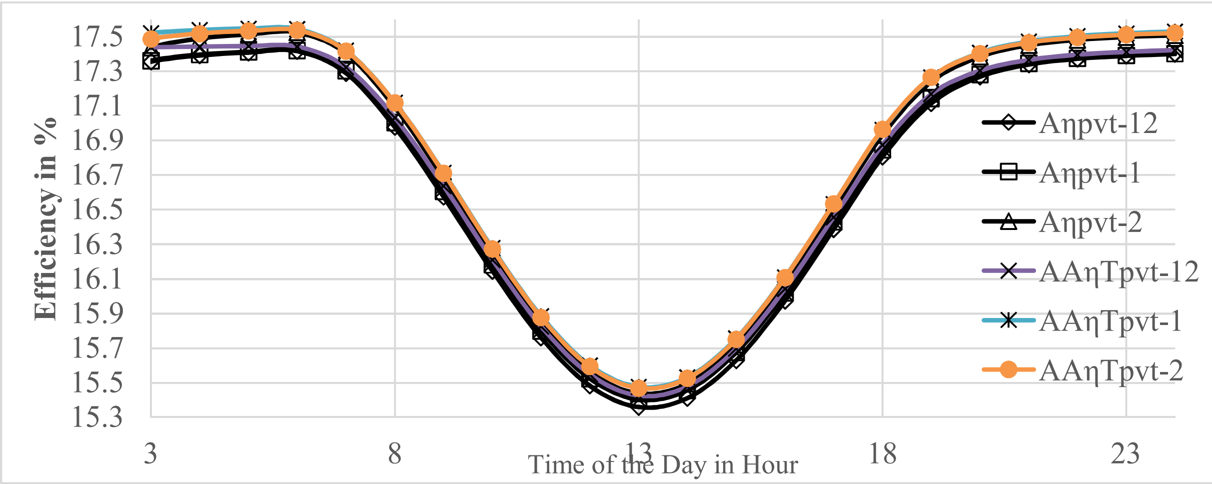

Figure 9. 24 Winter Season PV-T Collector Efficiency

9.2.2 Combine PV and PV-T Electrical Efficiency Profile

The theoretical background states in literature show that as the temperature of PV module increase, the electrical efficiency of PV module decrease is justified in the next figure.

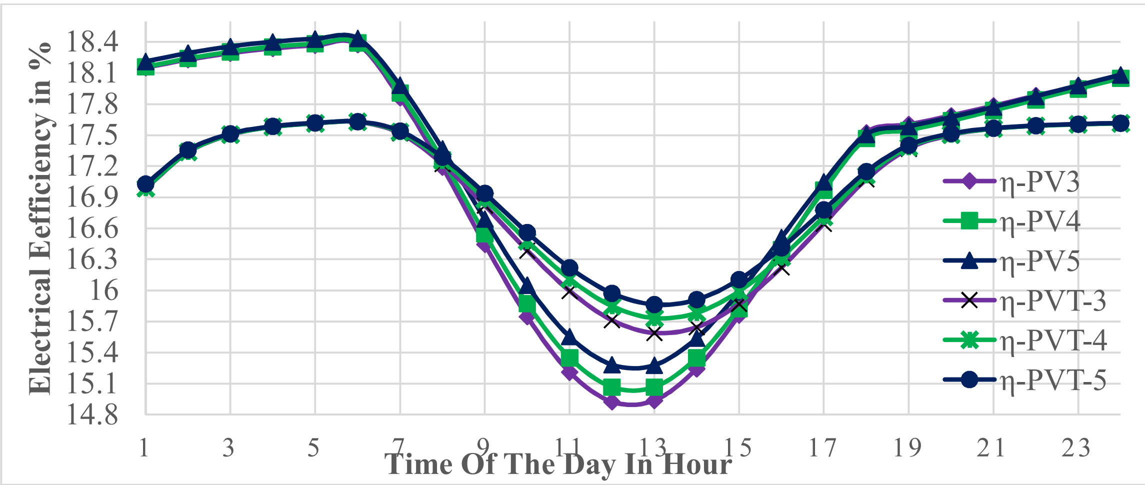

Figure 9. 25 Adama Spring Season Electrical Efficiency of PV Module And PV-T Collector

By using the spring season temperature, the efficiency of the two (PV and PV-T) system is clearly shown in following figure 9.14 for the temperature difference shown in figure 9.10, and the corresponding efficiency drop shown in figure 9.25.

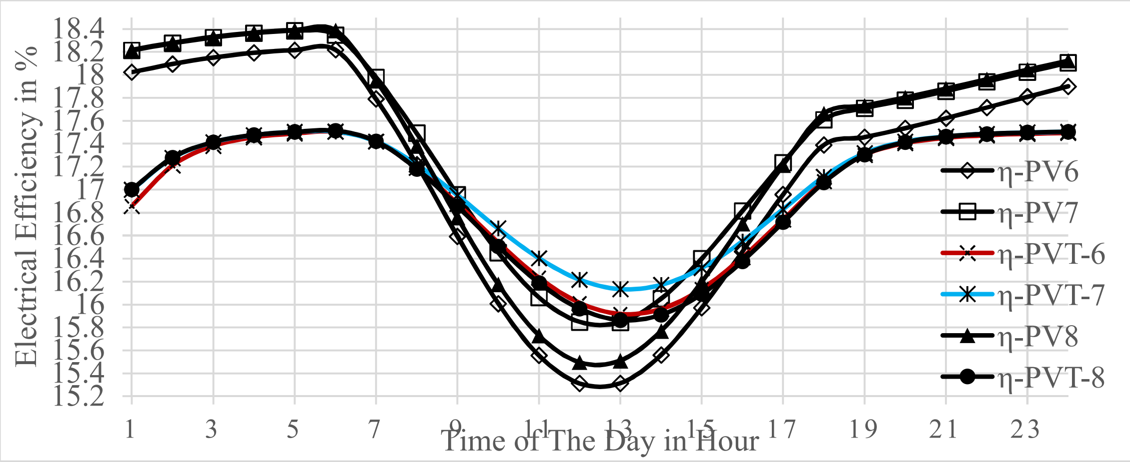

Figure 9. 26 Adama Summer Season Electrical Efficiency of PV Module And PV-T Collector

In the same manner by using summer season temperature is use to plot the following corresponding efficiency of summer.

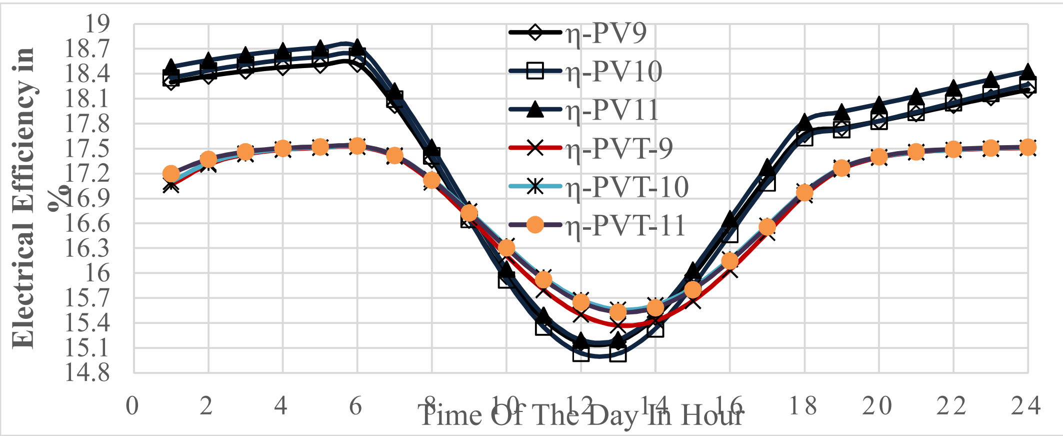

Figure 9. 27 Adama Autumn Season Electrical Efficiency of PV Module And PV-T Collector for Monthly Average hourly Data

The reference condition efficiency of the collector under investigation is 17.8%, but in all seasons and months the PV-T collector efficiency doesn't reach this reference value, because of the PV-T collector temperatures is greater than module reference temperature as discussed and shown in figure 8.10 to 8.13.

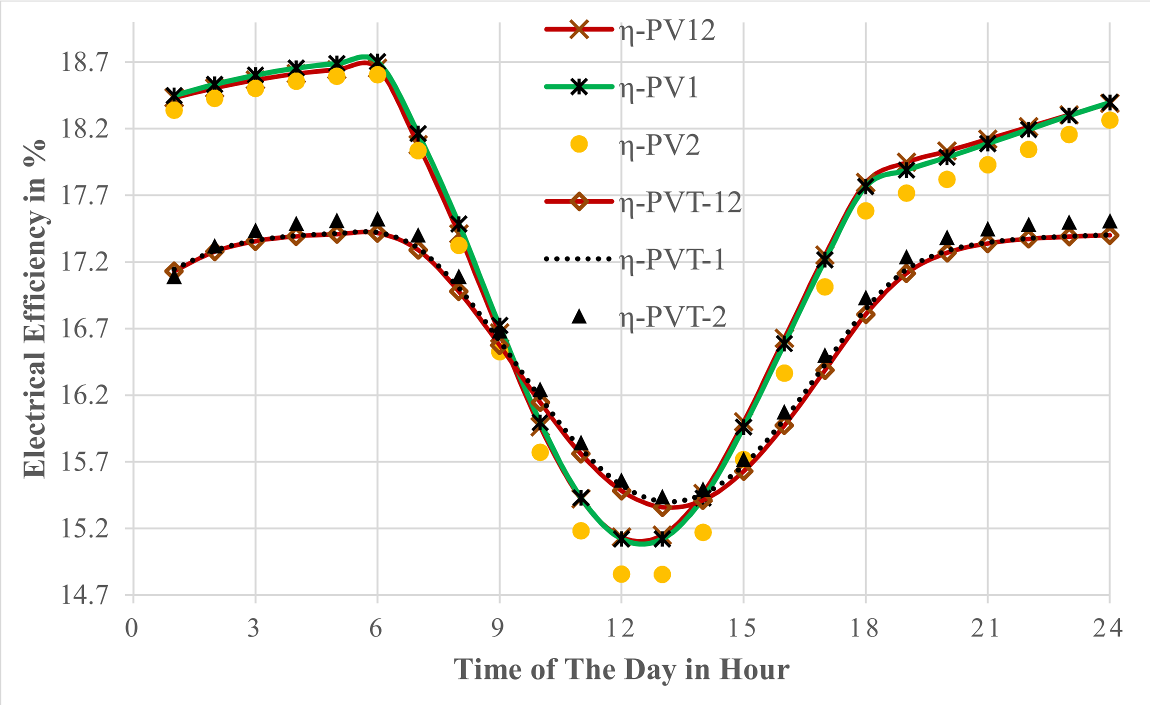

Figure 9. 28 Adama Winter Electrical Efficiency of PV Module And PV-T Collector

The all efficiency plots show the PV managed in some degrees, which gives the grant for efficiency is not less than the efficiency of separate PV module temperature at high temperature and solar insolation.

9.2.3 Total Electrical Gain

The total PV module electrical energy daily yield of Adama is greater than Addis Ababa corresponding day of the year in ten months.

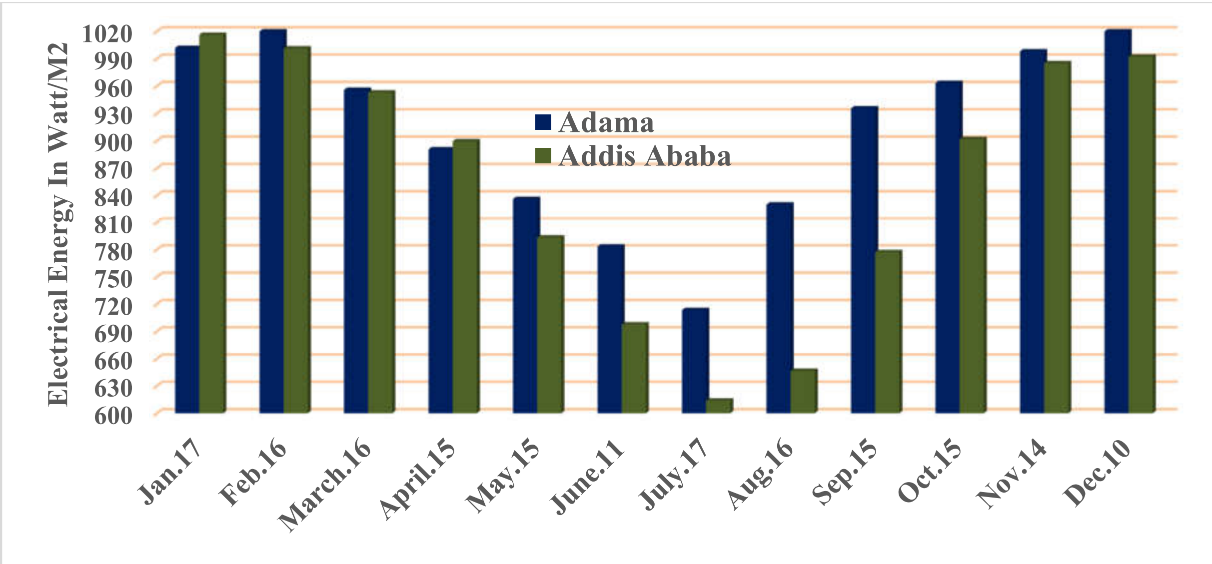

Figure 9. 29 PV module daily Total electrical energy gain

The following graph shows that the total PV-T collector electrical energy daily yield of Adama is greater than Addis Ababa corresponding day of the year in eleven months. Addis Ababa daily average electrical energy gained in January month is greater than Adama corresponding months due the higher solar irradiance in the stated month.

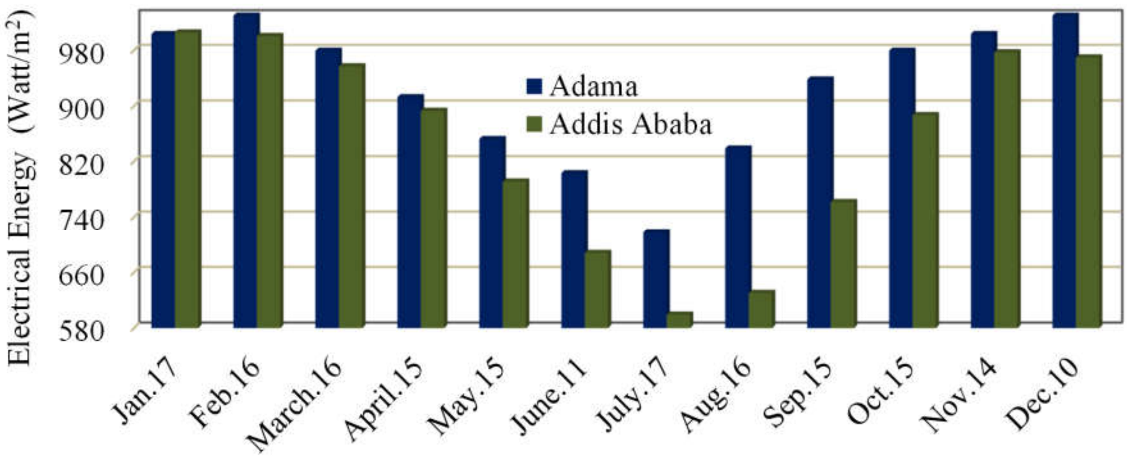

Figure 9. 30 PV-T Collector daily Total electrical energy gain

9.3 System Thermal characteristics

9.3.1 Water Temperature

The transient analysis of water outlet temperature mainly relies on the mass flow rates of the water, but the water flow rates 0.02kg/s used for temperature calculation and the following outlet temperature is achieved simulation. In this analysis the water outlet temperature is greater than 45℃ for all months except July which is less than 43℃. This temperature range in dairy industry use for different cleaning and for some intermediate process specially at 43℃ -55℃. The remaining process need more temperature range mainly greater than 62℃.

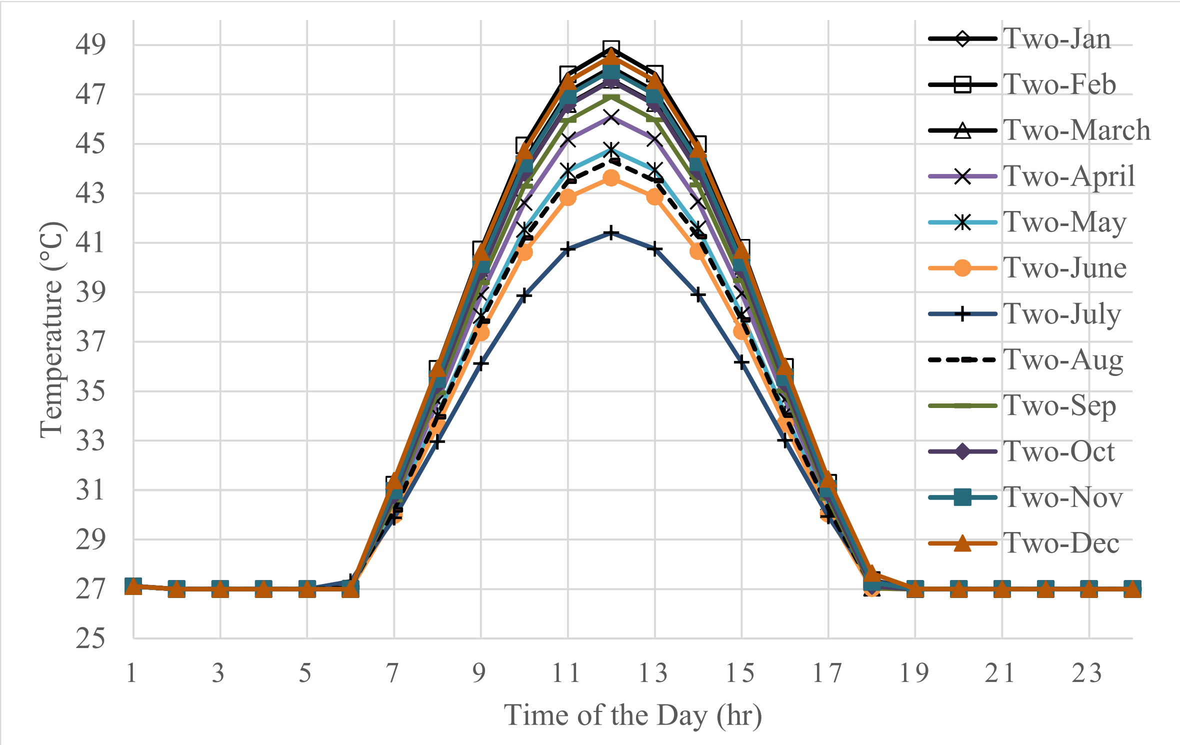

Figure 9. 31 ADAMA Water outlet Temperature from PV-T collector

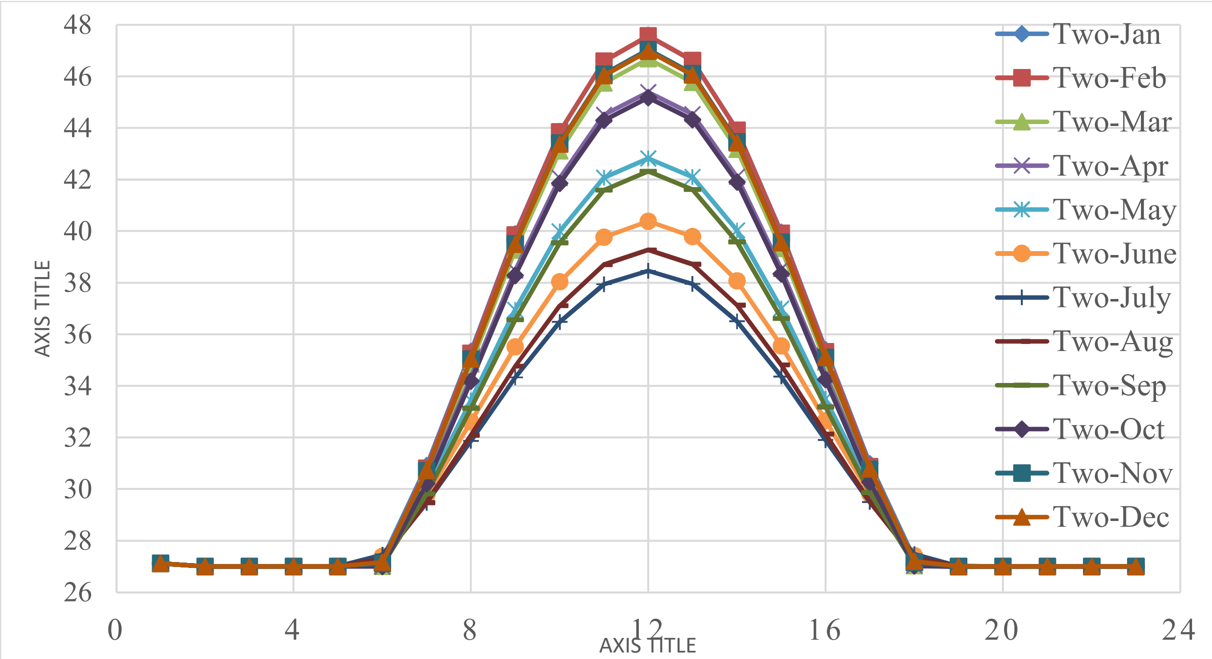

Figure 9. 32 Addis Ababa water outlet Temperature

9.3.2 Total Thermal Energy Gained

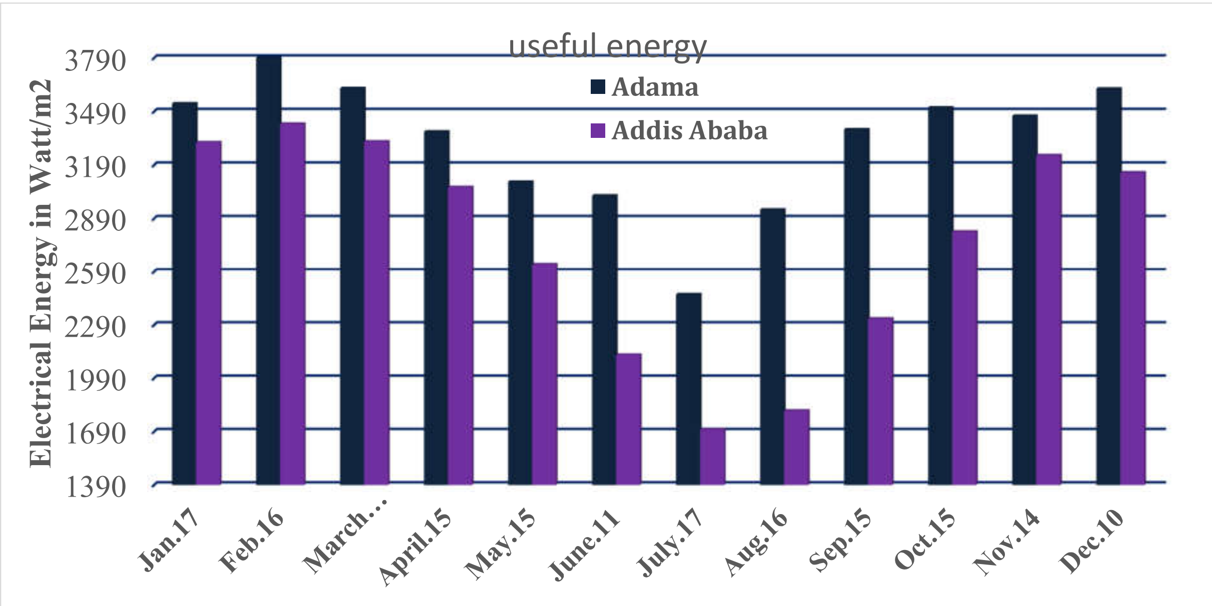

Figure 9. 33 Daily average useful energy gained

9.3.3 Therma efficiency

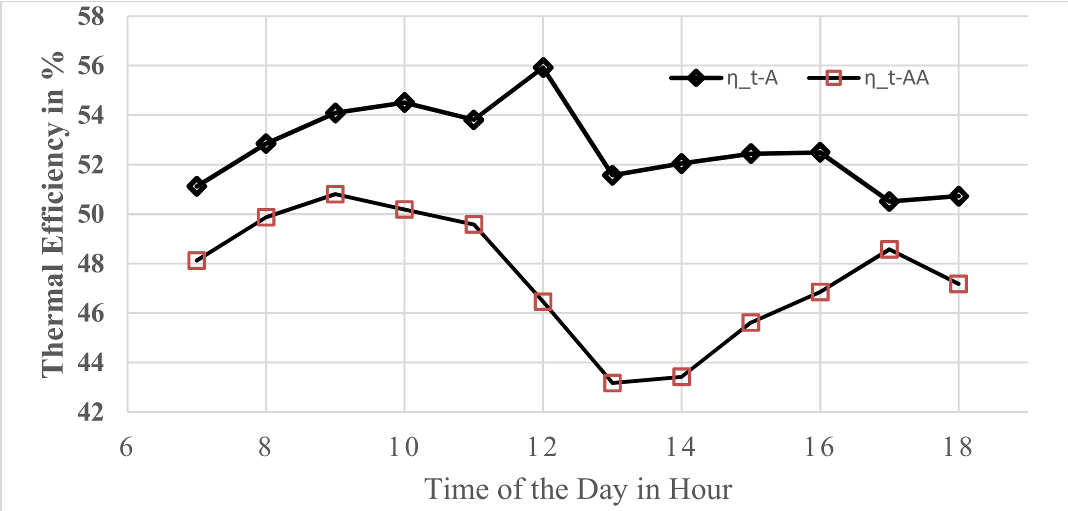

Figure 9. 34 Daily average thermal Efficiency

Using the hourly solar gain described in chapter 5 and the temperature data discussed in section 9.2 the following histography is plotted to differentiate the module and PV-T collector electrical energy gain.

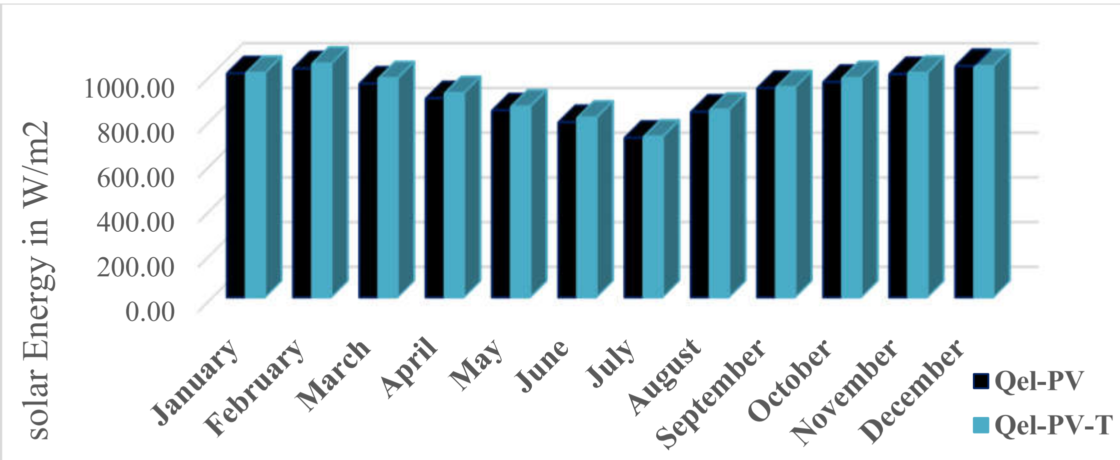

Figure 9. 35 Adama Monthly Average Daily Electrical Energy Gain from PV Module and PV-T Collector

The monthly electrical gained is comparatively greater than the separately used PV module which indicates that the desired cooling to save the dissipations of electrical energy is advantages.

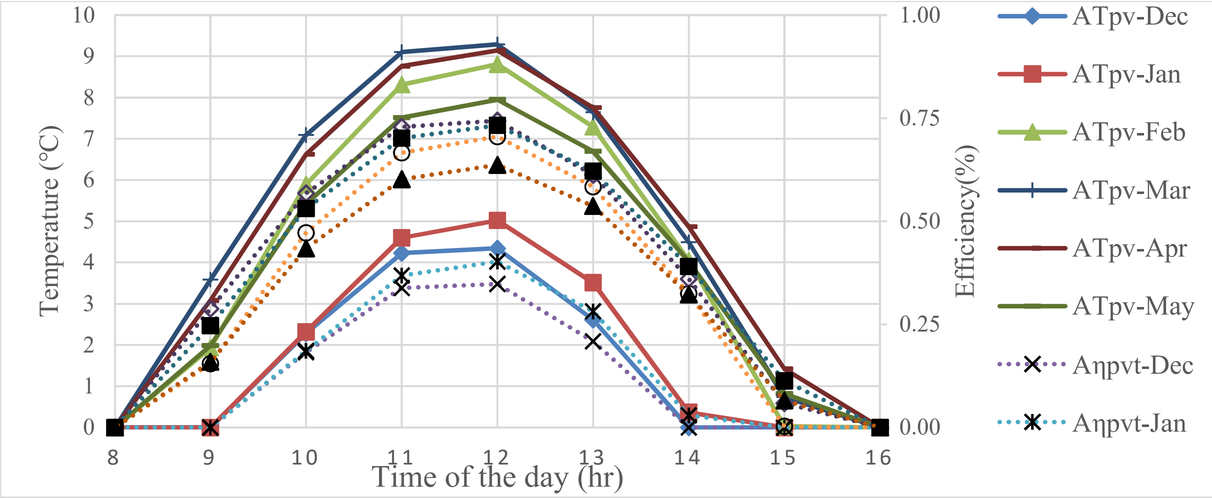

Figure 9. 36 PV Module Temperature reduce and net efficiency increase for Winter and Summer Season

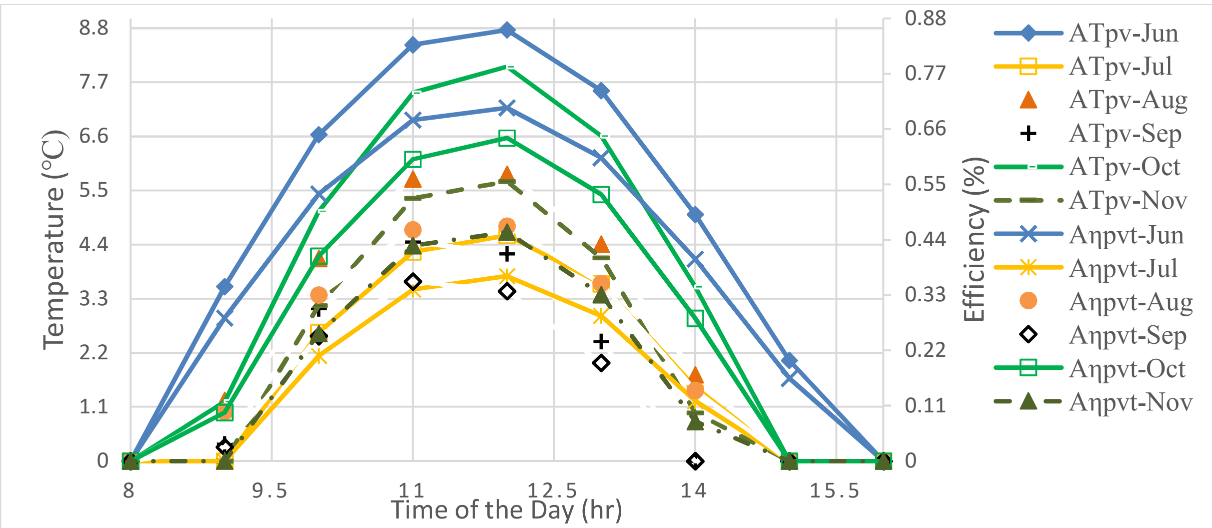

Figure 9. 37 PV Module Temperature reduce and net efficiency increase for Summer and Autumn Season

So, the numerical difference comparison also shows the same the meaning which shows the net solar power per square metre.

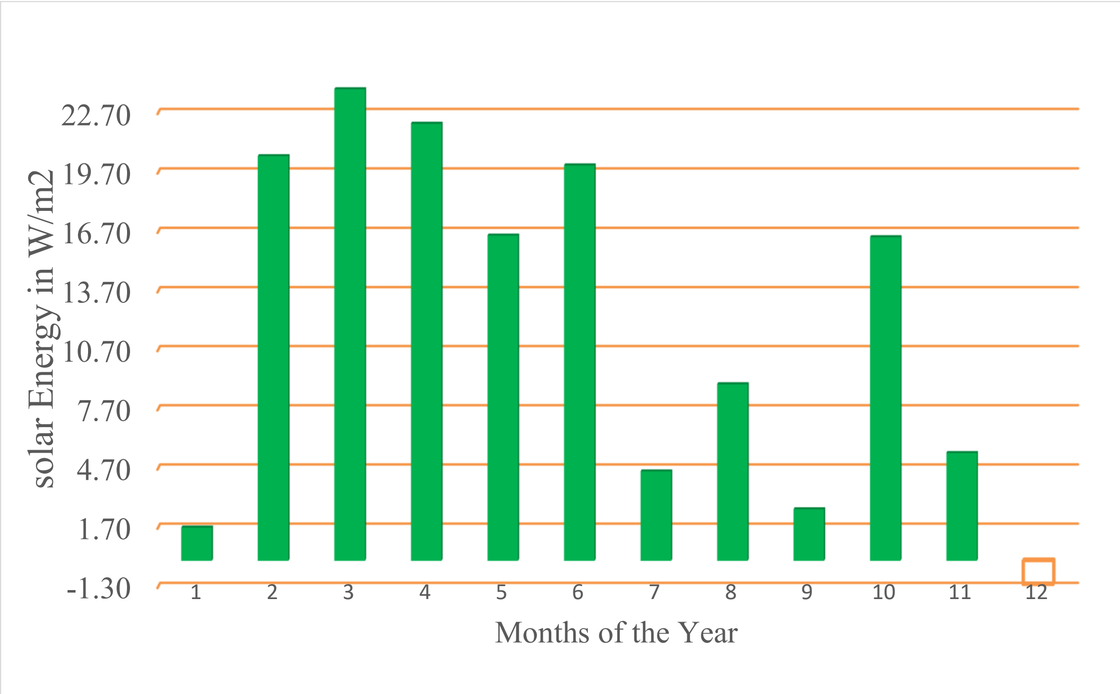

Figure 9. 38 Monthly Average Daily Net Electrical Energy Gain More than PV-Module

The technical meaning of the above chart and the below table is the amount of electricity this system save from dissipations in the form of heat from PV module if it's used separately and having the net electrical energy as the profit, the all the thermal energy generated by system is considered as the supplementary advantages of cooling the module by this design.

In Figure 9.38 the december monthly average daily net electrical energy gained by hybrid collector shows negative value that means the PV module net electrical energy generated is greater than PV-T collector in that month.

Table 9. 3 Adama Monthly Average Daily Electrical Energy Gain from PV Module

Hourly electrical energy gained by PV Module, in w/m2												
Hr.	Jan-17	Feb.16	Mr.16	Ap.15	Ma-15	Jun-11	Jul-17	Au-16	Se-15	Oct-15	No-14	De-10
6	0.00	0.00	0.00	0.00	0.00	0.00	2.45	0.50	0.00	0.00	0.00	0.00
7	31.50	32.63	28.70	26.33	24.11	22.73	22.21	24.65	27.77	29.29	31.06	33.92
8	64.01	65.90	60.42	56.05	52.19	48.74	44.52	51.72	58.87	61.24	63.54	66.44
9	94.41	96.79	90.08	83.92	78.62	73.36	65.94	77.43	88.03	91.08	93.97	96.90
10	118.00	120.56	113.16	105.70	99.41	92.88	83.18	97.88	110.84	114.19	117.63	120.63
11	132.03	134.55	127.00	118.82	112.03	104.88	93.97	110.50	124.61	127.92	131.78	134.85
12	135.72	138.10	130.78	122.40	115.55	108.34	97.19	114.21	128.43	131.50	135.56	138.71
13	129.38	131.65	124.73	116.63	110.06	103.25	92.70	108.96	122.47	125.26	129.26	132.47
14	113.80	115.96	109.55	102.21	96.25	90.28	81.15	95.42	107.43	109.97	113.64	116.85
15	90.12	92.05	86.34	80.27	75.30	70.60	63.77	74.84	84.49	86.72	89.88	93.03
16	60.73	62.25	57.56	53.24	49.62	46.59	42.80	49.71	56.15	57.91	60.42	63.45
17	29.86	30.79	27.29	24.94	22.86	21.67	21.29	23.64	26.44	27.65	29.50	32.37
18	2.25	2.51	0.17	0.00	0.00	0.00	2.35	0.48	0.00	0.56	1.88	4.61

Table 9. 4 Adama Monthly Average Daily Electrical Energy Gain from PV-T Collector

Hourly electrical energy gained by PV-T collector, in w/m2												
Hr.	Jan-17	Feb.16	Mar.16	Apr.15	My-15	Jun-11	Jul-17	Au-16	Se-15	Oct-15	Nov-14	De-10
7	30.01	31.49	27.97	25.60	23.36	22.26	21.52	23.92	26.82	28.19	29.73	32.44
8	62.25	65.02	60.18	55.70	51.64	48.66	43.83	51.13	57.95	60.25	62.09	64.79
9	93.77	97.70	91.65	85.17	79.37	74.62	65.91	77.88	88.18	91.61	93.75	96.37
10	119.37	124.16	117.24	109.23	102.10	95.97	84.24	99.87	112.56	117.11	119.49	122.01
11	135.19	140.45	133.09	124.25	116.37	109.45	95.97	113.73	127.49	132.92	135.42	137.81
12	139.33	144.66	137.30	128.35	120.36	113.31	99.44	117.65	131.28	137.12	139.62	141.90
13	131.79	136.83	129.85	121.44	113.92	107.32	94.39	111.44	124.04	129.67	132.08	134.30
14	114.02	118.44	112.13	104.81	98.25	92.61	81.76	96.27	107.14	112.00	114.22	116.45
15	88.50	92.06	86.66	80.85	75.61	71.33	63.45	74.35	82.88	86.60	88.57	90.87
16	58.65	61.15	56.81	52.79	49.12	46.45	42.13	48.73	54.37	56.86	58.56	60.96
17	28.50	29.86	26.62	24.46	22.39	21.39	20.79	22.95	25.41	26.82	28.26	30.75
18	2.14	2.42	0.17	0.00	0.00	0.00	2.28	0.47	0.00	0.54	1.79	4.36

Table 9. 5 Monthly Average daily Electrical Energy Achieved and Daily Net Energy

Date	Electrical El of PV	Electrical El. of PV-T	Net Electrical El
January-17	1001.83	1003.51	1.69
February-16	1023.73	1044.23	20.50
March-16	955.79	979.67	23.88
April-15	890.51	912.64	22.13
May-15	836.01	852.50	16.49
June-11	783.32	803.35	20.03
July-17	713.52	718.04	4.53
August-16	829.93	838.87	8.94
September-15	935.51	938.12	2.61
October-15	963.29	979.69	16.41
November-14	998.12	1003.58	5.46
December-10	1034.23	1033.01	-1.21

9.4 Solar PV-T System Array Sizing

9.4.1 Module Sizing

The PV-T system design and array sizing is performed based on **BSM340M-72/4BB** monocrystalline solar module with manufacturer specifications and characteristics given in Appendix B and using the average spring season irradiance on the tilted surface of Adama 4.983kWh/m²/day or 1.820Mwh/m2/year the manipulations is done, because the minimum insolation occurs in this season.

Using the peak hour approach calculation techniques: Energy demand per year equal to energy delivered by PV-T collector time consumption hour per day times number of the day per year.

Mathematically:

$$E_{demand} = E_{pv-t} * \frac{h}{day} * \frac{365days}{years}$$

$$E_{pv-t} = E_{demand} * \frac{days}{h} * \frac{years}{365days}$$

Using equation 4.1 and 4.1 the total energy required to process 3000l milk per day is calculated as:

$$E_{demand} = E_{total} * M_{milk}$$

$$\mathrm{M_{milk}} = \mathrm{V_{milk}\rho_{milk}} = 3000\mathrm{Litre} * 1.03\mathrm{kg/litre}$$

This means 3.09tonne of milk processed pasteurized milk products per days by using total energy of 0.1GJ/tonne of milk or 85.833KWh/day /31.3292MWh/year.

So, the amount of energy required from the collector is:

$$E_{ac} = \frac{\frac{31.3292\mathrm{MWh}}{\mathrm{year}}}{\frac{\frac{1.82\mathrm{Mwh}}{\mathrm{m2}}}{\mathrm{year}}} = 17.214\mathrm{kW}, \text{is the AC power required}$$

Consider the inverter loss, ignore the temperature effects due to temperature the collector efficiency is 0.78.

$$E_{dc} = \frac{17.214kw}{0.78} = 22069.2\mathrm{W} \text{ the amount of electrical energy needed}$$

Number of modules required=22069.2W/345W/module=63.96module approximate to 64module, add more two modules to reduce the battery size

To calculate the area required to install these 64 modules:

$$\mathrm{A_{module}} = \frac{\mathrm{E_{dc}}}{\frac{1\mathrm{kw}}{\mathrm{m2}} * \eta_0} = 123.9m^2$$

The array of this module mainly determined by the choice of the invertor and the size of the cable carry the currents from the arrays. Its better if the arrays off the string have the own invertor to make the system modularized, easy for maintenance.

9.4.2 Inverter

To tie 66 PV panels in a string, there are many possible combinations recommended by solar inverter manufacturers (sunny boy inverter is the best option in inverter technology), but the main problem is the arrange of inverter and the size of cable selected to carry currents and voltage from each string. By using five Sunny Boy 4000TL and one 3000TL inverter [26] for 22069.2W with six string all module connected in the following simple arrangement. The technical data for the Boy 3000TL and 000TL inverter is given in Appendix C.

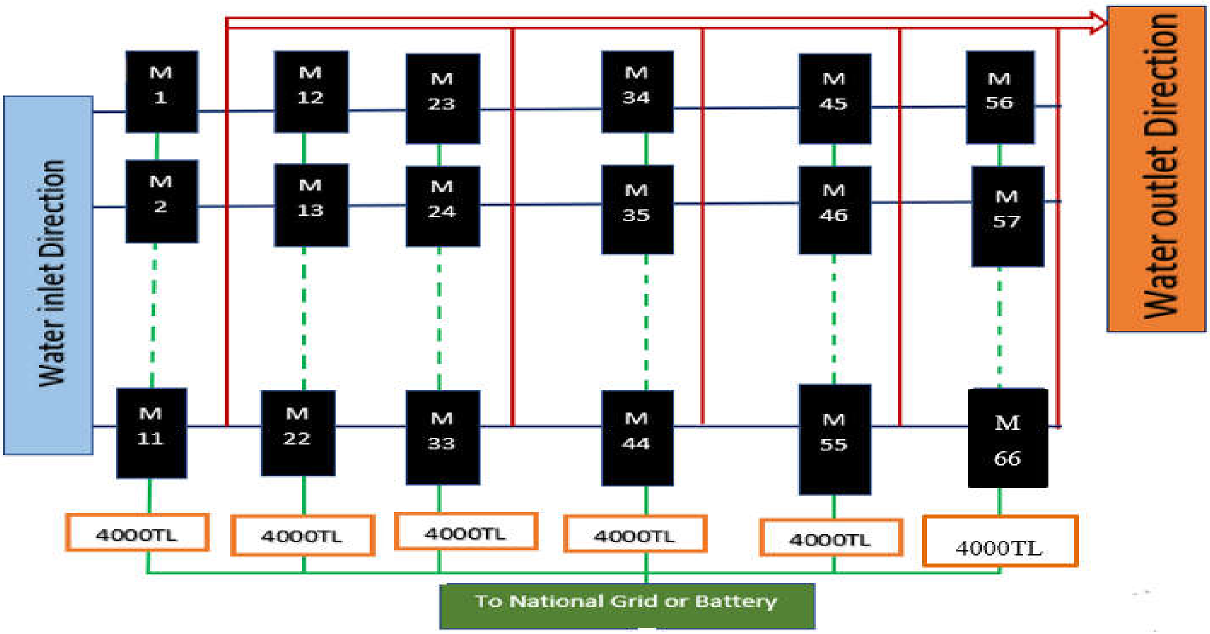

Figure 9. 39 PV-T collector String with Individual Inverter for each String.

The array output energy, current and voltage at maximum power tracking from the four strings of 16 modules each arrangement calculated as:

$$P_{inverter} = \text{number of modules in series} * P_{mpp}$$

$$I_{inverter} = I_{mpp} \text{ current in series connection is constant}$$

$$V_{inverter} = \text{number of modules in series} * V_{mpp}$$

For 4000TL Sunny Boy inverter connected string

$$P_{inverter} = 11module * \frac{345W}{module} = 3795W, \text{But the inverter can handle upto } 4200W$$

$$V_{inverter} = 11module * \frac{38.89volt}{module} = 422.29V, \text{But the inverter can handle } (175V - 500V)$$

For 3000TL Sunny Boy inverter connected string

$$P_{inverter} = 9module * \frac{345W}{module} = 3105W, \text{But the inverter can handle upto } 3200W$$

$$V_{inverter} = 9 * 38.89V = 345.51V, \text{But the inverter can handle } (175V - 500V) \mathit{Appendix\ C}$$

The Sunny Boy both 4000TL and 3000TL can handle the maximum input current of 17A per string and maximum power voltage range of 175V-500V.

9.4.3 Photovoltaic Cable

Solar Cables [35]used in Solar Farm installations are mainly categorized as given below:

A. PV module to PV module and PV modules to Array Junction Box: these cables though not exposed to direct sunlight are throughout the day time exposed to diffused/indirect sunlight and atmospheric temperatures in open air[35].
B. Array Junction Box to Main Junction Box and Main Junction Box to Inverter these Solar DC cables which are not exposed to sunlight and are always routed through PVC Pipes which are laid underground. Choice of cables can be done from any one of the options given. generally, option 3 is chosen for this route[35].
C. Inverter to Transformer Primary the three Phase AC output from the inverters is connected to the transformer Primary through underground armoured Cables[35].
D. Transformer Secondary to RMU/Switchyard the three Phase AC output from the transformer Secondary is connected to the Switchyard through armoured Cables[35].

9.5 Model Validation

In order to validate the simulation model developed for photovoltaic thermal solar collector system temperature profiles in each layer, water storage tank, electrical and thermal energy are compared with the authors previously published experimental data. The comparison of the experimental results to the simulation results is shown in the next two figure.

The simulation results closely agreed with experimental results, the model proposed thermal and electrical efficiency of PV-T collector with reduced temperature for Fig 2 design: [12] is given by regression lines $\eta_{th} = 28.74 - 41.24\frac{T_{in}-T_{am}}{G_T}$ which plotted in the graph for Adama and Addis Ababa data by Y_{1-A} & Y_{1-AA}, respectively. and the electrical efficiency for this configuration $\eta_{cell} = 11.81 - 11.94\frac{T_{in}-T_{am}}{G_T}$.

On another hand [10] proposed thermal and electrical efficiency of the glazed PV-T collectors as $\eta_{th} = Y_2 = 0.51 - 5.36\frac{\Delta T}{G}$ & $\eta_{el} = 0.108 - 0.15\frac{\Delta T}{G}$ which used for the comparison. The 1D daily yield simulation result obtained by (H. A Zondag et al) without producing electricity [36] is gives as Y_3 in the figure below.

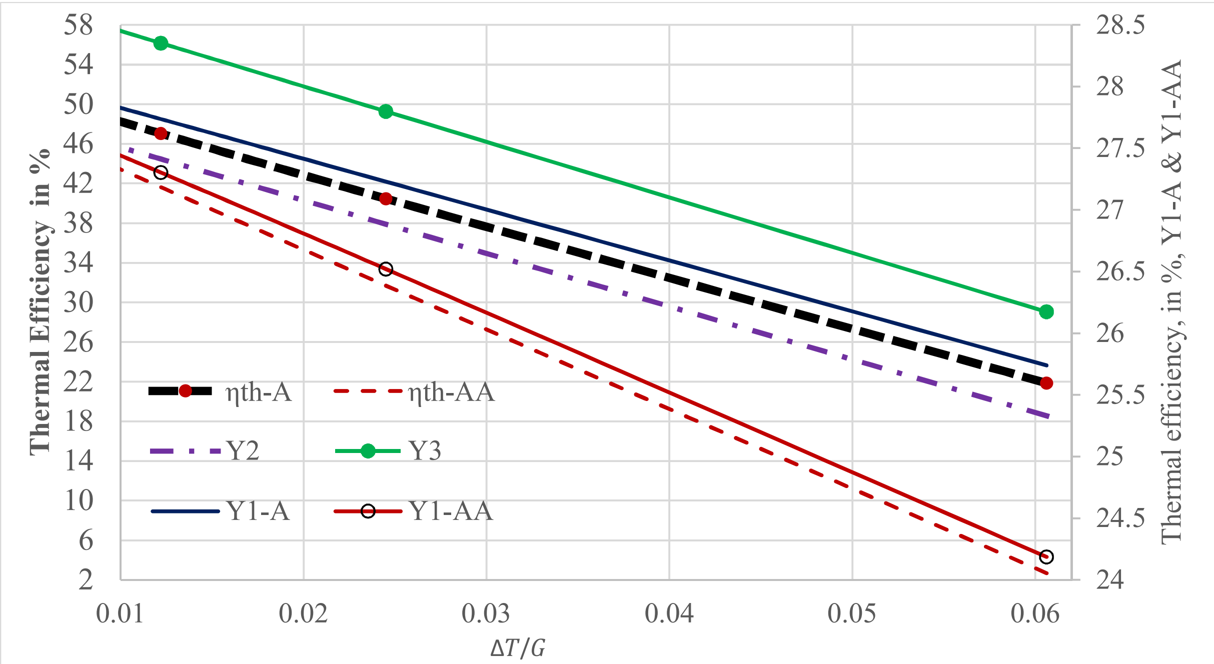

Figure 9. 40 validation chart 1

Where

Y_1 regressions line for oscillatory tube by [12]

Y_2 Single glazed sheet and tube PV-T collector thermal efficiency line

η_{th-A} Adama thermal efficiency

η_{th-AA} Addis Ababa thermal efficiency

Y_3 1D modelling PV-T collector thermal efficiency line

Based on validation graphs the desired modelling agree with the three-researcher stated above. So, the mathematical modelling followed is acceptable.

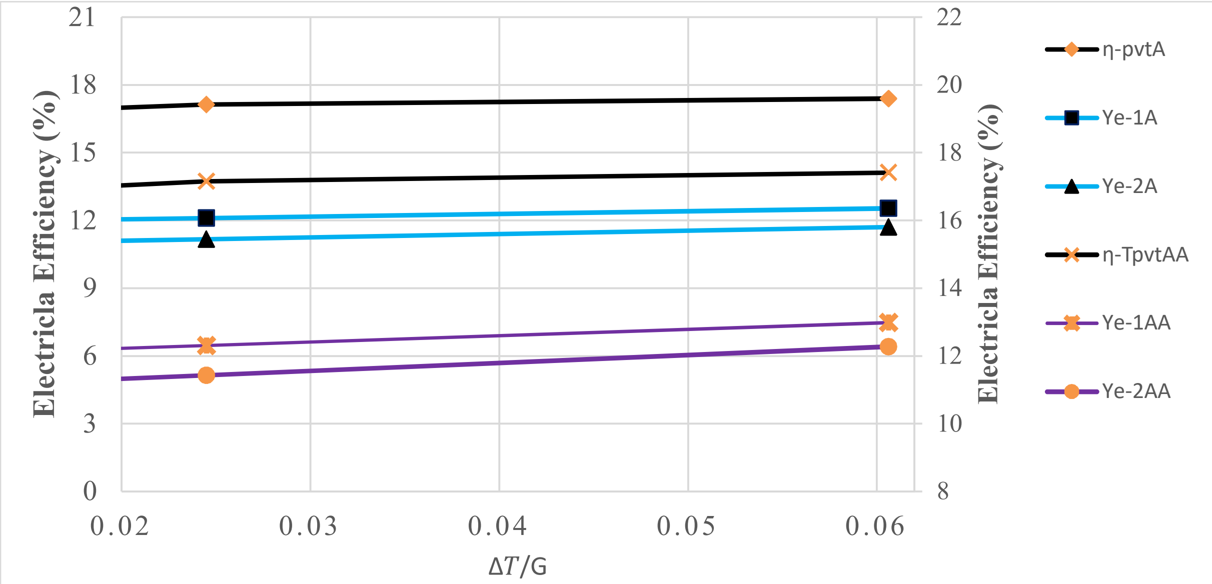

Figure 9. 41 Validation Chart 2

CHAPTER NINE

ECONOMIC EVALUATIONS

The numerical and technical evaluation discussed in the previous chapter is not sufficient to explain the advantages and disadvantages of this technology may be for technical and non-technical person, they need another alternative way to understand the profits in the form of economic benefit they can gain or lose from the desired system.

The economic profitability of the PV-T system under investigation and economic savings achieved by the proposed systems judged by comparing the system capital and operating costs with another alternative fuel source.

Techno-economic analysis is a fundamental subject of life-cycle cost analysis (LA). This is field of study where the cost of the system is optimized utilizing the engineering skills and experience in the particular field. Cost analysis is used for project-cost control through benefit–cost analysis, profitability analysis, planning, scheduling, and optimization of operational research, etc. In the case of solar-energy technology, it is necessary to determine its economic viability so that the users of the technology may know the importance.

9.1 Economic modelling

In this modelling the economic profitability of PV-T system achieved should be compared with the reference of diesel generator for thermal energy production.

The PV module manufacturer estimate the life span of the module as 25year and take the interest rate of 10% the life cycle cost found easily. The life cycle cost analysis of any solar-energy technology mainly depends on the following key parameters:

Initial investment for construction of solar-energy technology (P);

annual operating cost (O);

interest rate (i)

payback period (pbp); and

life time (n) and

annual maintenance cost (M) which is equal to 1.5%-time total investment cost

salvage value (S) of the system not considered in solar technology because after service year(25year) it's useless.

Life cycle cost (LCC)

Table 10. 1 Overall PV-T system cost list

No	Component	Price (Birr)
1	Glass cover	290
2	Al -Sheet	350
3	Inverter	1581.8
4	Controller (temperature controller)	730
5	Storage tank	3000
6	PV module	12000
7	Storage battery	636
8	Installation cost	1% of capital cost
9	Pump and pipe	1242
10	Copper tube	750
11	Maintenance cost	1.5% of total capital cost
12	Insulation material	500
13	Electrical wire	800
Total cost per PV-T collector		22,098.6
Total investment		1458507.468

The life cycle cost of any solar energy system calculated using the following mathematical expression:

$$\mathrm{LCC} = \mathrm{P} + \mathrm{P}\frac{1}{i * n}(1 - (1 + \mathrm{i})^{-n})$$

$$\mathrm{LCC} = 1422045 + 0.25 * 1422045 * 10 * (1 - 1.1^{-25})$$

$$\mathrm{LCC} = 4649034.843\text{birr for PV-T system}$$

LCC=3648787.921birr for PV system

The yearly average of PV module electrical, PV-T collector thermal and electrical energy generated found as 913.812, 3318.96 and 925.6 watt per square meter per day. So, to determine the price of energy from the life cycle cost, it may be equated with the yearly energy saving which the product of yearly energy achieved by the desired system times the fraction solar energy generated at standard operating conditions (0.85). finally, the annual total energy generated is 6530.8KWh for thermal. use the inflation rate of 9% throughout life span of the collector operation time to calculate the cost of the power.

$$C_{el} = \frac{LCC}{0.85 * 6530.8 * 66 * \frac{1 + if}{i - if}(1 - \frac{1 + if^{n}}{1 + i})}$$

$$C_{el} = \frac{4649034.843\text{birr}}{0.85 * 6530.8 * 66 * \frac{1 + 0.09}{0.1 - 0.09}(1 - \frac{1 + 0.09}{0.1 + 0.09}^{25}}$$

$$C_{el} = \frac{4649034.843\text{birr}}{8146778.54kwh}$$

$$\mathrm{C_{el}} = \frac{0.571\text{birr}}{\text{kwh}} \text{ for hybrid system or PV} - \text{T collector}$$

$$\mathrm{C_{el}} = \frac{4.52\text{birr}}{\text{kwh}} \text{ for PV system}$$

Where

if- inflation rate

C_{el} unit cost of electricity price delivered by hybrid system for invested cost.

To determine the profitability of PV and PV-T collector the above price compared with diesel fuel cost, which the market economic advantages are achieved or not. The calorific heating value diesel most of the time give as 39000KJ/L and one litre diesel weight is 0.85kg, and during industrial visit the cost of one litre diesel is 16.32birr only and the diesel cost (C_{diesel}) calculated as follows:

$$C_{diesel} = \frac{16.32\text{birr/litre}}{39000\text{KJ/litre}} = 0.0004185\text{birr/KJ}$$

$$C_{diesel} = \frac{0.0004185\text{birr}}{\text{kJ}} * \frac{3600\text{s}}{\text{hr}} = 1.506\text{birr/kwhr}$$

The two-energy comparison shows that energy generation cost of diesel is more expensive than PV-T collector and less expensive than PV system without considering the land cost and maintenance cost of the desired two system. This implies that using solar PV-T collector for dairy industry rather than diesel generator is more economical.

9.2 Payback period

The payback period (n) is defined as the number of years to recover the initial investment P. This can be calculated without considering discount rate of fuel and assuming uniform yearly saving, the life cycle cost saving at payback year is equal to the cash inflow in that year.

$$\text{pbp} = \ln(1 + \frac{\frac{P(if - i)}{1 + if}}{0.85 * C_{diesel} Q_{total\ yearly}} \frac{1}{\ln(\frac{1 + if}{1 + i})}$$

$$\text{pbp} = 2.688\text{years, approximately about 33month for PV-T system}$$

$$\text{pbp} = 4.426\text{years, approximately about 54Month for PV system}$$

Therefore, the economic evaluation shows the desired hybrid system more economical.

CHAPTER TEN

CONCLUSIONS AND RECOMMENDATIONS

10.1 Conclusion

The comparison is done between Adama and Addis Ababa for photovoltaic and hybrid photovoltaic thermal system using both locations weather data to give sufficient information's about solar energy location for dairy industry owners to establish the processing plate for better profit. The solar energy obtained in Adama weather conditions in all month is greater than each corresponding month of Addis Ababa weather conditions at the same collector dimensions and technical data which implies more energy potential available for the same investment in Adama.

Addis Ababa PV module temperature is less than Adama PV module temperature mainly due to ambient temperature and the electrical efficiency of Addis Ababa is greater than Adama in all months of the year which implies that this site is better for electrical energy applications. The Module temperature increment by 20°C above reference temperature cause the module efficiency drop by more than 0.66% which shorten the device life.

The temperature range (40-49°C) achieved by hybrid collector is used in dairy industry for washing, yoghurt maturation, mozzarella and cheese production, but the remain temperature requirement for pasteurisations achieved by using electrical energy parallelly generated.

For the same fluid inlet temperature more fluid outlet temperature obtained in Adama for PV-T collector, more combined efficiency and more useful energy gained with a smaller number of collector, space and the economic evaluations also results shows the 0.57birr/KWh, with this cost the payback period required is only 2.688years for desired hybrid system.

Generally, the hybrid collector is more advantages in all aspects of energy generations if installed in Adama rather than Addis Ababa.

10.2 Recommendations

The PV-T collector cannot heat water more than 50°C, but for pasteurization and sterilization process in dairy industry more water temperature is required, which needs auxiliary heater integrated design and the amount of this auxiliary energy demand requires another investigation which may be studied in the future.

By Cooling PV module its possible to increase the overall efficiency of the system, but beyond certain limit cooling the PV module may causes material damage (cracking) which needs serious analytical and experimental study to recognise the safely operating range of photovoltaic thermal collector.

REFERENCE

[1] C. Lation and F. Ation, “Tesfaye Bayou and Abebayehu Assefa Faculty of Technology Addis Ababa University,” vol. 8, pp. 7–16, 1989.

[2] Y. Mulugettaf, “Assessment of Solar and Wind Energy Ethiopia . i . solar energy resources,” vol. 57, no. 3, pp. 205–217, 1996.

[3] I. Description and W. Characteristics, “Dairy Industry,” pp. 295–297, 2007.

[4] “Summary of Requirements for Michigan Dairy Processing Plants.”

[5] “Extended Shelf Life Products (Milk , Cheese , Butter , Yogurt).”

[6] R. Fombad, “A Review of the Ethiopian Dairy Sector Edited by,” 2011.

[7] R. K. Mishra and G. N. Tiwari, “Evaluation of an integrated photovoltaic thermal solar (IPVTS) water heating system for various configurations at constant collection temperature,” pp. 3749–3756.

[8] T. T. Chow, G. N. Tiwari, and C. Menezo, “Hybrid Solar : A Review on Photovoltaic and Thermal Power Integration,” vol. 2012, 2012.

[9] R. C. Narayanan and A. K. Pv, “Performance Analysis of a Solar PVT / Water System,” vol. 1, no. 1, 2016.

[10] J. Kim and J. Kim, “Comparison of Electrical and Thermal Performances of Glazed and Unglazed PVT Collectors,” vol. 2012, 2012.

[11] N. Sítná and C. Republic, “Modeling Of Glazed Liquid Pv-T Collector With Use of Detail Model University Centre for Energy Efficient Buildings , Czech Technical University in Prague , Department of Environmental Engineering , Czech Technical University in Prague , Prague , Czech Rep,” pp. 2554–2560, 2015.

[12] A. Ibrahim et al., “Performance of Photovoltaic Thermal Collector (PVT) With Different Absorbers Design,” vol. 5, no. 3, pp. 321–330, 2009.

[13] S. E. Reviews, D. Version, and E. Reviews, “Flat-plate PV-Thermal collectors and systems : a review A review,” 2008.

[14] M. Ozgoren, M. H. Aksoy, C. Bakir, and S. Dogan, “Experimental Performance Investigation of Photovoltaic / Thermal (PV-T) System,” vol. 01106, 2013.

[15] A. Ramos et al., “Briefing paper No 22 Solar-Thermal and Hybrid Photovoltaic-Thermal Systems for Renewable Heating,” no. 22, 2017.

[16] A. Ramos, M. A. Chatzopoulou, I. Guarracino, J. Freeman, and C. N. Markides, “Hybrid photovoltaic-thermal solar systems for combined heating , cooling and power provision in the urban environment,” Energy Convers. Manag., 2017.

[17] J. Joe, S. Iniyan, and R. Goic, “Flat plate solar photovoltaic – thermal (PV / T) systems : A reference guide,” Renew. Sustain. Energy Rev., vol. 51, pp. 62–88, 2015.

[18] T. Arvind and T. Shyam, Handbook of Solar Energy. .

[19] A. Khelifa, K. Touafek, H. Ben Moussa, and I. Tabet, “Modeling and detailed study of hybrid photovoltaic thermal (PV / T) solar collector,” Sol. Energy, vol. 135, pp. 169–176, 2016.

[20] H. A. Zondag, D. W. De Vries, W. G. J. Van Helden, and R. J. C. Van Zolingen, “T he yield of different combined PV-thermal collector designs,” vol. 74, pp. 253–269, 2003.

[21] A. A. Ghoneim and A. M. Mohammedein, “Experimental and Numerical Investigation of Combined Photovoltaic-Thermal Solar System in Hot Climate,” vol. 16, no. 3, pp. 1–15, 2016.

[22] P. Y. Tripanagnostopoulos, “Hybrid Photovoltaic / Thermal Collectors,” pp. 1–24, 2016.

[23] S. Energy, “Hybrid Photovoltaic Thermal (PV / T) Air and Water Based Solar Collectors Suitable for Building Integrated Applications Adnan Ibrahim , Goh Li Jin , Roonak Daghigh , Mohd Huzmin Mohamed Salleh , Mohd Yusof Othman , Mohd Hafidz Ruslan , Sohif Mat and Kam,” vol. 5, no. 5, pp. 618–624, 2009.

[24] J. A. D. Deceased and W. A. Beckman, of Thermal Processes Solar Engineering. .

[25] C. Water, “Pump Selection Guide.”

[26] S. Boy, S. Boy, S. M. A. Solar, and T. Ag, “Operating Manual Sunny Boy 3000TL / 3600TL / 4000TL / 5000TL.”

[27] P. Production, Primary Production and Processing Standard for Dairy Products, no. June. 2009.

[28] U. States and U. States, “Solar Thermal Energy for Industrial Uses,” no. December, 2011.

[29] S. Energy and I. Areas, “Identification of Industrial Sectors Promising for Commercialisation of Solar Energy.”

[30] D. D. Desai, J. B. Raol, S. Patel, and I. Chauhan, “Application of Solar energy for sustainable Dairy Development,” pp. 131–140, 2013.

[31] P. K. Prabhakar, P. P. Srivastav, and K. Murari, “Energy consumption during manufacturing of different dairy products in a commercial dairy plant: A case study,” Asian J. Dairy Food Res., vol. 34, no. 2, p. 98, 2015.

[32] E. Inputs, “Sector Focus Dairy Processing,” pp. 1–4.

[33] F. Meteorology, N. Central, and S. Conservation, “Accuracy of hourly air temperatures calculated from daily minima and maxima*,” vol. 46, no. 15, pp. 193–209, 1989.

[34] “Numerical Investigation And Modelling Of Solar Photovoltaic / Thermal Systems Afroza Nahar Institute Of Graduate Studies,” 2017.

[35] S. Core, S. Core, and T. Copper, “Photovoltaic cables,” pp. 22–23, 2008.

[36] H. A. Zondag, D. W. D. E. Vries, W. G. J. V. A. N. Helden, R. J. C. V. A. N. Zolingen, and A. A. V. A. N. Steenhoven, “The Thermal and Electrical Yield of A Pv-Thermal Collector,” vol. 72, no. 2, pp. 113–128, 2002.

Appendix A: Solar Insolation Data Table

Adama monthly average hourly solar radiations in Watt/m2												
	Spring Season			Summer season			Autumn Season			Winter Season		
Time	Mar-16	Apr-15	May-15	Jun-11	Jul-17	Aug-16	Sep-15	Oct-15	Nov-14	Dec-10	Jan-17	Feb-16
6	0.0	0.0	14.6	3.0	0.0	0.0	0.0	0.0	0.0	0.0	0.0	0.0
7	147.0	140.1	135.5	150.6	169.0	177.5	187.2	205.8	190.2	198.4	176.2	161.2
8	329.6	310.4	279.2	326.4	371.8	385.7	397.8	418.5	401.5	417.2	385.5	356.1
9	516.7	484.8	426.5	506.8	580.2	600.0	614.7	637.7	619.2	642.3	600.7	556.2
10	679.3	636.3	554.5	663.6	761.5	786.7	803.7	828.7	809.0	838.4	788.0	730.3
11	789.9	739.4	641.6	770.4	885.1	913.9	932.6	959.0	938.4	972.0	915.7	848.8
12	829.2	776.0	672.5	808.3	928.9	959.1	978.4	1005.2	984.3	1019.4	960.9	890.8
13	789.9	739.4	641.6	770.4	885.1	913.9	932.6	959.0	938.4	972.0	915.7	848.8
14	679.3	636.3	554.5	663.6	761.5	786.7	803.7	828.7	809.0	838.4	788.0	730.3
15	516.7	484.8	426.5	506.8	580.2	600.0	614.7	637.7	619.2	642.3	600.7	556.2
16	329.6	310.4	279.2	326.4	371.8	385.7	397.8	418.5	401.5	417.2	385.5	356.1
17	147.0	140.1	135.5	150.6	169.0	177.5	187.2	205.8	190.2	198.4	176.2	161.2
18	0.0	0.0	14.6	3.0	0.0	3.5	11.6	28.4	13.9	15.7	1.1	0.0

Addis Ababa Monthly Average Hourly Solar Radiation In Watt/m2												
	Spring Season			Summer Season			Autumn Season			Winter Season		
TIME	Mar-16	Apr-15	May-15	Jun-11	Jul-17	Aug-16	Sep-15	Oct-15	Nov-14	Dec-10	Jan-17	Feb-16
6	0.4	0.0	8.2	19.0	21.9	14.4	2.0	0.0	5.8	8.2	12.4	6.0
7	171.5	160.3	145.4	132.9	118.3	118.9	134.9	154.2	178.1	179.3	188.0	183.3
8	376.2	351.8	308.4	268.3	233.0	243.6	293.8	344.0	384.9	385.0	398.8	395.7
9	586.7	548.5	475.6	407.0	350.5	371.5	457.2	539.4	598.1	597.2	616.2	614.6
10	770.0	719.6	620.9	527.5	452.6	482.9	599.5	709.8	784.1	782.3	805.9	805.3
11	894.9	836.1	719.8	609.5	522.2	558.7	696.5	825.9	910.9	908.5	935.2	935.3
12	939.3	877.4	754.8	638.6	546.8	585.6	730.9	867.1	955.9	953.3	981.1	981.4
13	894.9	836.1	719.8	609.5	522.2	558.7	696.5	825.9	910.9	908.5	935.2	935.3
14	770.0	719.6	620.9	527.5	452.6	482.9	599.5	709.8	784.1	782.3	805.9	805.3
15	586.7	548.5	475.6	407.0	350.5	371.5	457.2	539.4	598.1	597.2	616.2	614.6
16	376.2	351.8	308.4	268.3	233.0	243.6	293.8	344.0	384.9	385.0	398.8	395.7
17	171.5	160.3	145.4	132.9	118.3	118.9	134.9	154.2	178.1	179.3	188.0	183.3
18	0.4	0.0	8.2	19.0	21.9	14.4	2.0	0.0	5.8	8.2	12.4	6.0

Appendix B**: Blue Sun Monocrystalline Panels Manufacturer Data Sheet**

BSM340M-72/4BB

Monocrystalline 72 cells 325w-345w

Alibaba Trade Assurance Supplier

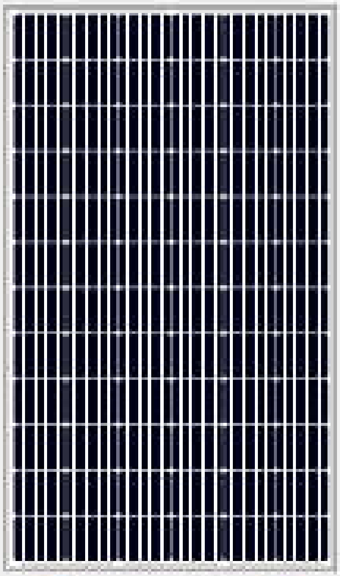

Key Features

- Monocrystalline modules designed for commercial and solar farm grid-tied applications
- High power output and highest conversion efficiency
- Anti-reflective and anti-soiling surface reduces power loss from dirt and dust
- Outstanding performance in low-light irradiance environments
- Excellent mechanical load resistance: Certified to withstand high wind loads (2400Pa) and snow loads (5400Pa)
- High salt and ammonia resistance certified by TÜV NORD

Superior Warranty

- 10-year product warranty
- 25-year linear power output warranty

Reliable Quality

- Positive power tolerance: 0~+5W
- 100% EL double-inspection ensures modules are defects free
- Modules binned by current to improve system performance
- Potential Induced Degradation (PID) Resistant

Mechanical Parameters

Cell (mm)	Mono 156×156
Weight (kg)	26 (approx)
Glass Thickness	4 mm
Dimensions (L×W×H) (mm)	1956×991×45
Cable Cross Section Size (mm^2)	4
No. of Cells and Connections	72 (6×12)
Junction Box	IP67, 3 diodes
Connector	MC4 Compatible
Packaging Configuration	23 Per Pallet

Working Conditions

Maximum System Voltage	DC 1000V (IEC)
Operating Temperature	-40℃~+85℃
Maximum Series Fuse	15A
Maximum Static Load, Front (e.g., snow and wind) Maximum Static Load, Back (e.g., wind)	5400Pa (112 lb/ft^2) 2400Pa (50 lb/ft^2)
NOCT	45±2℃
Application Class	Class A

I-V Curve

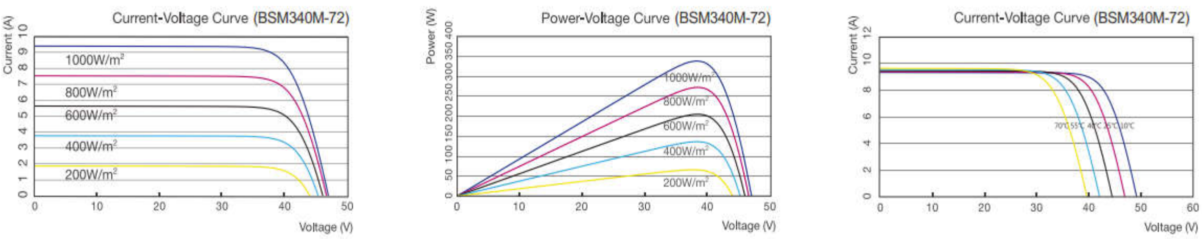

Electrical Parameters

Module	BSM325M-72	BSM330M-72	BSM335M-72	BSM340M-72	BSM345M-72
Rated Maximum Power at STC (W)	325	330	335	340	345
Open Circuit Voltage (Voc/V)	46.13	46.34	46.73	46.91	47.13
Maximum Power Voltage (Vmp/V)	37.21	37.57	37.92	38.17	38.39
Short Circuit Current (Isc/A)	9.25	9.29	9.32	9.41	9.48
Maximum Power Current (Imp/A)	8.73	8.78	8.83	8.91	8.99
Module Efficiency [%]	16 77	17.02	17 28	17.54	17.80
Power Tolerance (W)	-0~+5W				
Temperature Coefficient of Isc (αIsc)	+0.059%/℃				
Temperature Coefficient of Voc (βVoc)	-0.330%/℃				
Temperature Coefficient of Pmax (γPmp)	-0.410%/℃				
STC	Irradiance 1000W/m², Cell Temperature 25℃, Air Mass 1.5				

Appendix C: Sunny Boy Inverter Datasheet

Efficient

- Maximum efficiency of 97 %
- Multistring technology in all power classes
- Cost savings resulting from fewer parallel strings
- Shade management with OptiTrac Global Peak

Flexible

- Maximum DC input voltage of 750 V
- Integrated grid management functions and reactive power provision

Easy to Use

- Fanless
- Simplified wall mounting
- SUNCLIX DC plug-in system
- Fast connection without tools

Communicative

- Simple country configuration
- Bluetooth® and Speedwire/Webconnect technology as standard

SUNNY BOY 3000TL / 3600TL / 4000TL / 5000TL With Reactive Power Control

The same. Only better. The universal Sunny Boy.

Getting better all the time. The new transformerless Sunny Boy is the ideal solution, especially for demanding PV arrays and partly shaded systems. Version 20 of the successful Sunny Boy offers a further array of advantages. It's more flexible in its range of applications, provides even more efficient yields and it's easier to use. The high DC voltage of 750 V creates a cost advantage, since fewer parallel strings are required. In addition, the integrated grid management functions make the device suitable for universal applications and allow them to actively support the grid.

Technical Data	Sunny Boy 3000TL	Sunny Boy 3600TL
Input (DC)		
Max. DC power (at cos φ = 1)	3200 W	3880 W
Max. input voltage	750 V	750 V
MPP voltage range / rated input voltage	175 V to 500 V / 400 V	175 V to 500 V / 400 V
Min. input voltage / initial input voltage	125 V / 150 V	125 V / 150 V
Max. input current input A / input B	15 A / 15 A	15 A / 15 A
Max. input current per string input A / input B	15 A / 15 A	15 A / 15 A
Number of independent MPP inputs / strings per MPP input	2 / A:2; B:2	2 / A:2; B:2
Output (AC)		
Rated power (at 230 V, 50 Hz)	3000 W	3680 W
Max. AC apparent power	3000 VA	3680 VA
Nominal AC voltage / range	220 V, 230 V, 240 V / 180 V to 280 V	220 V, 230 V, 240 V / 180 V to 280 V
AC power frequency / range	50 Hz, 60 Hz / −5 Hz to +5 Hz	50 Hz, 60 Hz / −5 Hz to +5 Hz
Rated power frequency / rated grid voltage	50 Hz / 230 V	50 Hz / 230 V
Max. output current	16 A	16 A
Power factor at rated power	1	1
Adjustable displacement power factor	0.8 lagging to 0.8 leading	0.8 lagging to 0.8 leading
Feed-in phases / connection phases	1 / 1	1 / 1
Efficiency		
Max. efficiency / European Efficiency	97 % / 96 %	97 % / 96,4 %
Protective Devices		
Input-side disconnection point	●	●
Ground fault monitoring / grid monitoring	● / ●	● / ●
DC reverse polarity protection / AC short-circuit current capability / galvanically isolated	● / ● / –	● / ● / –
All-pole sensitive residual-current monitoring unit	●	●
Protection class (according to IEC 62103) / overvoltage category (according to IEC 60664-1)	I / III	I / III
General Data		
Dimensions (W / H / D)	490 / 519 / 185 mm (19.3 / 20.4 / 7.3 inch)	
Weight	26 kg (57.3 lb)	
Operating temperature range	−25 °C to +60 °C (−13 °F to +140 °F)	
Noise emission (typical)	25 dB(A)	25 dB(A)
Self-consumption (at night)	1 W	1 W
Topology	Transformerless	Transformerless
Cooling method	Convection	Convection
Degree of protection (according to IEC 60529)	IP65	IP65
Climatic category (according to IEC 60721-3-4)	4K4H	4K4H
Maximum permissible value for relative humidity (non-condensing)	100%	100%
Features		
DC connection / AC connection	SUNCLIX / spring-cage terminal	SUNCLIX / spring-cage terminal
Display	Graphic	Graphic
Interfaces: RS485 / Bluetooth® / Speedwire/Webconnect	○ / ● / ●	○ / ● / ●
Multifunction relay / Power Control Module	○ / ○	○ / ○
Warranty: 5 / 10 / 15 / 20 / 25 years	● / ○ / ○ / ○ / ○	● / ○ / ○ / ○ / ○
Certificates and approvals (others available upon request)	AS 4777, C10/11, CE, CEI 0-21, EN 50438¹, G59/3, G83/2, IEC 61727, MEA⁴, NEN-EN50438, NRS 097-2-1, PEA⁴, PPC, PPDS, RD1699, RD 661, SI 4777, UTE C15-712, VDE-AR-N 4105, VDE0126-1-1, VFR 2013, VFR 2014	

Technical Data	Sunny Boy 4000TL	Sunny Boy 5000TL
Input (DC)		
Max. DC power (at cos φ = 1)	4200 W	5250 W³
Max. input voltage	750 V	750 V
MPP voltage range / rated input voltage	175 V to 500 V / 400 V	175 V to 500 V / 400 V
Min. input voltage / initial input voltage	125 V / 150 V	125 V / 150 V
Max. input current input A / input B	15 A / 15 A	15 A / 15 A
Max. input current per string input A / input B	15 A / 15 A	15 A / 15 A
Number of independent MPP inputs / strings per MPP input	2 / A:2; B:2	2 / A:2; B:2
Output (AC)		
Rated power (at 230 V, 50 Hz)	4000 W	4600 W
Max. AC apparent power	4000 VA	5000 VA²
Nominal AC voltage / range	220 V, 230 V, 240 V / 180 V to 280 V	220 V, 230 V, 240 V / 180 V to 280 V
AC power frequency / range	50 Hz, 60 Hz / −5 Hz to +5 Hz	50 Hz, 60 Hz / −5 Hz to +5 Hz
Rated power frequency / rated grid voltage	50 Hz / 230 V	50 Hz / 230 V
Max. output current	22 A	22 A
Power factor at rated power	1	1
Adjustable displacement power factor	0.8 lagging to 0.8 leading	0.8 lagging to 0.8 leading
Feed-in phases / connection phases	1 / 1	1 / 1
Efficiency		
Max. efficiency / European Efficiency	97 % / 96.4 %	97 % / 96.5 %

Appendix D: Electric Cable

TYPE 1 – Dimensions

Single Core Size in Sq.mm	Max. Conductor Diameter in mm	XL-LSOH Insulation Thickness-Nominal in mm	XL-LSOH Sheathing Thickness-Nominal in mm	Overall Dia. Nominal in mm
SOLAR DC CABLES FROM PV MODULE TO ARRAY JUNTION BOX (as per TUV Specifications-2 Pfg 1169/08.2007)				
1.5	0.26	0.7	0.9	5.0 +/-0.5
2.5	0.26	0.7	0.9	5.5 +/-0.5
4	0.31	0.7	0.9	6.0 +/-0.5
6	0.31	0.7	0.9	6.5 +/-0.5
SOLAR DC CABLES FROM ARRAY JUNCTION BOX TO MAIN JUNTION BOX & MJB TO INVERTER (as per TUV Specifications-2 Pfg 1169/08.2007)				
10	0.41	0.7	0.9	7.5 +/-0.5
16	0.41	0.7	0.9	8.5 +/-0.5
25	0.41	0.9	1.0	10.5 +/-0.7
35	0.41	0.9	1.1	12.0 +/-0.7
50	0.41	1.0	1.2	14.0 +/-0.7
70	0.51	1.1	1.3	16.0 +/-1.0
95	0.51	1.1	1.5	18.5 +/-1.0
120	0.51	1.2	1.6	20.0 +/-1.0
150	0.51	1.4	1.7	22.5 +/-1.0
185	0.51	1.6	1.9	25.0 +/-1.0
240	0.51	1.7	2.1	28.0 +/-1.0

TYPE 2 – Dimensions

Single Core Size in Sq.mm	Max. Conductor Diameter in mm	HR 105°C PVC Insulation Thickness-Nominal in mm	UV HR 105°C PVC Sheathing Thickness-Nominal in mm	Overall Dia. Nominal in mm
SOLAR DC CABLES FROM PV MODULE TO ARRAY JUNTION BOX (as per IS 694 & IS 1554 Part I guidelines)				
1.5	0.26	0.6	0.9	5.0 +/-0.5
2.5	0.26	0.7	0.9	5.5 +/-0.5
4	0.31	0.8	0.9	6.5 +/-0.5
6	0.31	0.8	0.9	7.0 +/-0.5
SOLAR DC CABLES FROM ARRAY JUNCTION BOX TO MAIN JUNTION BOX & MJB TO INVERTER (as per IS 694 & IS 1554 Part I guidelines)				
10	0.41	1.0	0.9	8.5 +/-0.5
16	0.41	1.0	0.9	9.5 +/-0.5
25	0.41	1.2	1.0	11.0 +/-0.7
35	0.41	1.2	1.1	12.5 +/-0.7
50	0.41	1.4	1.3	15.0 +/-0.7
70	0.51	1.4	1.4	17.0 +/-1.0
95	0.51	1.6	1.5	19.5 +/-1.0
120	0.51	1.6	1.6	21.0 +/-1.0
150	0.51	1.8	1.8	23.5 +/-1.0
185	0.51	2.0	1.9	25.5 +/-1.0
240	0.51	2.2	2.2	29.5 +/-1.0

TYPE 3 – Dimensions

Single Core Size in Sq.mm	Max. Conductor Diameter in mm	XLPE Insulation Thickness-Nominal in mm	UV-PVC-ST2 Sheathing Thickness-Nominal in mm	Overall Dia. Nominal in mm
SOLAR DC CABLES FROM PV MODULE TO ARRAY JUNTION BOX (as per IS 7098 Part I guidelines)				
1.5	0.26	0.7	0.9	5.0 +/-0.5
2.5	0.26	0.7	0.9	5.5 +/-0.5
4	0.31	0.7	0.9	6.0 +/-0.5
6	0.31	0.7	0.9	6.5 +/-0.5
SOLAR DC CABLES FROM ARRAY JUNCTION BOX TO MAIN JUNTION BOX & MJB TO INVERTER (as per IS 7098 Part I guidelines)				
10	0.41	0.7	0.9	7.5 +/-0.5
16	0.41	0.7	0.9	8.5 +/-0.5
25	0.41	0.9	1.0	10.5 +/-0.7
35	0.41	0.9	1.1	12.0 +/-0.7
50	0.41	1.0	1.2	14.0 +/-0.7
70	0.51	1.1	1.3	16.0 +/-1.0
95	0.51	1.1	1.5	18.5 +/-1.0
120	0.51	1.2	1.6	20.0 +/-1.0
150	0.51	1.4	1.7	22.5 +/-1.0
185	0.51	1.6	1.9	25.0 +/-1.0
240	0.51	1.7	2.1	28.0 +/-1.0

TYPE 1 – Current Carrying Capacity

SOLAR DC CABLES AS PER TUV SPECIFICATIONS-2 PfG 1169/08.2007

Single Core Size in	Tinned Copper Maximum Resistance @20°C	Current Carrying Capacity of DC Solar Cable with XL-LSOH Insulation and XL-LSOH Sheathing at 60°C		
		Single Cable in Air	Single Cable on Surface	2 Adjacent Cables on Surface
Sq.mm	Ohms-Ω/Km	in Amps-A	in Amps-A	in Amps-A
1.5	13.700	30	29	24
2.5	8.210	41	39	33
4	5.090	55	52	44
6	3.390	70	67	57
10	1.950	98	93	79
16	1.240	132	125	107
25	0.795	176	167	142
35	0.565	218	207	176
50	0.393	274	260	219
70	0.277	406	386	325
95	0.210	491	467	393
120	0.164	576	547	461
150	0.132	670	637	536
185	0.108	784	745	627
240	0.0817	944	897	755

TYPE 2 – Current Carrying Capacity

SOLAR DC CABLES FROM JUNCTION BOX TO INVERTER AS PER IS 694 & IS 1554 PART I GUIDELINES

Single Core Size in	Bare Copper Maximum Resistance @20°C	Current Carrying Capacity of DC Solar Cable with HR 105°C PVC Insulation and UV Stabilised HR 105°C PVC Sheathing at 40°C		
		Single Cable in Air	Single Cable on Surface	2 Adjacent Cables on Surface
Sq.mm	Ohms-Ω/Km	in Amps-A	in Amps-A	in Amps-A
1.5	13.3	28	26	22
2.5	7.98	39	37	31
4	4.95	50	48	40
6	3.30	64	61	51
10	1.910	89	84	71
16	1.210	119	113	95
25	0.780	150	143	120
35	0.554	191	182	153
50	0.386	253	240	202
70	0.272	374	355	299
95	0.206	451	429	361
120	0.161	530	504	424
150	0.129	618	587	494
185	0.106	721	685	577
240	0.0801	869	825	695

TYPE 3 – Current Carrying Capacity

SOLAR DC CABLES FROM JUNCTION BOX TO INVERTER AS PER IS 7098 PART I GUIDELINES

Single Core Size in	Bare Copper Maximum Resistance @20°C	Current Carrying Capacity of DC Solar Cable with XLPE Insulation and UV Stabilised PVC ST2 Sheathing at 40°C		
		Single Cable in Air	Single Cable on Surface	2 Adjacent Cables on Surface
Sq.mm	Ohms-Ω/Km	in Amps-A	in Amps-A	in Amps-A
1.5	13.3	25	24	20
2.5	7.98	35	33	28
4	4.95	45	43	36
6	3.30	58	55	46
10	1.910	80	76	64
16	1.210	106	101	85
25	0.780	135	128	108
35	0.554	173	164	138
50	0.386	226	215	181
70	0.272	336	319	269
95	0.206	406	386	325
120	0.161	476	452	381
150	0.129	555	527	444
185	0.106	649	616	519
240	0.0801	781	742	625